7-2022

EFFECT OF INJURY MECHANISM AND SEVERITY ON THE MOLECULAR PATHOPHYSIOLOGY OF TRAUMATIC BRAIN INJURY

Brandon McDonald
University of Nebraska-Lincoln, brandon.mcdonald@huskers.unl.edu

EFFECT OF INJURY MECHANISM AND SEVERITY ON THE MOLECULAR PATHOPHYSIOLOGY OF TRAUMATIC BRAIN INJURY

by

Brandon Z. McDonald

A THESIS

Presented to the Faculty of

The Graduate College at the University of Nebraska

In Partial Fulfillment of Requirements

For the Degree of Master of Science

Major: Agricultural and Biological Systems Engineering

Under the Supervision of Professor Forrest Kievit

Lincoln, Nebraska

July, 2022

EFFECT OF INJURY MECHANISM AND SEVERITY ON THE MOLECULAR PATHOPHYSIOLOGY OF TRAUMATIC BRAIN INJURY

Brandon McDonald, M.S

University of Nebraska, 2022

Advisor: Forrest M. Kievit

Traumatic brain injury (TBI) mechanism and severity are heterogenous clinically, resulting in a multitude of physical, cognitive, and behavioral deficits. However, approximately 80% suffer from milder injuries. Thus, examining pathophysiological changes associated with mild TBI is imperative for improving clinical translation and evaluating the efficacy of potential therapeutic strategies. Through this work, we developed models of TBI, ranging in both injury mechanism and severity, using an electromagnetic controlled cortical impact (CCI) device. First, we characterized and optimized a closed head, mild TBI model (DTBI) to determine the clinical translatability and practicality of producing repeated mild injuries. Interestingly, we determined that impact speed was highly dependent on both input velocity and depth. Indeed, impact conditions differed from input parameters, and we suggest researchers characterize closed head models using CCI devices to ensure data is interpreted based on the true impact conditions. Additionally, we investigated how impact speeds influenced pathophysiology, specifically autophagic flux. Our results show that autophagic flux was impaired acutely in the hippocampus, regardless of impact speed, providing rationale for evaluating autophagic flux following mild, diffuse impacts. Thus, we continued investigating pathophysiological changes associated with a spectrum of TBI, including severe CCI, modified mild TBI (MTBI), and previously characterized DTBI. Following impacts, we

observed distinct differences in gross neuropathology, which corresponded with changes in the progression of cell death. Indeed, severe CCI resulted in dramatic increases in oncosis, while mild models differed regarding apoptotic response, suggesting injury mechanism and severity shift the progression of cell death. Interestingly, each of the three impact models resulted in impaired autophagic flux, which coincided with changes in both oncotic and apoptotic cell death. Thus, these results provide evidence that the pathophysiological mechanisms affiliated with TBI heterogeneity may be linked through common upstream events, namely impaired autophagic flux and lysosomal dysfunction. Therefore, therapeutic strategies designed to intervene in the amelioration of these consequences may alleviate molecular dysfunction, in addition to the cognitive and behavioral deficits observed following TBI.

DEDICATION

To those who risk their lives playing the game they love. My hope is that one day this work, and the work of other neurotrauma researchers, will help establish effective diagnostic and therapeutic protocols to ensure your continued health and safety.

ACKNOWLEDGEMENTS

This work would not have been possible without the continuous support of so many incredible people. I would like to first acknowledge my primary advisor, Dr. Forrest Kievit. Your mentorship and tutelage over these last 4 years has sparked my passion for neurotrauma research. I am grateful for how you have helped me grow as a person, and I thank you for your compassion and guidance. I would also like to acknowledge my committee members, Dr. Rebecca Wachs and Dr. Xinghui Sun. You have given me valuable insight into what it means to be an excellent teacher and diligent researcher. I look forward to working with you in the future and continuing to learn by your example. Special thanks to Aria Tarudji, Connor Gee, Evan Curtis, Hunter Miller, Brittany Schweiger, and other past and current members of the Kievit lab. It has been an honor and privilege to learn from you during my graduate program. I am thankful for the friendships and memories that we have made, and I can't wait to see what the future holds for our careers. I would also like to thank my friends and family including my father and mother, Kevin and Letitia, and my two younger brothers, Colin and Trevor. You all have molded me into the man I am today, and I will forever be appreciative of your love and support. Lastly, I would like to thank my beautiful, loving wife, Hannah. I know it is not easy being married to a graduate student, but your warmhearted personality eased the stresses associated with work and school. Thank you for all that you have done for me, and will continue to do for me, as we grow old together.

TABLE OF CONTENTS

TABLE OF FIGURES

TABLE OF TABLES

CHAPTER 1: INTRODUCTION

1.1 Traumatic Brain Injury

Adapted from my previously published literature review [1]:

Traumatic brain injury (TBI) is currently the leading cause of injury related morbidity and mortality worldwide with an estimated global cost of $400 billion annually [2]. Injury severity and mechanism are heterogenous clinically, leading to a multitude of physical, cognitive, and behavioral outcomes. These outcomes originate from primary head impact leading to a spread of secondary injury [3]. External forces can be generated from direct collision impacts or through non-impact situations, including rotational acceleration of the head or the energy waves produced from blasts (Figure 1.1) [4, 5]. Impacts result from falls, motor vehicle accidents, assault, domestic violence, military warfare, and even recreational sports including football, soccer, and boxing [3]. These multiple mechanisms of impact are a primary cause of heterogenous behavioral outcomes, leading to difficulties in developing diagnostic and prognostic protocols, let alone effective treatments. Thus, there is still no approved therapy that has shown efficacy in reducing the long-term secondary effects following TBI.

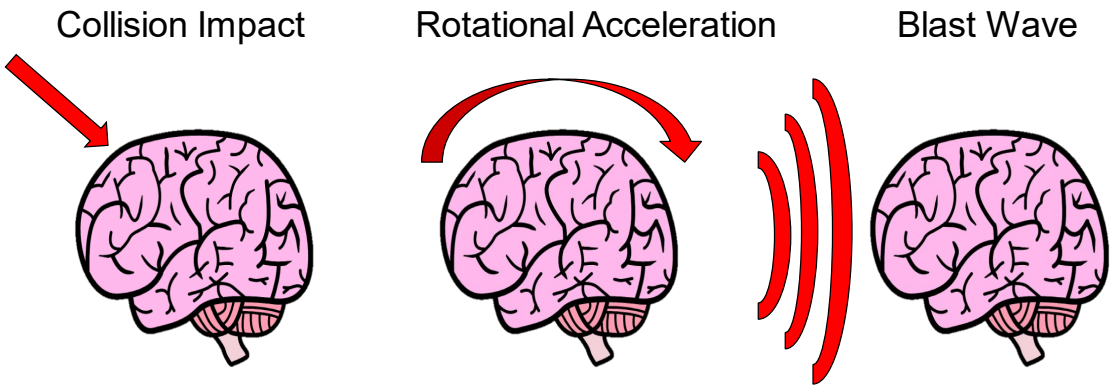

Figure adapted from Gabriel Peterman

Figure 1.1. Mechanisms of Traumatic Brain Injury. Primary impacts are caused by three primary mechanisms of impact including collision impacts through direct contact, rotational acceleration of the head, and energy produced from blast waves.

TBI patients have a 2–4-fold increase in the risk of developing dementia later in life, due to even a single instance of TBI followed by a loss of consciousness (LOC) [6]. In conjunction with aging, individuals who have experienced TBI are at increased risk for developing Alzheimer's disease, at 2.3 and 4.5 times more likely for moderate and severe TBI, respectively [7]. Even repeated mild injuries, such as those with retired professional American football players, have been correlated to long term cognitive deficits. Retired players who had suffered three or more concussions in their careers had a 5-fold increase in mild cognitive impairments as compared to their counterparts with no history of concussions [6]. Additionally, Parkinson's disease, amyotrophic lateral sclerosis, Creutzfeldt-Jakob disease, and chronic traumatic encephalopathy (CTE) were also all found to be associated with the progression of chronic TBI [6]. Due to the association of TBI with these progressive neurodegenerative diseases, viable treatment options must be developed with an in-depth knowledge of the injury's pathophysiology lest the current therapeutic stalemate continue.

Unfortunately, these differences between patients and their injuries provide a variety of complications for medical personnel in determining efficient diagnoses and effective treatments. Current treatment options include surgical and pharmacological intervention, including relieving intracranial pressure through craniotomy or ameliorating symptoms following TBI through antidepressants, anticonvulsants, and stimulants [8]. However, none of these methods have shown efficacy in alleviating the long-term deficits associated with injury [9-11]. Although there has been success in Phase II trials, all treatments options have failed during larger, multi-center Phase III trials [12]. These failures have resulted due to a variety of problems during testing for the efficacy of

treatments. Clinical trials for testing the efficacy of the pharmacological intervention of progesterone, the glutamate antagonist, CP 101-606, and the antioxidant, Tirilazad, each resulted in negative outcomes during Phase III trials [11-14]. Researchers postulate that these failures were the result of suboptimal dosing during Phase II trials suggesting inadequate delivery into the brain and poor target engagement. Additionally, heterogeneity between injuries can result in vastly different secondary pathophysiology requiring in multiple strategies in pharmacological intervention [15, 16]. Other clinical trials have had similar issues including problems with clinical trial design, lack of accurate injury phenotyping, and inadequate outcome assessment tools [16]. Challenges with injury heterogeneity and inadequate outcome assessment tools are capable of being mitigated with effective classification systems. Classification systems have been previously constructed for categorizing the injury severity of TBI in humans immediately following diagnostic exams from medical professionals. Initial methods for classifying TBI in a clinical setting are efficient, but simplistic in approach, leaving room for error between different degrees of human injury. However, recent literature has investigated the most important variables for assessing TBI in hope of improving upon the original designs to create a more effective classification system [17, 18].

While methods for classifying degrees of injury in humans have advanced, efforts have also been directed towards developing animal models for TBI to provide an effective comparison to human injuries [19, 20]. These models have been used to understand the pathophysiological mechanism for the progression of different degrees of TBI. Additionally, animal models have aided in the development of potential treatments for the reduction of oxidative stress, BBB dysfunction and various other biochemical

impairments [19-21]. Recently, Operation Brain Trauma Therapy (OBTT) was developed as a multi-center pre-clinical consortium to identify therapies that are beneficial in alleviating damage from head trauma in animal models [16]. The OBTT makes use of several animal models in three distinct injury categories, focal, diffuse, and non-impact injury, creating a broad spectrum of potential pathophysiological outcome [3, 19]. Each model has unique procedures and outcomes in hopes to provide a sufficient translation to the variety of head traumas that occur in humans. Through these models, comparisons can be derived between the various degrees of human injury severity, which will ultimately lead to improvements in diagnostics and treatment protocols.

Thus, the role of this research is to understand how injury heterogeneity influences the changes in molecular pathophysiology following TBI. This goal will be accomplished through three primary aims including: 1) utilize one impact device to develop and optimize mild TBI animal models to produce injury variability 2) identify the effects of injury heterogeneity on pathophysiology, and 3) determine how injury variability influences the mechanisms of pharmacological targets. These results will provide insight into how the progression of secondary injury differs in animal models which reflect the heterogeneity observed clinically. Ultimately, this work will elucidate pathophysiological similarities and differences to optimize strategies for therapeutic intervention and provide a more rigorous method for assessing their efficacy.

1.2 Clinical Classification of TBI Severity

The severity of a patient's TBI is primarily affiliated with the mechanism and severity of injury in which the initial applied force is delivered to the head. This force will drive the secondary progression of damage and can provide valuable insight into the

overall development of the condition. However, there are several additional variables that are required to effectively characterize a patient's level of injury. These factors help determine the overall injury progression of the individual. While patient's injuries can range from mild, presenting with concussive symptoms, to severe, leading to probable death, the classification methods developed by previous literature have determined the different categories of human TBI in between these broad outcomes.

1.2.1 Glasgow Coma Scale

Initial analysis for categorizing the behavioral deficits following TBI in a clinical setting is based on the Glasgow Coma Scale (GCS), originally developed in 1974 [22, 23]. Although the classification criteria for this system was developed nearly 50 years ago, the system is still regularly used by medical professionals to evaluate the degree of injury immediately following head trauma. The GCS provides a reference score calculated following an examination from a medical professional to identify the strength of a patient's response in three main areas: eye movement, verbal response, and motor function (scale shown in Table 1.1.) [22-24]. Each category is scored based on criteria increasing in cognitive complexity from a score of 1-6. Summing the three scores allows for a better understanding of a patient's TBI severity and enhances the ability to explore the relationships between score and outcome on an academic level. The GCS scoring system is categorized into three sections: mild, moderate, and severe TBI (Figure 1.2.) [25]. Mild injuries receive scores ranging from 13-15, where patients experience a LOC for less than 30 minutes, followed by post-traumatic amnesia (PTA) for up to 24 hours [26]. In contrast, severe injuries receive scores of 3-8, with an LOC of over 24 hours and PTA lasting for over 7 days. Most patients suffer from mild TBI, approximately 80%,

while moderate and severe TBI represent about 10% of the clinical population, respectively [27]. Concussions are one specific example of mild TBI, when individuals experience deficits in cognition or behavior. However, even sub-concussive impacts have resulted in the chronic progression of behavioral deficits seen in neurodegenerative diseases [28].

Table 1.1. Assessment criteria of the Glasgow Coma Scale used for determining injury severity in a clinical setting [22-24].

Response **1**	**2**	**3**	**4**	**5**	**6**
Eye None	To Pain	To Speech	Spontaneous	N/A	N/A
Verbal None	Incomprehensible Sounds	Inappropriate Words	Confused Conversation	Oriented	N/A
Motor None	Extension (Decerebrate)	Abnormal Flexion (Decorticate)	Withdrawal (Normal Flexion)	Localizes Pain	Obeys Commands

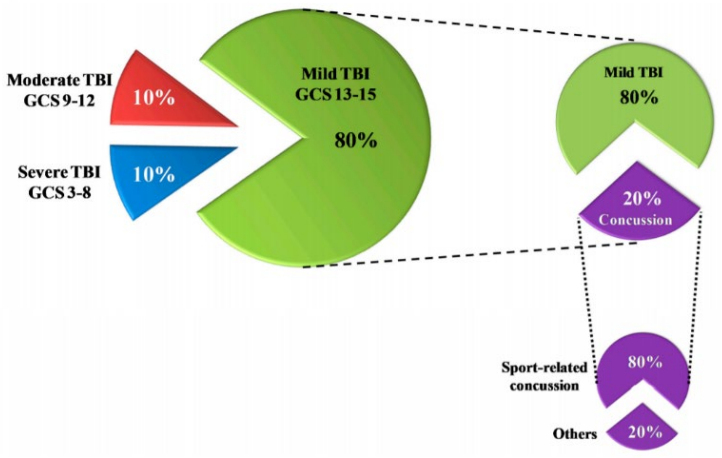

Figure 1.2. TBI Epidemiology. The Glasgow Coma Scale provides guidelines for evaluating the severity of injuries in the clinical population. Scores are categorized into three groups: Mild (13-15), Moderate (9-12), and Severe (3-8). Reproduced with permission from [25].

The GCS system has been used for several decades due to its effectiveness in predicting outcomes of TBI. A study taking place in 1999 showed that outcome predictions made using this model were accurate 76.3% of the time at admission, 82.5% preoperatively, 77.1% at 24 hours, 63.3% at 3 days, and 69.7% at 7 days post TBI [29]. Additionally, in 2014, GCS scores obtained following patient's exams were shown to be positively correlated with assessments of metabolism, neuroimaging, collected biomarkers, and prediction of mortality [23]. However, the GCS method suffers from limitations when predicting severe TBI outcomes. From the 1999 study, 75.8% of the overall outcome predictions were correct, however, predictions for an outcome of severely disabled were only correct 12.2% of the time [29]. It is also important to note that successful predictions for severe TBI (71.2%) were much lower than predictions of moderate (90%) and mild (92.9%) TBI [30]. Additionally, GCS scores may be impacted by a variety of circumstances including behavioral changes from drug and alcohol intoxication, misinterpretation of patients' responses, and even early medical intervention such as intubation which can lead to inaccurate assessment from the GCS [31]. Ultimately, GCS has continued to provide value in TBI classification due to its simplicity and overall efficiency, specifically for triage while stabilizing patients. However, this method lacks the ability for an ultimate diagnostic report due to external circumstances and poor predictability for determining differences between moderate and severe TBI based on the criteria provided in the scoring system.

1.2.2 Mayo Classification of TBI

To build upon the GCS method and provide a more complete classification system for the evaluation of TBI injuries, in 2007, the Mayo Clinic developed a model

incorporating a variety of variables including: death, LOC, post-traumatic anterograde amnesia (PTA), and computed tomography (CT) imaging [17]. Each of these variables was used to help categorize injuries into three sections ranging from symptomatic (possible) TBI, mild (probable) TBI and moderate-severe (definite TBI) [17]. Mayo's method was able to improve upon the GCS method by utilizing additional details following a patient's exam to effectively achieve a diagnosis [17]. Comparisons were evaluated between Mayo's classification system to GCS, PTA, and LOC classifications alone for the evaluation of 1,678 patients [17]. Mayo's model was shown to identify additional patients presenting with moderate-severe TBI that other methods classified as mild due to the lack of additional parameters. Additionally, Mayo's classification system was able to provide a category for patients with possible TBI based on symptoms that no other model was able to establish previously. Over 50% of the patient study fell into this symptomatic TBI classification, indicating that a large percentage of head trauma may not result in pronounced cognitive deficits detected by the GCS system. Individuals experiencing symptoms of TBI from concussions and minor head trauma may still require medical care, which may have been overseen from previous classification methods. Unfortunately, Mayo's system fails to distinguish between moderate and severe TBI which lacks details for a wide range of treatment possibilities for the medical community.

1.2.3 Collaborative European NeuroTrauma Effectiveness for Research for TBI

In April of 2020, analysis conducted in the Collaborative European NeuroTrauma Effectiveness Research for TBI (CENTER-TBI) expanded upon previous models for evaluating TBI injuries in humans using a wide variety of variables and characteristics

[18]. Data was collected from 4,509 patients across Europe and categorized into clusters using a range of five collective "building blocks" that included: demographics, clinical severity, secondary insults, cause of injury, and imaging characteristics, such as CT imaging or Magnetic Resonance Imaging (MRI) [18]. Variables were evaluated to determine strength of significance, where cause of injury remained the most significant determinant for the condition's progression, followed by presence of major extracranial injury, GCS, and imaging characteristics. Following characterization, CENTER-TBI provided four separate categories for TBI injury in humans including: mild, upper intermediate, lower intermediate, severe; and identified the likelihood of each respective outcome using the Glasgow Outcome Scale Extended (GOSE) [18]. The additional category for dividing moderate TBI is an improvement from previous classification models, allowing for additional prognostic guidance. The study also established probabilities for expected behavioral outcomes in each of the categories. The percentage of patients remaining in their previously affiliated category after resampling was 97.4%, confirming a 95% confidence interval [18]. Following this study, researchers developed a prediction model for determining an individual's functional outcome based on the variables described previously, along with additional vitals. Researchers applied baseline admissions characteristics from examinations and a prediction of the prognostic results for a 6-month mortality time frame was collected. This prediction model represents the potential growth in the field of TBI classification. Researchers and medical personnel would be able to determine an individual's treatment based on a handful of characteristics capable of being tested upon entry into the hospital following their initial TBI. While initial results from GCS scores are efficient and useful for providing an assessment for

the urgency in treating a patient following admission to a medical facility, developing classification methods based on additional information is necessary to determine the overall progression of TBI.

1.3 Clinical Classification of TBI Mechanism

1.3.1 Focal TBI

TBI can often be used to describe a broad condition with varying degrees of damage, however, the causal injuries associated with TBI are categorized into three distinct forms: focal, diffuse, and non-impact. Focal injuries in the patient population are created through direct impact forces acting on the skull, which causes compression of the underlying tissue. Focal injuries include skull fractures, contusions, lacerations, hemorrhages, and subdural, epidural and intraparenchymal hematomas [32]. Contusions from focal injuries are often due to penetrating impacts or severe blunt force trauma, differing from other ailments that may be caused by diffuse injury. Contusions can occur in two different forms, coup, also known as ipsilateral, or contrecoup contusions [32]. Coup contusions occur below the impact site when the head absorbs impact and contrecoup contusions occur opposite of the impact site. For example, impact forces applied to the frontal lobe (hitting head against wall), produce contrecoup contusions near the occipital lobe. Contusions differ from lacerations simply by the forces causing the injury, as contusions are caused by direct blunt forces while lacerations are caused by shearing forces placed upon the tissue [32]. Additionally, contusions are associated with damage to small blood vessels, while hemorrhaging is associated with bleeding in the subarachnoid or subdural space. Subarachnoid hemorrhaging may result from either focal or diffuse injuries but is more often seen in diffuse injuries [15]. Subdural hematomas are

usually caused by ruptured veins due to quick acceleration and deceleration forces [15]. A concern with focal injuries is with intracerebral hematomas which can develop over 24 hours following contusions and, specifically, the subset of intracerebral hematomas that develop with a delayed onset 1 to 3 days after TBI. Delayed intracerebral hematomas are incredibly dangerous with a mortality rate between 50% to 75% [32].

1.3.2 Diffuse TBI

While focal injuries are particularly dangerous and concerning, special attention must be paid to diffuse injuries due to the underwhelming sense of urgency following trauma. Diffuse injuries describe an injury mechanism where rapid acceleration and deceleration results in semi-independent movements of brain structures due to the heterogeneous nature of tissue fixation with other structures and the skull, as well as tissue consistency [33]. This phenomenon is similar to the effect of whiplash following a traffic vehicle accident where the brain's inertia continues in the direction of the applied force, followed by a rapid deceleration against the inner wall of the skull. Directional movement influences the diffuse injury severity, as lateral movement tends to cause worse damage than sagittal movement [15]. This movement can result in vascular injury, brain swelling or edema, and most commonly a diffuse axonal injury (DAI) [15, 32]. DAI refers to the tearing of axons which, under normal conditions, would remain intact due to their high elasticity. However, when enough force is applied, the axons can tear or deform, resulting in permanent and irreversible damage to the fibers of neurons [15, 32]. It is thought that this irreversible damage is caused by an initial swelling of the axon due to mitochondrial dysfunction leading to the collapse of the microtubular system throughout the cell, 6 to 12 hours after the initial swelling [15]. However, there are other

bodies of evidence that argue axonal swelling continues for years after the primary injury and could potentially contribute to increased disability in some patients [15]. Furthermore, Doppenberg et al. 2004, recommends excluding patients who are diagnosed with DAI from clinical trials until a proven therapy specifically for DAI is found in animal models [15]. Figure 1.3. provides both CT (A-F) and MRI (G-I) images of pathophysiological changes following both focal and diffuse TBI [32]. This figure highlights the structural differences between focal and diffuse injuries, which is important to keep in context when discussing the comparisons between animal models of TBI.

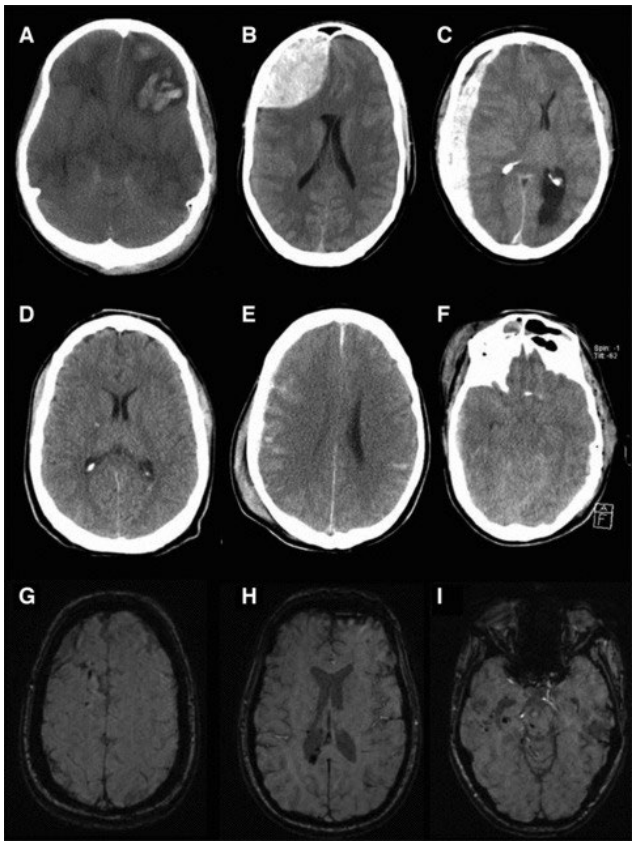

Figure 1.3. Clinical examples of focal and diffuse TBI. Examples of structural changes following Focal and Diffuse TBI represented by CT Imaging (A-F) and MRI (G-I). A, B and C are of CT images following focal injuries, indicated by the presence of a focal contusion in A, as well as hematomas in B and C. Figures D, E and F are of CT images following diffuse injuries, indicated by hemorrhages in D and E, and diffuse swelling in F. Images G, H and I are of susceptibility weighted MRI images of one patient presenting with DAI indicated by hemorrhaging in different regions of the brain. Reproduced with permission from [32].

1.3.3 Non-Impact TBI

The final mechanism of injury seen in TBI refers to non-impact injuries. Unlike focal injuries, non-impact TBI implies damage from injuries which did not result from direct penetrating or blunt force impact with the skull and is typically induced through alterations in pressure or acceleration/deceleration from the brain inside the skull. The associated pathophysiological consequences of non-impact injuries are unique due to the mechanism of impact, but share features observed in both focal and diffuse TBI. Additionally, clinical presentation of non-impact injuries is typically coupled with focal and diffuse injuries leading to compounding effects on the pathological outcome. For example, members of military warfare can often be exposed to blast injuries, in which multiple mechanisms of injury are acting on the body. These elements include 1) primary blast injury: blast wave acting on the brain, 2) secondary blast injury: accelerated projectiles penetrating the skull, 3) tertiary blast injury: acceleration/deceleration effects acting on the body, and 4) quaternary blast injury: thermal and chemical injuries to the head following the initial explosion [34]. However, in this section of the review we will be referring to the primary blast injury only. Blast waves result in accelerated air pressure which interacts with the head and body creating acceleration or rotation of the head, and transfer of the kinetic energy from the blast through fluid circulating in the thorax [35, 36]. Acceleration of fluid within the body, results in increased intracranial pressure which can result in BBB disruption, vasculature damage, edema, and hemorrhaging [34]. Cognitive deficits from blast injuries include headache, fatigue, problems with sleep and concentration, and even post-traumatic stress disorder, which is one of the behavioral aspects most relevant to members of the military [36]. Additionally, road traffic incidents,

as discussed briefly in the diffuse injury section, can produce rapid acceleration and deceleration of the brain inside the chamber of the skull, producing edema, vascular injury, and DAI [15, 32, 37].

While there are similarities between focal, diffuse, and non-impact injuries, each of these types of traumas produce unique pathological outcomes that are specific to mechanism of injury delivered to the brain. Therefore, animal models must be developed with an in-depth knowledge of the mechanism of injury to enhance translation between the pathophysiological consequences seen following animal injury and clinical TBI. Through these animal models, researchers will be able to develop therapeutic options for alleviating the conditions presented within each type of TBI.

1.4 TBI Animal Models

Animal models are valuable tools used for providing an effective comparison to a variety of human conditions. Understanding the mechanism for the progression of various diseases allows researchers to develop treatment protocols which can be modified prior to human testing for optimal results. These models have been created for a multitude of ailments affecting the brain, including TBI [19, 38]. TBI animal models have aided in the development of potential treatments for the reduction of oxidative stress, improving BBB permeability, and other various biochemical impairments following TBI [19, 21, 38]. Several models have been developed, sectioned into three distinct categories as seen in clinical presentations of TBI: focal, diffuse, and non-impact injury [3, 19]. Each of these models has distinct procedures and outcomes in hopes of providing a sufficient translation to the variety of situations for which head trauma occurs in humans. Additionally, several of these models can be manipulated to alter the levels of

injury severity, leading to a greater understanding of injury progression. Based on these experiments, comparisons are derived between the various degrees of human injury severity, which will ultimately lead to improvements in diagnostics and treatment protocols.

1.4.1 Controlled Cortical Impact

The controlled cortical impact (CCI) model is currently one of the most used and well characterized models of TBI, due to the model's reproducibility and specificity regarding mechanical parameters [39-42] (57-60). CCI models use a pneumatic or electromagnetic (Figure 1.4.) impact system to deliver a rigid impactor onto the exposed dura of the animal, following craniectomy [40]. Originally developed in ferrets, the CCI model has been adapted for a variety of species including mice, rats, swine, and monkeys [19, 41]. Features of injury include subdural hematoma, subarachnoid hemorrhage, axonal injury, in addition to cortical contusions and cortical tissue loss which have been shown in clinical presentations of TBI [40-42]. Primary advantages for using CCI models include precise automated control over a variety of factors including impactor diameter, velocity, depth, and dwell time of impact [42]. Previous literature has identified the appropriate depths for inducing mild, moderate, and severe TBI's at 0.0-0.2 mm, 0.5-1.0 mm, and 1.2-2.0 mm, respectively [42]. Figure 1.5. shows whole brain images and histological images of coronal brain slices following a moderate TBI with a velocity of 3.0 m/s, tip diameter of 3 mm and depth of 1 mm. Images from 24 hours and 6 weeks following moderate injury show cortical tissue loss in the ipsilateral hemisphere (Figure 1.5. C-D), in addition to the loss of Nissl-stained neurons (Figure 1.5. F) [42].

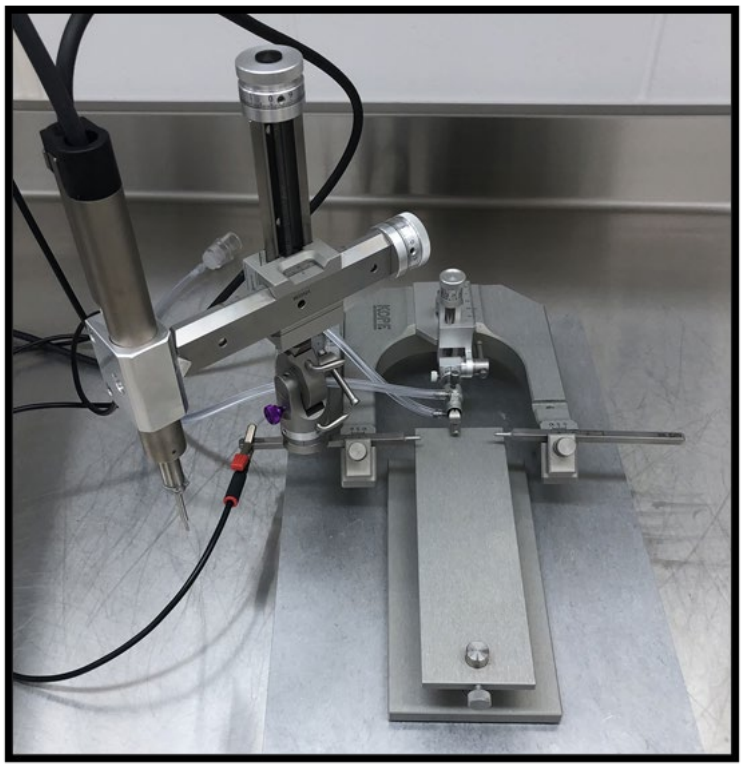

Figure 1.4. Example of an Electromagnetic Controlled Cortical Impact System with stereotaxic frame for stabilizing mice.

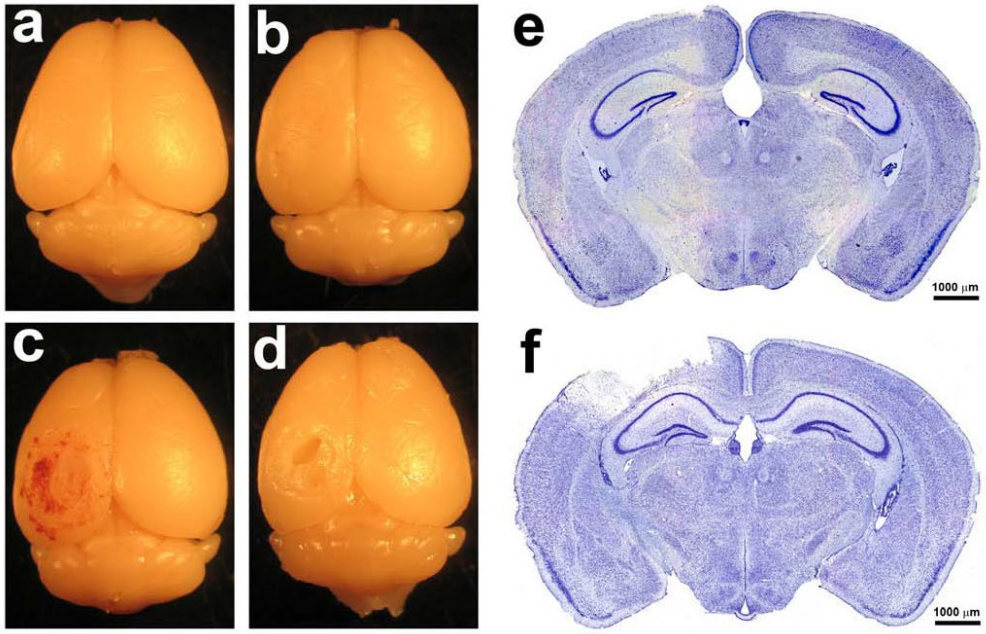

Figure 1.5. Brains collected from experimentation in the CCI model. a) 10-Week-Old Mouse, b) Sham (Craniectomy Only), c) 24 Hr. Post Moderate TBI, d) 6 Weeks Post Moderate TBI, e) Nissl Staining of Sham, f) Nissl Staining of Moderate TBI. This is adapted from Romine, J., Gao, X., Chen, J. Controlled Cortical Impact Model for Traumatic Brain Injury. *J. Vis. Exp.* (90), e51781, doi:10.3791/51781 (2014).

1.4.2 Modified Controlled Cortical Impact

For the investigation into the biomechanics involved in mild TBI, in 2014, Meaney et al. introduced a modified CCI model through adjustments to the mechanical parameters discussed previously, in addition to the material and size of the impactor tip [43]. This modified CCI model uses similar methodology and equipment as the previously discussed CCI model, but with a much lower impact velocity of 0.43 m/s and a larger impact depth of 2.1 mm [43]. The material and size of the impactor tip was adjusted to produce a diffuse, mild injury. In this study, the impactor tip (4.0 mm diameter) was manufactured from Sylgard-184 to produce a soft silicone tip capable of producing a diffuse injury across a greater surface area of the brain [43]. Figure 1.6. (Top) illustrates the comparison in tip size and region of injury between the mild CCI (mCCI) impactor tip developed in this study and the traditional CCI impactor tip comprised of metal, typically stainless steel [43]. Features of this model include subcortical axonal injury, with no presence of visible lesions or hemorrhaging (Figure 1.6. Bottom) [43]. An additional point of consideration highlighted in this figure is the lack of cortical lesion represented in both the sham and mCCI brain images. Several reports have discussed the impact of craniectomies in elucidating changes in inflammatory and behavior responses. Therefore, the incorporation of a sham model is crucial in separating the effects from injury and surgical perturbation of the skull. This injury design further illustrates the variation established with the use of CCI methods. While this method requires further standardization, the variation in impactor tip hardness provides the possibility for additional studies with ranging injury outcomes.

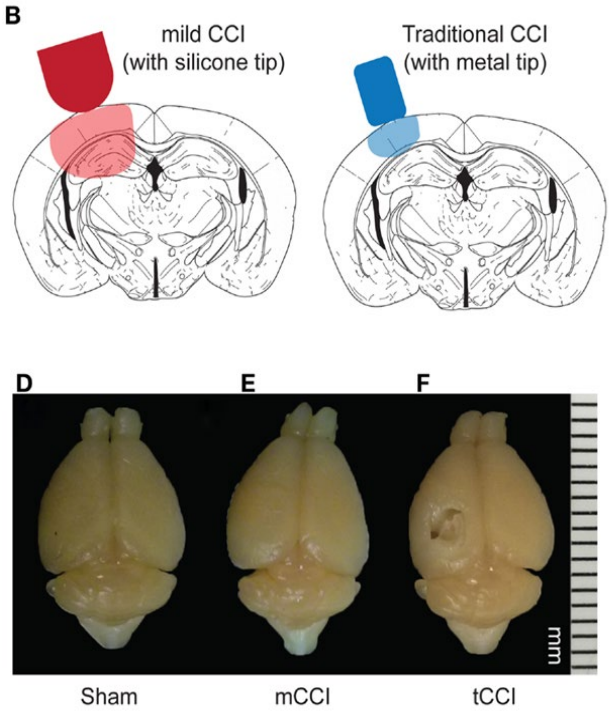

Figure 1.6. Modified controlled cortical impact model. Top (B): Comparison between the impactor tip size and region of injury between mild and traditional CCI (64). Bottom (D–F): Brains 8 days post injury showing comparisons between sham, mild (mCCI) and traditional CCI (tCCI). Reproduced with permission from [43].

1.4.3 Marmarou Weight Drop Model

The Marmarou weight drop model has a distinct experimental design that mimics diffuse axonal injury experienced in clinical TBI, through impacting a greater surface area of the skull and diffusing the primary injury throughout the brain [44, 45]. Following a midline incision into the animal's scalp, a stainless-steel disc is attached to the skull with an adhesive glue between the lambda and bregma [44, 45]. This disc prevents skull fractures upon impact from the free-falling weight, which is more frequent in the focal injury weight drop models. Additionally, the animal is placed onto a foam bed to reduce the deceleration of the animal's head following impact (Figure 1.7.) [46].This reduction in deceleration mitigates the risk of producing contrecoup injuries opposite the impact

[19]. In a study conducted on rats in 1994, animals were impacted with a weight of 450 grams from heights of 1 or 2 meters [44]. Animals injured from 1 meter resulted in no mortalities, while heights from 2 meters resulting in a 59% mortality rate [44]. However, groups receiving intervention in the form mechanical ventilation did not result in mortality for either height [44]. Both heights produced diffuse brain injuries with no presence of focal lesions, while petechial hemorrhaging was associated with injuries produced from the 2-meter height [44]. Neuronal injury was noticed in both ipsilateral and contralateral cortices, in addition to DAI present in the corpus callosum, long tracts in the brain stem, and to the cerebral and cerebellar peduncles [44]. Due to the presentation of DAI following impact, Marmarou's model has been well characterized in literature, however it has been associated with a high mortality rate due to respiratory depression without mechanical ventilation following injury.

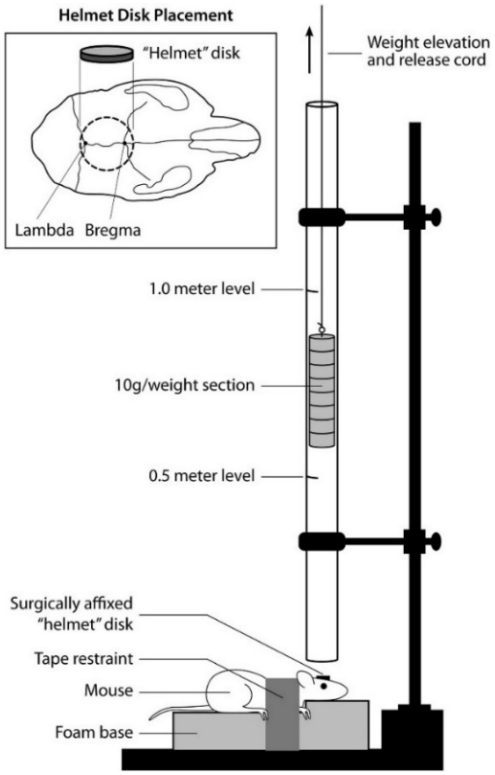

Figure 1.7. Illustration of a modified grade 1A Marmarou weight drop model. The impact is delivered through a free-falling weight colliding with a helmet secured to the animal's head. The animal is placed onto a foam pad to decelerate impact and reduce the risk of contrecoup injuries. Reproduced with permission from [46].

1.4.4 Modified Marmarou Weight Drop Model

While Marmarou's weight drop model has shown to be successful in producing features of diffuse injuries such as DAI, limitations in reproducibility have led researchers to explore alternatives to the original methods established in 1994. The diffuse injury model developed by Cernak, I et al. in 2004 incorporates a variety of factors from the Marmarou Weight Drop Model and CCI model to develop a reproducible diffuse moderate injury [47]. Following a midline incision through the scalp, a steel disc (10 mm diameter, 3 mm thickness) is cemented to the animal's skull using a polyacrylamide adhesive [47]. The impactor tip uses the same steel disc as the one attached to the animal's head, so that there is no impact to the unprotected skull,

minimizing the risk of fractures [47]. Lastly, the animal's head is supported by a molded, gel-filled base, similar to the foam base in Marmarou's model [44, 47]. This base is used to decelerate the animal's head upon impact to prevent any injuries produced between the animal and the hard surface below. The impact is produced by an air-driven high-velocity impactor, similar to the pneumatic system used in CCI with a velocity of 3.25 m/s [40-42]. Additionally, the depth of impact was 18-mm for this moderate TBI, with a mortality rate of 26%. However, a range of depths from 16 mm to 20 mm was tested, with depths of 19 and 20 mm representing severe TBI at 56 and 90% mortality rates, respectively. This model showed increased edema and BBB permeability as early as 20 min following moderate injury. Additionally, measurements in arterial blood pressure increased immediately following injury and declined, reaching a minimum at 1 min post injury, which was shown previously in Marmarou's weight drop model [44]. Features of this diffuse model include no focal lesions or contusions, with presence of subarachnoid and intraventricular hemorrhages (Figure 1.8. C, black arrows) [47]. Overall, this model provides unique advantages for producing DAI with enhanced reproducibility and reduced mortality rate through the incorporation of an air-driven impactor capable of making precise, automated adjustments to parameters such as speed and depth.

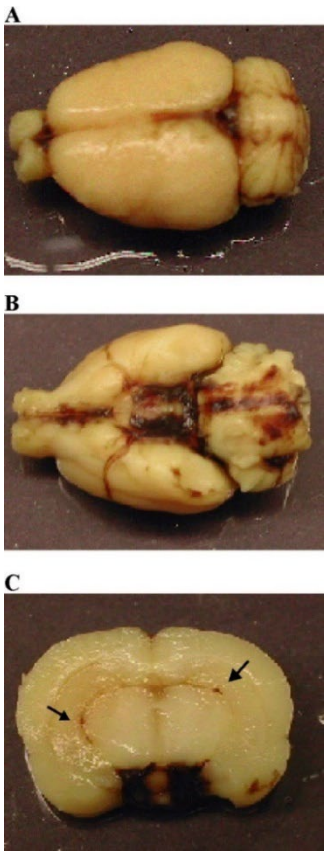

Figure 1.8. Brain from a moderate diffuse injury model 24 hr following impact. a) Superior surface, b) Inferior surface, c) Coronal view. Black arrows indicate presence of subarachnoid and intraventricular hemorrhages. Reproduced with permission from [47].

1.5 Molecular Pathophysiology and Therapeutic Intervention in TBI

Several safety precautions have been implemented to prevent head trauma including the provision and advancement of helmets, seatbelts, and airbags. However, the major problem facing TBI patients is the spread of secondary corrosive damage to surrounding brain tissue following primary impact. This lethal progression of secondary damage is caused by a variety of biochemical malfunctions including blood brain barrier (BBB) disruption, glutamate excitotoxicity, oxidative stress, and neuroinflammation (Figure 1.9.) [21]. The BBB is a tightly regulated network of semi-permeable vasculature designed to transport blood, ions, and molecules to the central nervous system, while preventing the import of harmful toxins and pathogens [48, 49]. Impact forces associated

with TBI generate excess mechanical stress, which compromises the structural integrity of the brain, resulting in a disruption of this vascularized system [49]. BBB breakdown results in hemorrhaging from damaged blood vessels and impedes the flow of blood and oxygen throughout the brain, corresponding to ischemia and hypoxia, respectively [6, 50]. Insufficient blood and oxygen intake halts neuronal ATP production, inhibiting the ATP-dependent Na+/K+ pump, required to maintain a sufficient electrochemical gradient [51-53]. These events lead to rapid neuronal depolarization lending to a corresponding influx of calcium ions [51]. Under physiological conditions, calcium influx triggers the synaptic release of a variety of neurotransmitters including glutamate [54]. Glutamate is an excitatory neurotransmitter necessary for adequate brain functioning and plays a primary role in learning and memory [54, 55]. Following TBI, excess influx of calcium into the neuron leads to an upregulated release of glutamate which overstimulates glutamate receptors, specifically NMDA, AMPA, and kainite receptors [56, 57]. Increased receptor activation contributes to an excess influx of calcium into the cell which increases mitochondrial dysfunction, drives the production of reactive oxygen species (ROS), and can eventually lead to apoptotic cell death [33, 56, 57]. Upregulated cellular ROS induces oxidative stress which forces a biochemical imbalance in the oxidant/antioxidant equilibrium of the brain [21]. Oxidative stress leads to the damage of lipids, proteins, and DNA in the brain and results in deterioration similar to the development of some neurodegenerative diseases [21, 58]. Cellular damage facilitates neuroinflammation, where neutrophils, lymphocytes, inflammatory cytokines, and microglia are recruited to the site of injury to alleviate further damage [59, 60]. However, this pro-inflammatory response persists and perpetuates an oversaturation of cytokines, specifically tumor

necrosis factor alpha (TNF-α), leading to cell death [59-61]. Overall, these pathophysiological consequences are primary factors influencing a cyclical cascade of damage inducing cell dysfunction, cell death, and eventually the neuropathological changes and behavioral deficits observed clinically. While these sequalae differ in their mechanisms of biological dysfunction, their molecular consequences play a primary role in the fate of the cell. Researchers have identified several forms and derivatives of cell death, including apoptosis, ferroptosis, oncosis, and necroptosis [62-65]. Each of these cellular processes is classified based on whether their induction is regulated or not. Recommendations from the Nomenclature Committee on Cell Death 2018 conclude that regulated cell death must be induced through an activation in signaling molecules[62]. These regulated mechanisms can be exploited, either through genetic or pharmacological intervention[62]. Thus, understanding how the progression of cell death differs following TBI provides valuable insight into potential therapeutic strategies.

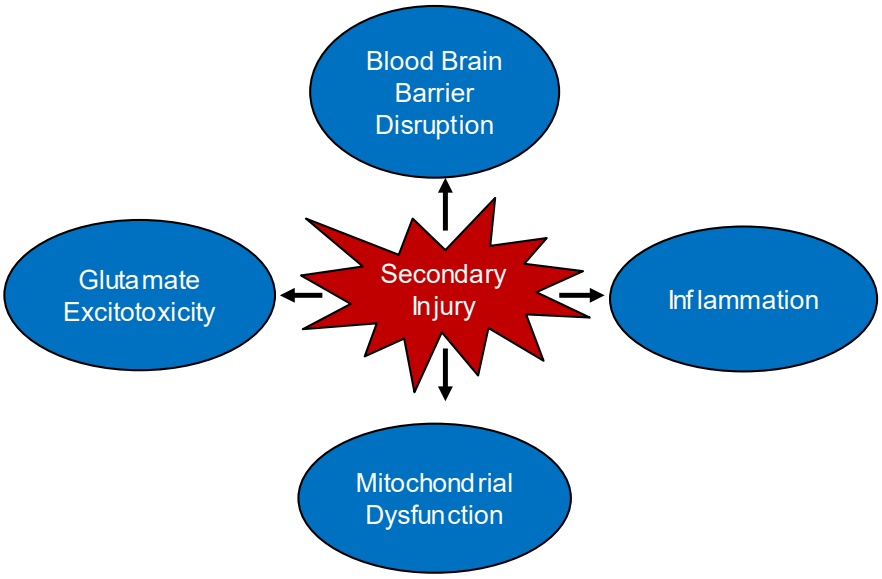

Figure 1.9. Secondary Consequences of TBI. Following TBI, the progression of secondary injury leads to a variety of pathophysiological consequences including blood brain barrier disruption, glutamate excitotoxicity, mitochondrial dysfunction, and inflammation. Figure adapted from [21].

1.5.1 Apoptosis, Necrosis, and Oncosis

Apoptosis is a form of caspase-mediated cell death induced by disruptions in the microenvironment, including oxidative stress and DNA damage[62, 63, 66]. Mechanistically, apoptosis is subdivided into two pathways: intrinsic or extrinsic (Figure 1.10.)[62, 67]. Intrinsic apoptosis results in the formation of pores along the surface of the outer membrane of the mitochondria, referred to as mitochondrial membrane permeabilization (MMP)[62, 68]. MMP is regulated by apoptotic proteins in the BCL2 family, including BCL2 and BAX, which establish roles as anti-apoptotic and pro-apoptotic proteins, respectively[63]. MMP results in the release of cytochrome c from the mitochondria. Cytochrome c binds and activates apoptotic protease activating factor 1 (APAF-1) resulting in the downstream activation of pro-caspase-9[62, 63, 69]. Pro-caspase 9 activation ultimately leads to the activation and cleavage of caspase-3 inducing the progression of apoptosis[62, 63].

In contrast, extrinsic apoptosis is regulated through receptors located on the surface of the plasma membrane[70]. This pathway relies on two distinct types of receptors including death receptors and dependence receptors[62, 70, 71]. Death receptors are dependent on ligand binding for activation, where in contrast, dependence receptors are activated when the amount of binding substrate falls below a physiological threshold[62]. Fas and tumor necrosis factor receptor 1 (TNFR1) are two types of death receptors, whose substrates include Fas ligand (FasL) and TNF-α, respectively[62, 67, 70, 72]. Upon ligand binding, death-inducing signaling complex (DISC) is assembled at the intracellular tail of the receptor leading to the downstream activation of pro-caspase-8[62, 73]. Pro-caspase 8 is cleaved upon activation leading to the activation and cleavage of

caspase-3, as discussed in intrinsic apoptosis[63]. Cells undergoing both intrinsic and extrinsic apoptosis maintain plasma membrane structural integrity and limited, but sufficient, metabolic activity[62]. Thus, apoptosis is dependent on adequate levels of ATP throughout the progression of cell death. This maintenance phase during apoptosis allows for rapid clearance of damaged cellular components through macrophages, reducing the likelihood of an inflammatory response[62, 74].

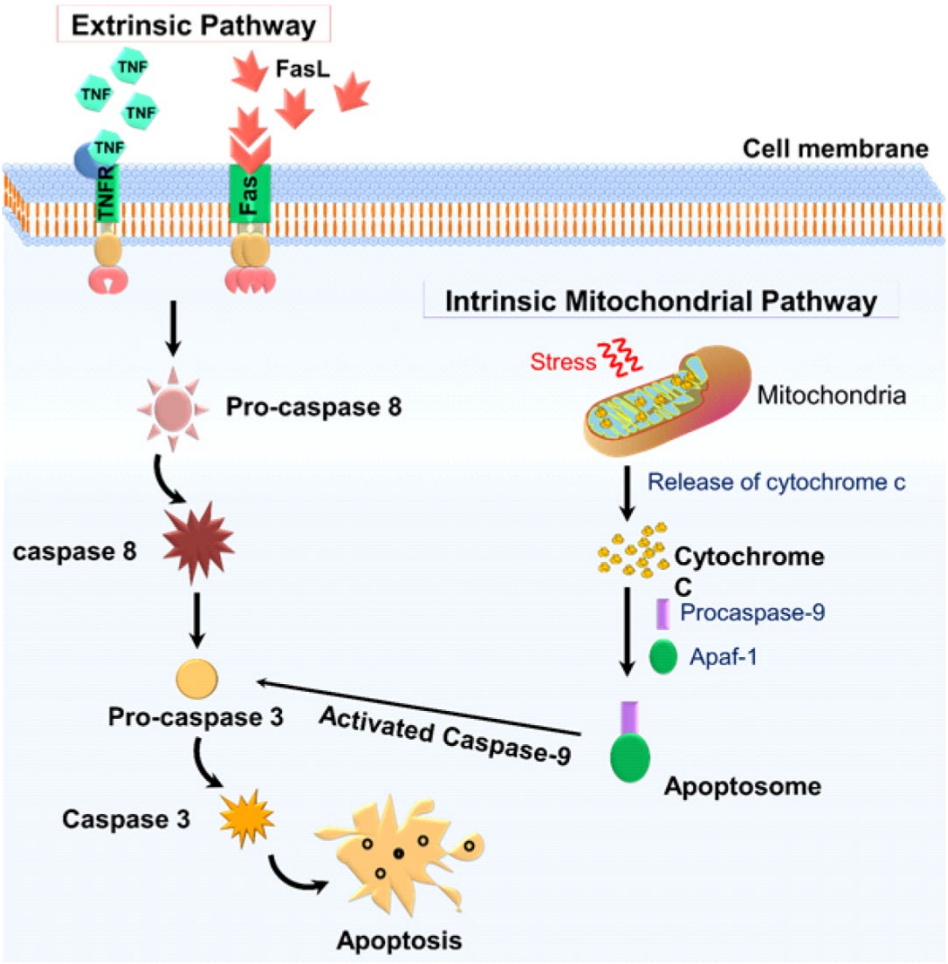

Figure 1.10. Mechanistic differences between intrinsic and extrinsic apoptosis. Apoptosis is subdivided into two pathways: intrinsic and extrinsic. Intrinsic apoptosis is initiated from mitochondrial stress leading to the release of cytochrome c and the downstream activation of pro-caspase-9. In contrast, extrinsic apoptosis is induced through from activation of death receptors located on the plasma membrane. Receptor activation leads to activation of pro-caspase-8. Ultimately, both mechanistic pathways lead to the activation and cleavage of pro-caspase-3 resulting in apoptosis. Reproduced with permission from [67].

Necrosis is a term used to describe the death of cells, or tissue, due to the extreme physiological conditions caused by disease or injury [75, 76]. Previously, necrosis was associated with the spontaneous, uncontrolled, pathological reaction of cell death, used to contrast the mechanisms of apoptosis [64, 75]. However, following the induction of damage, the cell undergoes three distinct phases including activation through signaling transduction (pre-lethal), destruction associated with cell death (breaking point), and cell lysis and degradation (post-mortem) [64]. Therefore, the term necrosis is more accurately used to describe the end stage changes associated with cell death, rather than the cellular and mechanistic changes inducing cell death. The cellular pathology opposite of apoptosis is oncosis [64].

Oncosis is a cellular pathology caused by extreme pathophysiological consequences including ischemia and hypoxia [64]. Both ischemia and hypoxia are highly relevant in the context of TBI, specifically severe, focal TBI [77, 78]. Oncosis is a regulated form of cell death induced through genetic, enzymatic, and environmental factors, similar to apoptosis [62, 63, 79]. For example, recent evidence suggests that oncosis can be triggered through increased mitochondrial permeability, resulting in a dramatic decrease in mitochondrial membrane potential and reduction in intracellular levels of ATP [62, 79]. However, oncosis differs primarily in three distinct aspects of cell death including ATP dependence, cellular pathology, and inflammatory response. Oncosis is initiated when external stimuli induce a disruption in the mechanisms involved in ATP synthesis, resulting in decreased levels of ATP and an increase in intracellular Na^+ and Cl^- [79, 80]. These increased intracellular ions lead to increased fluid uptake inside the cell [62, 64, 79, 80]. Extracellular fluid builds up in the cell resulting in cell

swelling, which is where the term “oncosis” originates, from the Latin translation for swelling [64]. Cellular swelling continues leading to a complete physical breakdown of the plasma membrane causing the release of damage-associated molecular patterns (DAMPs) and other inflammatory cytokines [79, 81]. Ultimately, this inflammatory response is a primary distinctions between the mechanisms of apoptosis and oncosis and is actively being investigated in the context of TBI severity and mechanism [77].

1.5.2 Role of Apoptosis and Oncosis in TBI

Due to the relationship between secondary injury and cell death, apoptosis and oncosis have been researched extensively in both clinical and pre-clinical TBI [77, 82-85]. Moderate to severe focal models, including CCI and fluid percussion injury, result in an acute development of oncotic cell death, accompanied by apoptosis [82-84]. Closed head mild TBI, including blast injuries, are typically absent of oncosis, but have been associated with apoptotic cell death in both the acute and subacute period following TBI [82, 85]. These observations have also been seen in clinical TBI studies [77]. Recent reports have shown levels of caspase-3 in cerebrospinal fluid are correlated with TBI severity [86]. Indeed, when coupled with intracranial pressure monitoring, apoptosis was found to be significantly correlated with GCS scores and may play a role as a biomarker for TBI prognosis [86]. Biomarkers of necrosis have also been correlated with clinical TBI severity, including, α-II spectrin breakdown products (SBDP’s) [77]. A-II spectrin is a molecular scaffold protein which is cleaved by both apoptotic, caspase-dependent, and oncotic, calpain-dependent, pathways [77, 87]. Researchers identified a significant correlation between oncotic SBDP’s, and GCS scores classified in the upper portion of

the severe category (3-5) [77]. Thus, investigating these mechanisms of cell death is critical for assessing potential therapeutic strategies of TBI.

1.5.3 Autophagy

While the mechanisms of apoptosis and necrosis differ, the stress response experienced by the cell will end in the same result: cell death. However, cells also possess specific machinery for overcoming these methods of cellular termination. In these scenarios, the stress response is assessed, and rather than complete destruction, the cell combats the stressor and adapts. This adaptive process experienced by the cell is known as autophagy, translated from Greek meaning "self-eating" [88]. Autophagy is the major metabolic pathway involving the assembly of aggregated proteins, and damaged organelles, into autophagosomes to be degraded by lysosomes and further recycled for the cell's usage [89]. This evolutionarily conserved biological process is key for repairing the body during periods of nutrient deprivation or during periods of stress [90, 91].

The mechanisms involved in the activation and continuation of autophagy are vastly complex, containing multiple feedback loops, activation/inhibitory checkpoints, and are still an active area of research and discovery. However, the generalized mechanism is rather straightforward. During periods of cellular stress or nutrient deprivation, metabolic processes involved in cell proliferation are stopped; namely lipid, protein and nucleotide synthesis, to conserve energy and available resources [89, 92, 93] (Figure 1.11.). This process begins with two primary upstream regulatory processes, including the inhibition of the master regulatory protein complex, mechanistic target of rapamycin (mTOR), as well as activation of AMP-activated protein kinase (AMPK) [92, 93]. Inhibiting mTOR allows for the translocation of transcription factor EB (TFEB) into

the nucleus, which acts as the master regulator in lysosomal biogenesis and autophagy [93, 94]. AMPK activates the unc-51 like autophagy activating kinase 1 (ULK1) complex, leading to the phosphorylation of Beclin1, a core subunit of the PI3K complex, which initiates the production of autophagosomes [92, 95, 96]. Autophagy related genes 3 & 7 (ATG3 and ATG7) are involved in the covalent linkage of phosphatidylethanolamine, converting LC3-I into LC3-II [97-99]. LC3-II, or Microtubule-associated protein 1A/1B light chain 3B, is involved in the formation of the autophagosome, specifically the elongation of the phagophore [97, 98]. During this process, ubiquitin-binding protein P62 (also referred to as sequestome-1, SQSTM1), selectively binds to autophagic substrates tagging them for autophagic accumulation [100]. The autophagosome continues to grow, and expands around the tagged targets, until advancing into a mature autophagosome. The final steps in autophagy involve autophagosomes fusing with lysosomes leading to degradation, where nutrients can be recycled for the specific needs of the cell [89].

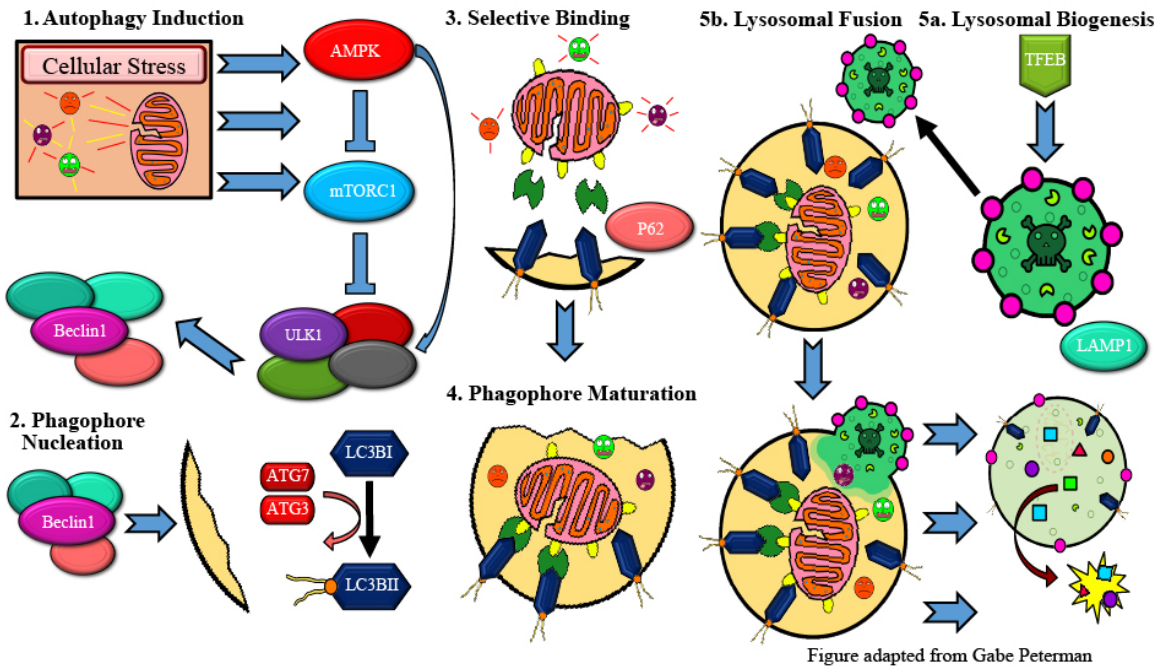

Figure 1.11. Brief overview into the mechanisms of autophagy. Autophagy is induced through cellular stress leading to the activation of AMPK. Downstream signaling leads to the activation of Beclin1 initiating phagophore formation. ATG3 and ATG7 convert LC3-I into LC3-II involved in the elongation of the phagophore. P62, selectively binds to autophagic substrates tagging them for autophagic accumulation. Following maturation, autophagosomes fuse with lysosomes to degrade these substrates where nutrients can be recycled for the specific needs of the cell.

1.5.4 Role of Autophagy in TBI

Due to the implications for autophagy as a potential therapeutic target, there has been a recent push to understand how autophagy is influenced following TBI [101, 102]. Autophagy activation was first reported following injury from a weight drop TBI model [101]. Western blot analysis concluded that Beclin1 was significantly upregulated in the ipsilateral hemisphere in the acute phase and remained elevated for three weeks following injury [103]. Beclin1 was localized with both neurons and astrocytes, confirmed with double immunofluorescence staining for NeuN and GFAP, respectively[103]. Additionally, autophagy activation has been reported clinically in children following severe TBI [104]. ELISA analysis confirmed a significant upregulation of both Beclin1

and P62 in cerebrospinal fluid [104]. These studies provide primary rationale for investigating the mechanisms of autophagy following TBI. However, there is still debate as to whether this biological process provides a positive or negative role following injury.

Rationale in support of autophagy as a protective role in TBI, originates from the mechanistic understanding of the cross talk between apoptosis and autophagy [105, 106]. Both autophagy and apoptosis are induced by external stressors to the cell [63, 89]. However, both biological processes have shown to exhibit a mutual inhibition on one another [107, 108]. Evidence has shown that upregulation of BCL-2 proteins inhibits the mechanisms involved in Beclin1 autophagy activation [107]. Additionally, autophagy is upregulated under physiological stress during nutrient deprivation and exercise, inhibiting apoptosis and increasing the likelihood of cell survival [109]. Thus, autophagy activation following TBI suggests a competitive inhibition of apoptosis to reduce cell death following injury. Additional support for the protective role of autophagy in TBI is based on evidence with the pharmaceutical, rapamycin [110] Rapamycin activates autophagy through inhibition of the mTOR signaling pathway and was shown to improve neurological severity scores as early as 48 hours following TBI, suggesting increased neurobehavioral functioning [110, 111].

In contrast, several studies have reported that autophagy plays a negative role following TBI [112, 113]. Treatment with the antioxidant, γ-Glutamyl cysteinyl ethyl ester, was shown to reduce levels of LC3BII following controlled cortical impact and improved performance in the Morris-water maze [112]. These results suggest that antioxidant administration following TBI inhibits the activation of autophagy leading to improved outcomes in behavioral assessments. Additionally, previous studies have

shown that the autophagy inhibitors, 3-methyladenine (3-MA) and bafilomycin (BFA) provide a therapeutic effect following impact [113]. Data concluded that these autophagy inhibitors improved scores in behavioral outcomes and reduced lesion volume [113].

However, recent literature suggests a unique explanation for the changes in autophagy following TBI, potentially providing rationale for the discrepancy between previous studies [114, 115]. Following controlled cortical impact, researchers identified a decrease in the activity of cathepsin D (CTSD), a lysosomal aspartyl protease, in the lysosomal fraction of tissue lysates, and a corresponding increase in CTSD levels in the cytosolic fraction [115]. Additionally, they observed a decrease in the colocalization of LC3BII puncta with CTSD, when compared to sham [115]. These results, coupled with significant increases in both LC3BII and SQSTM1, suggest autophagy may be dysfunctional, leading to an accumulation in autophagic substrates caused by lysosomal dysfunction [114, 115]. Indeed, further studies have shown that cytosolic phospholipase A2 Group IVA (PLA2G4A), involved in the hydrolysis of phospholipid membranes, is activated following TBI leading to a breakdown of the lysosomal membrane [114]. Additionally, these studies show that PLA2G4A inhibition attenuates autophagic dysfunction and improves behavioral outcomes [114]. Therefore, autophagy may be activated following TBI, but impaired due to lysosomal damage via lysosomal membrane permeabilization (LMP) (Figure 1.14) [116]. LMP is induced through a variety of mechanisms, including increased ROS production, resulting in the release of cathepsins and other hydrolases from inside the lysosome [116-118]. Ultimately, LMP inhibits lysosomal degradation and disrupting the mechanisms of autophagy [114-116]. Thus,

developing therapeutic strategies for mitigating the production of ROS, may mitigate LMP and lead to the physiological activation and continuation of autophagy.

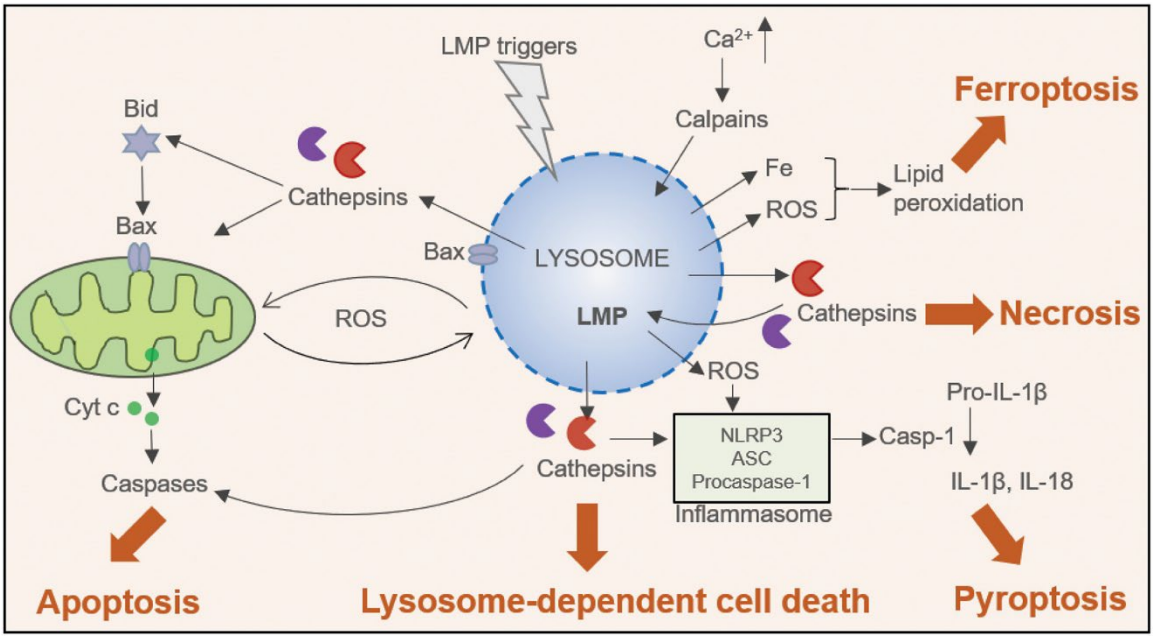

Figure 1.12. Lysosomal Membrane Permeabilization (LMP) is induced through the formation of pores in the lysosomal membrane leading the release of cathepsins and other hydrolases involved in lysosomal degradation. LMP contributes to multiple pathways involved in cell death including necrosis, apoptosis, and lysosome-dependent cell death. Reproduced with permission from [116].

CHAPTER 2: CHARACTERIZATION AND OPTIMIZATION OF A CLOSED HEAD INJURY MODEL FOR ASSESSING VARIABILITY IN TRAUMATIC BRAIN INJURY

2.0 Abstract

Animal models have been used extensively in neurotrauma research to simulate injuries observed amongst the patient population. Due to the prevalence of mild traumatic brain injury (TBI) clinically, researchers have emphasized the use of models which produce diffuse, mild impacts. However, there are still no clinically approved therapeutics for treating the secondary consequences associated with these injuries. Thus, developing animal models which can produce mild TBI with automated, reproducible, precision is imperative for understanding the pathophysiological consequences associated with mild injuries. Here, we optimized and characterized a closed-head, mild injury model using an electromagnetic controlled cortical impact (CCI) device. In our preliminary evaluation, we determined that the actual impact speed produced from our modified device was inconsistent with the input velocity parameter for our impact system. Indeed, both input depth and velocity, influenced our actual impact speed, and we found our maximum impact speed to be with an input velocity of 3.59 m/s and input depth of 7.08 mm. Therefore, researchers should be cautious when using electromagnetic CCI devices for replicating closed head mild TBI, to ensure results are interpreted based on the appropriate impact parameters. Additionally, following impact, we examined autophagic flux acutely following impact. Previous literature has shown that autophagic flux is impaired acutely following severe impacts to the central nervous system. Following DTBI, we observed autophagic dysfunction in the hippocampus at 1 day post

impact in each of the three DTBI conditions. Overall, these results suggest that even mild, diffuse TBI results in impaired cell turnover, thus may provide a therapeutic target in a range of injury severities.

Key Words: Mild TBI, Controlled Cortical Impact, Marmarou Weight Drop

2.1 Introduction

Animal models have been used extensively in traumatic brain injury (TBI) research to simulate clinical injuries and examine how primary impact influences the progression of secondary damage [1, 19, 20, 38]. Most TBI models contain scalable impact parameters, such as impact height, weight, velocity, and depth, capable of producing a spectrum of injury severities, ranging from mild to severe TBI. Due to the adjustable nature of these parameters, researchers have optimized impact models for producing the relevant pathophysiological changes observed clinically. However, secondary consequences following TBI are also influenced by the mechanism of injury including focal impacts, diffuse impacts, and even non-impact TBI [3, 38]. Diffuse impacts result from rapid acceleration and deceleration of the head driving compressive, tensile and shear forces throughout the brain [33, 119]. This array of independent directional forces is primarily due to the heterogeneous nature of tissue fixation and tissue consistency in the brain [33]. For example, following a road traffic collision, the brain continues accelerating in the direction of the applied force, where it meets against the inner wall of the skull. However, diffuse injuries are observed in many other situations, and are especially common amongst sports-related concussions. Currently, no therapeutic interventions have been successful in treating the secondary damage associated with diffuse impacts, owing to the current complications associated with injury

heterogeneity and inadequate drug delivery [2, 14, 16]. Previously, the Marmarou weight drop model was designed to simulate diffuse TBI for pre-clinical studies, and has been characterized and used extensively throughout the field [44-46]. Due to the success of Marmarou's model, his methods have been modified and adapted to improve upon his original experimental design. Indeed, several models have been developed with specific emphasis on improving injury reproducibility and efficiency [47, 120]. Additionally, current research has investigated these models for replicating pathophysiology associated with repeated mild TBI [120-122]. Injury reproducibility is a primary criterion associated with the controlled cortical impact (CCI) impactor device. CCI devices contain modifiable impact parameters designed to generate precise, automated impacts. Thus, this work aims to optimize and characterize a closed head injury model through modifications to an electromagnetic controlled cortical impact device and evaluate the changes in molecular pathophysiology associated with a range of impact parameters.

2.2 Materials and Methods

2.2.1 Antibodies

For Western Blot analysis, the following primary antibodies were used: β-Actin (Mouse, Cat. #A2228, Sigma-Aldrich, 1:2,000) LC3B (Rabbit, Cat. #ab192890, Abcam, 1:1,000), and SQSTM1 (Mouse, Cat. #ab56416, Abcam, 1:500). β-Actin was used as a loading control. Secondary antibodies for respective host species included Goat Anti-Rabbit (Cat. #1705046, Bio-Rad, 1:10,000) and Goat Anti-Mouse (Cat. #1705047, Bio-Rad, 1:10,000).

2.2.2 Modified Marmarou Weight Drop Model

All surgical procedures and experiments were performed in accordance with the Animal Care and Use Committee at the University of Nebraska Lincoln. All injuries were performed on 8-week old C57BL/6J mice (N=3) using an electromagnetic CCI device (PCI3000, Hatteras Instruments). Prior to impact, mice were anesthetized under 3.0% isoflurane in a plexiglass chamber, placed onto a bed platform and secured using a stereotaxic frame (David Kopf Instruments, Model 963). Isoflurane was held at 1.5% for the remainder of the procedure. Buprenorphine SR (0.5 mg/mL) was administered via dorsal subcutaneous injection to the skin flap of the mouse. Hair was removed from the scalp with Nair and a lidocaine/bupivacaine (20 mg/ml) solution was applied dropwise as a local anesthetic. Iodine was applied to the scalp, followed by a 1 cm incision through the midline to expose the skull. Following surgical preparation, a steel helmet comprised of stainless-steel (10 mm diameter x 3 mm thickness) was secured to the midline of the exposed skull using an adhesive glue. The impactor is also comprised of stainless steel and is the same size as the helmet to ensure the skull is completely protected from impact. For impact speed analysis without the use of animals, impacts were delivered using the electromagnetic CCI device with input velocities of 2, 3, and 4 m/s and depths at 3, 9 and 15 mm. For *in vivo* analysis, input velocity was fixed at 3.3 m/s with depths at 3, 9 and 15 mm. Impact dwell time remained constant at 80 ms. Additionally, the mouse was placed onto a 1-in foam pad, with head placed onto a smaller foam pad (~15 mm), to dissipate the acceleration from impact.

2.2.3 Phantom Miro 310 Videography and Impact Speed Calculations

The Phantom Miro 310 high speed camera was used to record videos of impacts from each experimental condition, without the use of animals, to be used for calculating the actual impact speed. Video parameters are included here: (Resolution: 256x128; Frame Rate: 2,000 fps; Exposure Time: 490 μs). Images were captured throughout the impact including: the starting position, where the impactor was at the highest point prior to impact, the ending position, where the impactor would contact the steel helmet, and 5 frames prior to reaching the end position. Positions at 5 frames prior to impact were used as an arbitrary metric to compare relative impact velocities between each of the experimental conditions. Impact heights were determined using a proportional relationship between the size of the red sticker, placed on the impactor, and the pixel size of the sticker (Equation 1). The actual impact speed was calculated by determining the change in position between the impact height at 5 frames prior to impact to the end position (Equation 2).

Equation 1: $\frac{D_R}{D_{PR}} = \frac{H_I}{H_{PI}}$

Equation 2: $\frac{H_I}{X} * FR = V$

Variables:

D_R: Diameter of Red Sticker (In.)

D_{PR}: Diameter of Red Sticker (Px.)

H_I: Height of Impactor (In.)

H_{PI}: Height of Impactor (Px.)

X: # of Frames until End Position

FR: Frame Rate (FPS)

V: Final Impact Speed (m/s)

2.2.4 Regression Model of Impact Speed

Impact speeds for each experimental condition were used for generating a regression model of impact speed using Statistical Analysis System (SAS). Briefly, SAS was used to generate an analysis of variance table for determining which factors provided

a significant effect on impact speed. Results were used to create an analysis of contrasts table. Analysis of contrasts was used to determine how each factor influenced the impact speed response, and whether those factors behaved linearly or quadratically. Significant contrasts were used to determine which parameter coefficients would be incorporated in our regression model. Relevant SAS Code used for our impact speed analysis is provided (Appendix A.)

2.2.5 Tissue Lysate Preparation

For *in vivo* analysis, mice from each group (N=3) were perfused with PBS at a fluid pressure of 80 mmHg. Perfusions were conducted at days 1, 3, and 7 post injury. Following perfusions, brains were harvested and separated into four regions: left cortex (LC), right cortex (RC), left hippocampus (IH) and contralateral hippocampus (CH) using methods described previously [123]. Samples were homogenized using bead disruption (TissueLyser II, Qiagen) in 300 µL of RIPA buffer (50 mM Tris HCl pH 8.0, 150 mM NaCl, 1% Triton X-100, 0.5% Na Deoxycholate, 0.1% SDS, 1 mM EOTA, 0.5 mM EGTA, 1 mM PMSF, 1 mM Na3VO4, 1 mM NaF). Brain samples were sonicated using a horn sonicator for 20s at 20% pulse frequency and then centrifuged in 4 ºC for 5 minutes at 17,740 rcf. Tissue supernatant was collected, and total protein content was measured using a bicinchoninic acid (BCA) assay. Aliquoted tissue lysates were loaded with B-Mercaptoethanol and 4x Laemlli Buffer (1:9 ratio), boiled at 95 °C for 5 minutes and stored at -20 °C.

2.2.6 Western Blot Analysis

Western blot analysis was used for assessing changes in protein biomarkers. Casted polyacrylamide gels (13%) were loaded with tissue lysates at 30 µg of total

protein content. Proteins were separated through gel electrophoresis at 120 V for approximately 60 minutes. Proteins were transferred onto PVDF membranes, using a wet transfer tank, overnight at 25 V. Membranes were washed with TBS (2 x 5 minutes) and incubated for 1 hour at room temperature in blocking buffer (5% Blot-Quick Blocker Reagent in TBST). Membranes were then incubated overnight in primary antibody solution and washed with TBST (3 x 5 minutes). After washing, membranes were incubated with secondary antibody for 1 hour and washed with TBST (3 x 10 minutes). ECL was then added dropwise and left to set for approximately 5 minutes prior to imaging. Imaged bands were quantified using the adjusted volume quantity from drawn regions of interest.

2.2.7 Statistical Analysis

All data are represented as mean ± standard deviation (SD) with N=3 for all groups. Statistical analysis was performed using GraphPad Prism (version 9.3.1) and all graphs were generated using this software. Prior to running comparative analysis, all data was first analyzed for normality using the Shapiro-Wilk Test, and all data collected passed this test. For examining comparisons of injury timeline to control, data was analyzed using Two-way ANOVA with Dunnett's multiple comparisons test for post hoc analysis (#: CTRL vs DTBI). For examining comparisons between injuries, data was analyzed using Two-Way ANOVA with Tukey's Honest Significantly Difference test for post hoc analysis (*: Differences between DTBI groups)

2.3 Results

2.3.1 Inconsistency between input parameters and output conditions

Impact parameters from our electromagnetic impact system, including depth and velocity, were adjusted to determine an optimal impact speed for reproducing diffuse, mild TBI. Upon preliminary investigation, we observed that the starting impact height for each condition was dependent on the parameter depth. These preliminary observations suggested that the actual impact speed from our modified Marmarou weight drop model was inconsistent with the parameter velocity. To assess these inconsistent results, we used a high-speed camera (Phantom Miro M310) to record videos from an experimental matrix of DTBI conditions, without the use of animals. Images were captured throughout the duration of impact and used to calculate the actual impact speed. Parameters for this experiment included input velocities at 2, 3, and 4 m/s with depths at 3, 9 and 15 mm. Videos were recorded, and captured images were used to determine how starting impact height and impact velocity differed for each of the 9 experimental conditions (Figure 2.1.). We observed that the actual impact speed was the greatest at an impact depth of 9 mm for each of the three input velocities (Figure 2.2.). In addition, the actual impact speed was lowest at an impact depth of 15 mm for each respective velocity, which did not coincide with our original hypothesis. Interestingly, we observed that the difference between impact speeds for 3 and 9 mm depths decreased as we increased our input velocity, such that actual speeds for these depths were the most similar at 4 m/s (Figure 2.3.). These results coincided with our previous findings, which suggested that both input depth and velocity influenced our actual impact speed. Additionally, impact speeds were fairly constant at 15 mm depths, regardless of input velocity. Overall, these results

suggest that both velocity and depth are important factors for influencing our impact speed response.

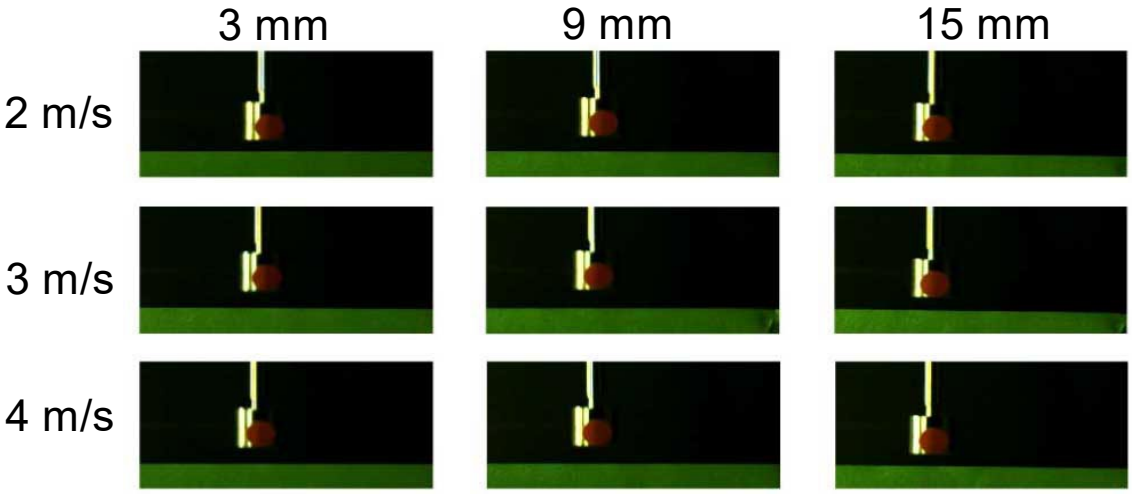

Figure 2.1. Images captured during impact for each experimental DTBI condition. Impact position was located at 5 frames prior to contact with the green tape for each experimental condition. Impact position was different for each DTBI impact, suggesting final impact speeds were different between groups.

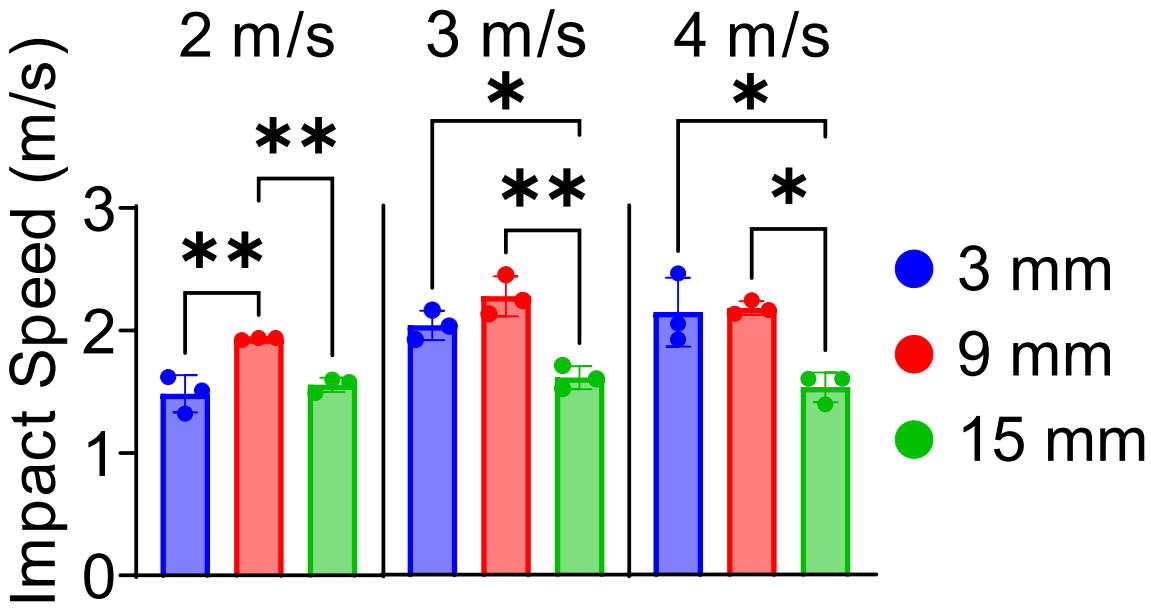

Figure 2.2. Calculated impact speeds for each experimental condition of the DTBI matrix. Impact speeds were the greatest at a depth of 9 mm, and lowest at 15 mm regardless of input velocity. Additionally, the difference between impact speeds for 3 and 9 mm depths decreased as we increased input velocity.

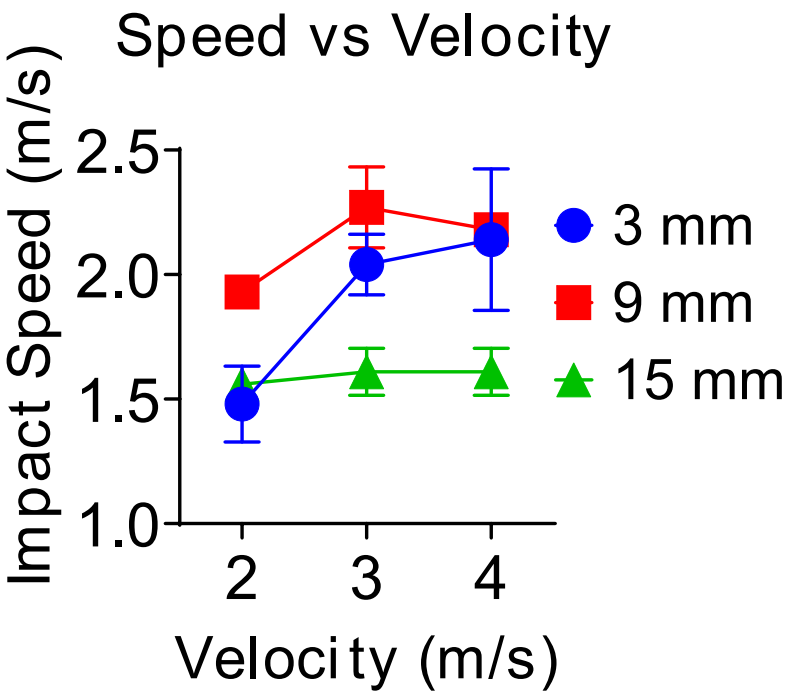

Figure 2.3. Calculated impact speed with respect to input velocity. We observed that the difference between impact speeds at 3 and 9 mm depths decreased as we increased our input velocity. Additionally, actual impact speeds were fairly constant at 15 mm depths. Overall, these results suggest a combinatorial effect from both input depth and velocity.

2.3.2 Impact speed highly influenced by impact depth

Our previous results for calculated impact speed suggested there was interaction between depth and velocity indicating each factor is dependent on the other, providing a combinatorial effect. Results from our analysis of variance (ANOVA) table conclude that the actual impact speed was significantly affected by both factors (depth and velocity), as well as the interaction effect between the two factors determined by the p-values highlighted inside the blue box (Table 2.1.). Due to the nature of our experimental conditions; equally spaced, quantitative factors (Velocity: 2.0, 3.0, 4.0 m/s and Depth: 3, 9 and 15 mm), we used analysis of contrasts to determine how each factor influences our actual impact speed response. Results from our analysis of contrasts table conclude that our impact speed response curve increases both linearly and quadratically with respect to

both factors, based on the p-values highlighted inside the blue box (Table 2.2.). Additionally, we identified a linear interaction between each factor, which suggests that actual impact speed increased linearly with respect to linear changes in depth. However, this information does not provide a complete picture for the accurate interpretation of our impact speed response curve. Therefore, using SAS, we identified the relevant parameter coefficients for fitting our regression model. Table 2.3. provides a list of coefficients used for fitting the appropriate regression model shown below in Equation 7. Ultimately, this regression model was used for accurately describing the effect of both factors on actual impact speed, and the parameters needed for achieving a maximum impact speed can be derived using multivariate implicit differentiation (Appendix B.) Previous impact calculations, along with the derived maximum impact speed of 2.32 m/s, were compared against actual impact speeds from our equation (Table 2.4.). However, the maximum impact speed can also be found using the response curve plot created from our fitted regression model (Figure 2.4.).

Table 2.1. Analysis of variance (ANOVA) table used to determine the significance of input factors. We determined that depth, velocity, and their interaction were each significant regarding their influence on impact speed response. Abbreviations: d (Depth), v(Velocity) d*v (Depth*Velocity interaction).

Type 3 Analysis of Variance								
Source	DF	Sum of Squares	Mean Square	Expected Mean Square	Error Term	Error DF	F Value	Pr > F
d	2	1.432563	0.716281	Var(Residual) + Q(d,d*v)	MS(Residual)	18	37.06	<.0001
v	2	0.556541	0.278270	Var(Residual) + Q(v,d*v)	MS(Residual)	18	14.40	0.0002
d*v	4	0.390726	0.097681	Var(Residual) + Q(d*v)	MS(Residual)	18	5.05	0.0066
Residual	18	0.347867	0.019326	Var(Residual)	.	.	.	.

Table 2.2. Analysis of contrasts table used to determine the shape of the response curve regarding actual impact speed. Impact speed behaved linearlly and quadratically with respect to both factors. Additionally, there was a linear interaction between both factors suggesting that impact speed increased linearly with respect to linear changes in depth.

Contrasts				
Label	Num DF	Den DF	F Value	Pr > F
D Lin	1	18	24.18	0.0001
D Quad	1	18	49.95	<.0001
V Lin	1	18	19.88	0.0003
V Quad	1	18	8.91	0.0079
D Lin * V Lin	1	18	18.30	0.0005
D Lin * V Quad	1	18	1.27	0.2746
D Quad * V Lin	1	18	0.28	0.6043
D Quad * V Quad	1	18	0.37	0.5501

Table 2.3. Coefficients for factors found to be significant from analysis of contrasts table. These coefficients were used for generating our fitted regression model shown below.

Parameter	Estimate	Standard Error	t Value	Pr > |t|
Intercept	-1.155925926	0.42109421	-2.75	0.0710
d	0.259537037	0.02813970	9.22	0.0027
v	1.420277778	0.27783155	5.11	0.0145
d*d	-0.011141975	0.00126097	-8.84	0.0031
v*v	-0.169444444	0.04539493	-3.73	0.0335
d*v	-0.028611111	0.00534984	-5.35	0.0128

Equation 7: Fitted regression model of impact speed response curve.

$$Y = -1.156 + 0.26d + 1.42v - 0.011d^2 - 0.169v^2 - 0.029dv$$

Table 2.4. Data table for comparing calculated impact speeds with actual impact speeds generated from fitted regression model. Input parameters for achieving a maximum impact speed are highlighted below in blue.

Depth (mm)	Input Velocity (m/s)	Calculated Impact Speed (m/s)	Actual Impact Speed (m/s)
3	2	1.48	1.52
9	2	1.93	1.94
15	2	1.56	1.56
3	3	2.04	2.00
9	3	2.27	2.25
15	3	1.61	1.70
3	4	2.14	2.15
9	4	2.18	2.23
15	4	1.53	1.51
7.08	3.59	N/A	2.32

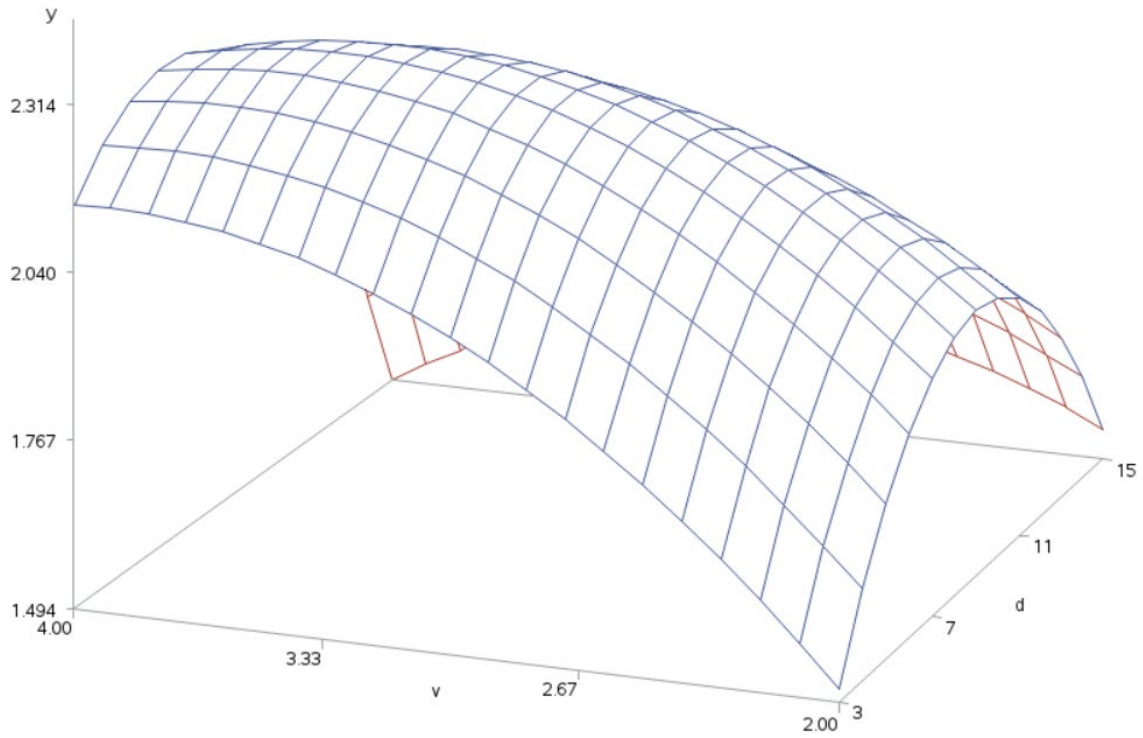

Figure 2.4. Surface response curve generated from our fitted regression model.

2.3.3 Effect of input parameters on molecular pathophysiology

Based on our previous analyses, we determined that the maximum impact speed was 2.32 m/s, with an input velocity and depth at 3.59 m/s and 7.08 mm, respectively. However, we were primarily interested in understanding how biomarkers changed over a range of impact depths. Indeed, for an impact depth of 9 mm, an input velocity of 3.3 m/s would achieve the highest actual impact speed at 2.28 m/s, comparable to our maximum impact speed (Table 2.5.). Thus, for *in vivo* impacts, we chose to examine each depth (3, 9, 15 mm) at an impact speed of 3.3 m/s (Figure 2.5.). For identifying changes in pathophysiology, we chose to investigate biomarkers associated with cell turnover, specifically autophagy. Autophagy is a metabolic pathway involved in the aggregation and degradation of damaged or dysfunctional organelles [89]. Previous literature has

demonstrated that following TBI autophagy is dysfunctional, suggesting impaired autophagic flux [114, 115]. Autophagic flux refers to the activity of autophagic degradation completed by lysosomes. Both autophagosomes and their substrates are degraded by lysosomes following a complete cycle of cellular turnover. Thus, corresponding increases in LC3BII, representing autophagosomes, and SQSTM1, representing autophagic substrates, suggest autophagic flux is disrupted leading to an accumulation of cellular components inside the lysosome. Impaired autophagic flux has been reported previously following severe injuries to the central nervous system and plays an active role in a variety of neurodegenerative processes [114, 115, 124, 125]. Thus, we sought to determine if autophagic flux was impaired following mild, diffuse TBI. Following injuries from each respective impact depth, we observed impaired autophagic flux in the hippocampus (HC) at 1 day post impact (Figures 2.6., 2.7., 2.8.). However, autophagy recovered at days 3 and 7, suggesting that diffuse, mild injuries result only in acute autophagic dysfunction. Additionally, we observed a peak in LC3BII only in the cortex at 3 days post injury following both the 3 mm and 15 mm impact depths. Interestingly, following the 9 mm impact depth, we observed a peak in SQSTM1 at 3 days post injury in the cortex, with no corresponding increase in LC3BII. Overall, these results suggest that diffuse mild impacts result in acute autophagic dysfunction in the hippocampus. However, there may be an impact threshold for observing autophagic dysfunction in the cortex, as we did see increases in SQSTM1 in the cortex, produced from the highest impact speed.

Table 2.5. Data table of calculated impact speeds used in our *in vivo* experiment. For an input velocity of 3.3 m/s, at an impact depth of 9 mm, we achieved our peak impact speed at 2.28 m/s.

Depth (mm)	Input Velocity (m/s)	Actual Impact Speed (m/s)
3	**3.3**	**2.08**
9	**3.3**	**2.28**
15	**3.3**	**1.68**

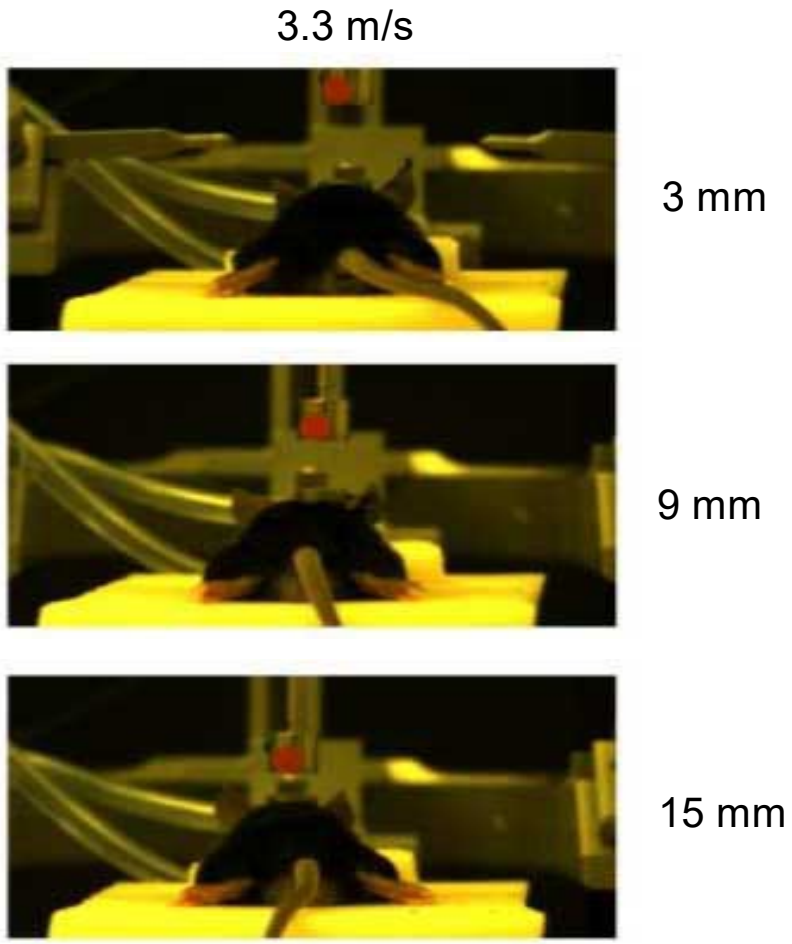

Figure 2.5. Images captured at the starting impact position for each of the three experimental DTBI conditions with an impact velocity of 3.3 m/s. Starting impact positions were different for each of the three conditions, coinciding with our previous findings.

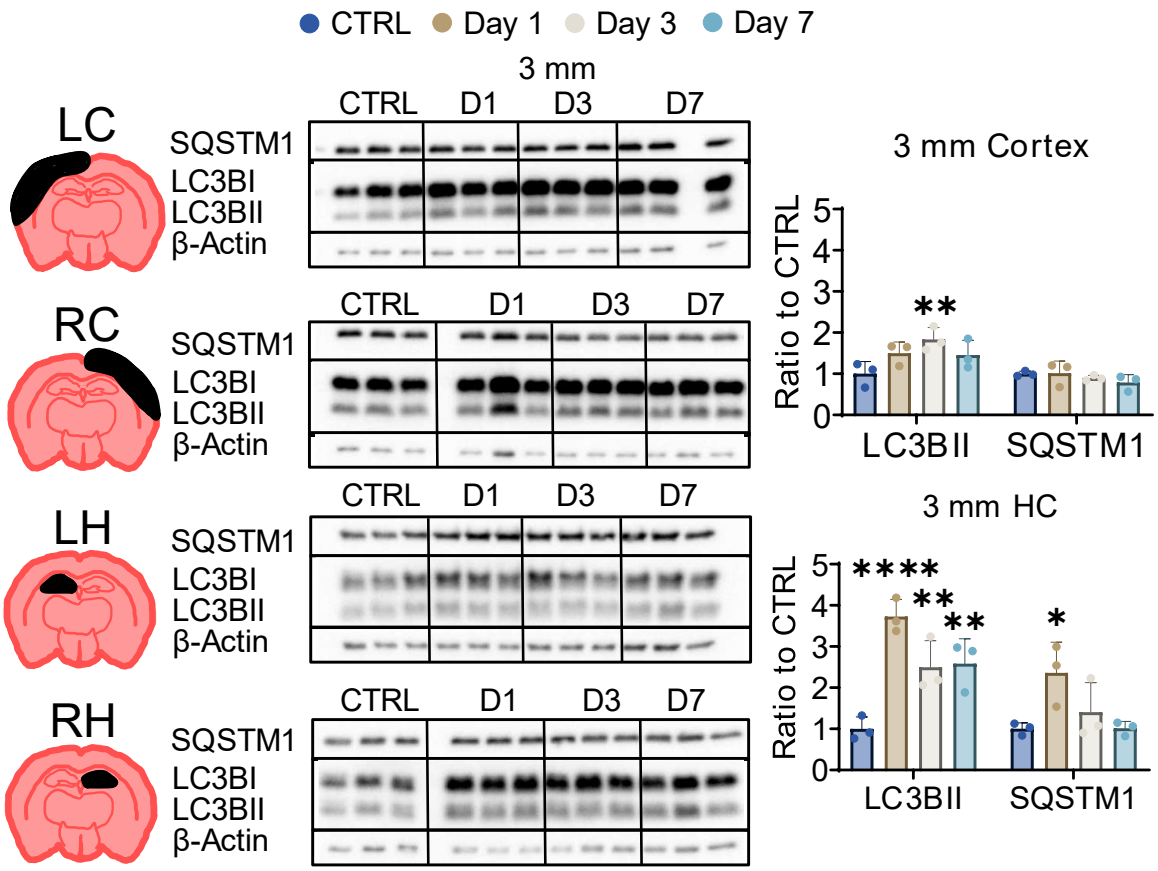

Figure 2.6. Western blot images and quantified data for autophagy biomarkers at 1, 3 and 7 days post DTBI at 3 mm impact depth. LC3BII peaked at 3 days post impact in the cortex, with no corresponding increase in SQSTM1. However, impaired autophagic flux was observed in the hippocampus at 1 day post impact.

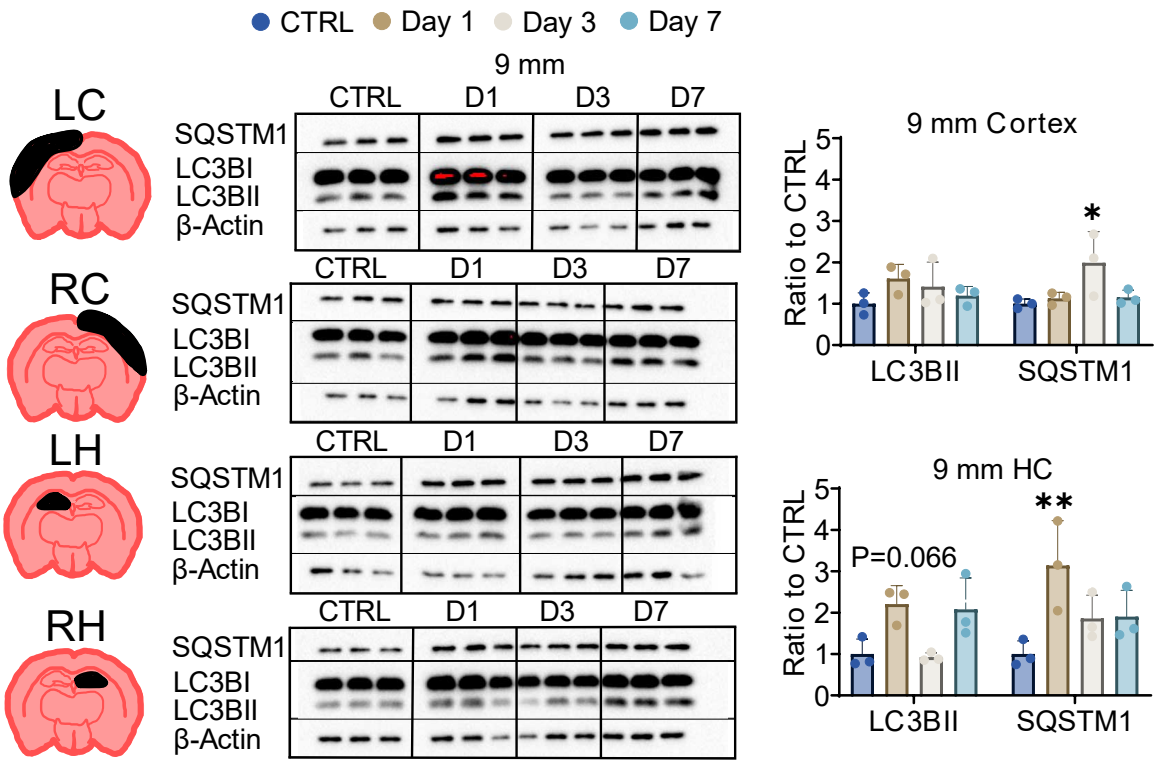

Figure 2.7. Western blot images and quantified data for autophagy biomarkers at 1, 3 and 7 days post DTBI at 9 mm impact depth. SQSTM1 peaked at 3 days post impact in the cortex, with no corresponding increase in LC3BII. However, impaired autophagic flux may be present in the hippocampus at 1 day post impact.

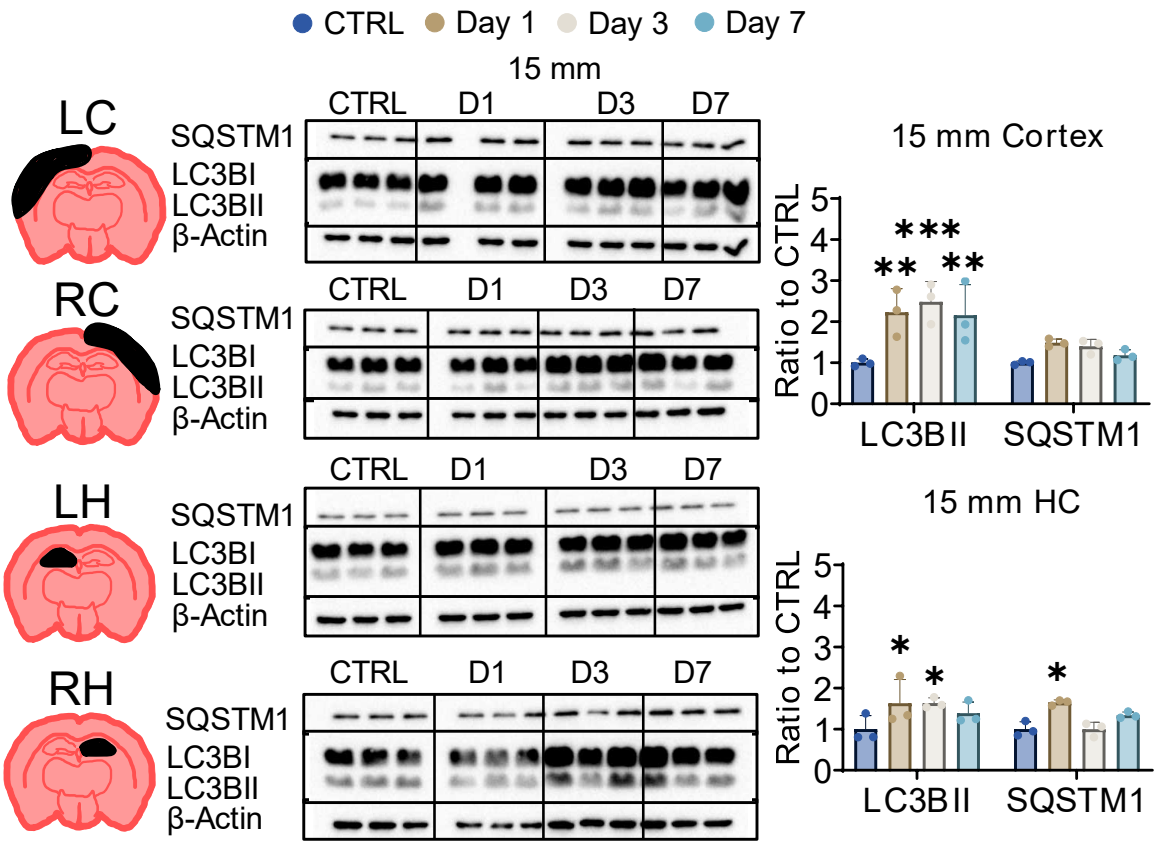

Figure 2.8. Western blot images and quantified data for autophagy biomarkers at 1, 3 and 7 days post DTBI at 9 mm impact depth. LC3BII peaked at 3 days post impact in the cortex, with no corresponding increase in SQSTM1. However, impaired autophagic flux was observed in the hippocampus at 1 day post impact.

2.4 Discussion & Limitations

Recent efforts in the field of neurotrauma have prioritized developing mild TBI models, due to the overwhelming abundance of mild injuries observed clinically. Current challenges facing clinical trials and pre-clinical translation are primarily due to an incomplete understanding of the pathophysiology associated with closed head, diffuse injuries. Thus, investigating mild, diffuse impact models is imperative for overcoming these current limitations. Through this work, we characterized and optimized a closed head, mild injury model (DTBI) using an electromagnetic CCI device. These impact devices are valuable for producing injuries, due to the precise, automated, reproducibility associated with the impactor. However, our results suggest that these impacts may not be

directly correlated with the set experimental parameters of our electromagnetic impact system. Results from videographic analysis using the Phantom Miro 310 concluded that actual impact speeds were highest with an impact depth of 9 mm, and we observed similar impact speeds at 15 mm impact depth regardless of impact velocity. Additionally, using our fitted regression model, we calculated a maximum impact speed of 2.32 m/s, with an input impact velocity of 3.59 m/s and depth at 7.08 mm. This maximum impact speed is far lower than the maximum input velocity of 4 m/s, ultimately leading to reduced impact forces and cognitive deficits. Overall, these results suggest that the actual impact speed for our DTBI model does not reflect the input parameter for impact velocity and is highly influenced by the impact depth. Therefore, we believe that it is imperative that researchers first characterize their closed head injury models when using the CCI system to ensure that data is interpreted based on the actual injury outcome, and not the input parameters. Additionally, we investigated how actual impact speed influenced the mechanisms of cell turnover, specifically autophagy. Previous literature has shown that autophagic flux is impaired following severe, focal CCI [114, 115]. However, these injuries are not representative of the patient population, and the mechanisms of autophagy may remain functional following closed head, mild impacts. Thus, we sought to determine if autophagic flux was impaired following mild, diffuse TBI using a range of impact depths, which corresponded with ranges in impact speed. Interestingly, following DTBI at each respective impact depth of 3, 9 and 15 mm, we observed impaired autophagic flux in the hippocampus (HC) at 1 day post impact. Autophagy recovered at days 3 and 7, suggesting that diffuse, mild injuries result only in acute autophagic dysfunction. However, this acute dysfunction resulted from a single impact,

suggesting that impaired autophagic flux may be exacerbated following repeated mild impacts. Additionally, we observed that autophagy remained functional in the cortex following both the 3 mm and 15 mm impact depths. Interestingly, following the 9 mm impact depth, we observed a peak in SQSTM1 at 3 days post injury in the cortex, with no corresponding increase in LC3BII. While these results do not confirm autophagic dysfunction in the cortex following DTBI, there may be an impact threshold for observing autophagic dysfunction in the cortex, as we did see increases in SQSTM1 in the cortex, produced from the highest actual impact speed. Overall, these results suggest that autophagy is dysfunctional following a range of closed head, diffuse impacts. Thus, impaired autophagic flux may play a role as a potential therapeutic target for treating the secondary consequences associated with the spectrum of injury severities and mechanisms observed clinically.

CHAPTER 3: EFFECT OF INJURY SEVERITY AND MECHANISM ON THE CROSSTALK BETWEEN THE MECHANISMS OF CELL DEATH AND SURVIVAL

3.0 Abstract

Traumatic brain injury (TBI) mechanism and severity are heterogenous clinically, resulting in a multitude of physical, cognitive, and behavioral deficits. However, approximately 80% suffer from milder injuries. Thus, examining pathophysiological changes associated with mild TBI is imperative for improving clinical translation and evaluating the efficacy of potential therapeutic strategies. Here, we employed derivations of the controlled cortical impact (CCI) model, including traditional, severe CCI (CCI, 4 m/s velocity, 2.5 mm depth), mild CCI with silicone tip (MTBI, 0.4 m/s velocity, 2 mm depth), and closed skull CCI with protective helmet (DTBI, 3.3 m/s velocity, 9 mm depth). Injuries were performed on 8-week old male C57BL/6J mice (N=3), and perfused at 1, 3, and 7 days post-injury. Western blot results of α-II spectrin breakdown products (SBDP's) confirmed a peak in oncotic cell death at 3 days post CCI in all regions, and both mild models were absent of oncosis. However, SBDP's for total cell death and apoptosis did differ between mild models, suggesting that impact mechanism alone is enough to influence molecular pathophysiology. These differences in apoptosis were also observed by measuring changes in the pro-apoptotic protein, BAX. Additionally, Western blot results for autophagic markers, LC3BII and SQSTM1, indicated autophagic flux was impaired in the LH following impacts from each TBI model. Preliminary results confirmed autophagic dysfunction in the left cortex by evaluating LC3BII localization through confocal microscopy at 3 days post injury, which corresponded with peaks in

oncotic cell death. Thus, mechanisms of cell death and turnover are highly variable depending on mechanism and severity of TBI, and autophagic dysfunction may play a critical role in the progression of secondary injury following impact.

Key Words: Concussion/mTBI, Secondary Injury, Cell Death, Autophagy

3.1 Introduction

Traumatic brain injury (TBI) is currently the leading cause of injury related morbidity and mortality worldwide, with an estimated global cost of $400 billion annually [2]. Injury mechanism and severity present heterogeneously in the patient population resulting in a multitude of physical, cognitive, and behavioral deficits. Based on the Glasgow Coma Scale, an assessment used for classifying TBI clinically, injury severity can be categorized into three distinct groups: mild, moderate, and severe [22, 23]. Epidemiological reports from the CDC conclude that mild TBI represents approximately 80% of the patient population, while moderate and severe injuries represent approximately 10%, respectively [27]. Additionally, injury severity can be sub-categorized based on the mechanism of impact including focal, diffuse, and non-impact TBI [32, 36, 37]. Following impact, a progression of secondary damage results in a cascade of pathophysiological events including blood brain barrier disruption, glutamate excitotoxicity, and oxidative stress [21]. These injury sequalae evolve over time resulting in corresponding changes in biomarkers, imaging characteristics, and behavioral outcomes. Overall, this heterogeneity amongst the clinical population, with respect to both injury and outcome, is one of the primary contributors to problems currently facing clinical trials and preclinical translation [9, 11, 14, 15]. Indeed, this hallmark of variability has critically impacted the lack of success experienced in phase III clinical trials for TBI,

and yet, researchers are still faced with an incomplete understanding of pathophysiology regarding injury heterogeneity [12]. Thus, there is a critical need to identify these changes in molecular pathophysiology, to improve upon our understanding of how injury variability influences the progression of secondary damage following TBI. Previous research has employed the use of animal models designed to mimic the biochemical and neuropathological changes experienced following TBI [1, 19, 20]. However, investigating changes associated with individual models limits the scope of discovery regarding injury heterogeneity. In addition, several previously developed models have the propensity to produce moderate to severe, focal injuries, which are currently underrepresented in the clinical population [39, 126, 127]. While these pre-clinical injuries are valuable for testing the efficacy of theranostic tools, these interventions must be evaluated amongst of a spectrum of injuries to ensure adequate targeting and efficacious drug delivery. Additionally, these assessments could provide insight for understanding how molecular pathophysiological mechanisms are influenced following injury. Previous studies in both pre-clinical and clinical TBI have already identified several differences regarding mechanisms of cell death and cell turnover in response to injury severity [77, 83, 104, 115]. Results from these studies indicate a shift in oncosis following severe TBI and these changes may influence the functionality of autophagic turnover. Thus, this work aims to determine how cell death and autophagic turnover are influenced based on TBI injury severity and mechanism.

3.2 Materials and Methods

3.2.1 Antibodies

For Western Blot analysis, the following primary antibodies were used: β-Actin (Mouse, Cat. #A2228, Sigma-Aldrich, 1:2,000), α-II Spectrin (Mouse, Cat. #MAB1622, Sigma-Aldrich, 1:1,000), BAX (Rabbit, Cat. #2772, Cell Signal.), LC3B (Rabbit, Cat. #ab192890, Abcam, 1:1,000), and SQSTM1 (Mouse, Cat. #ab56416, Abcam, 1:500). β-Actin was used as a loading control. Secondary antibodies for respective host species included Goat Anti-Rabbit (Cat. #1705046, Bio-Rad, 1:10,000) and Goat Anti-Mouse (Cat. # 1705047, Bio-Rad, 1:10,000). Immunostaining for confocal microscopy was done with the following primary antibodies: LC3B (Rabbit, Cat. #ab192890, Abcam, 1:250) and LAMP1 (Rat, Cat. #ab25245, Abcam, 1:250). Secondary antibodies for respective host species included Donkey Anti-Rabbit (Cat. #ab150063, Abcam, 1:250) and Goat Anti-Rat (Cat. #ab150158, Abcam, 1:250).

3.2.2 Controlled Cortical Impact Model

All surgical procedures and experiments were performed in accordance with the Animal Care and Use Committee at the University of Nebraska Lincoln. All injuries were performed on 8-week old C57BL/6J mice (N=3) using an electromagnetic controlled cortical impact (CCI) device (PCI3000, Hatteras Instruments). Prior to impact, mice were anesthetized under 3.0% isoflurane in a plexiglass chamber, placed onto a bed platform and secured using a stereotaxic frame (David Kopf Instruments, Model 963). Isoflurane was held at 1.5% for the remainder of the procedure. Buprenorphine SR (0.5 mg/mL) was administered via dorsal subcutaneous injection to the skin flap of the mouse. Hair was removed from the scalp with Nair and a lidocaine/bupivacaine (20 mg/ml) solution was

applied dropwise as a local anesthetic. Iodine was applied to the scalp, followed by a 1 cm incision through the midline to expose the skull. Following surgical preparation, craniectomy was performed using a 2.5 mm trephine drill tip to remove a cranial flap, located at 2 mm posterior of bregma and 2 mm left of the midline. Following bone flap removal, injury was induced using the CCI device with a stainless steel impactor (2.0 mm diameter). Velocity, depth, and dwell time are input at 4 m/s, 2.5 mm depth, and 80 ms, respectively.

3.2.3 Modified Mild TBI Models

Modified mild TBI models were established based on methodology from previously developed protocols [43, 47]. In the MTBI model, the size of craniectomy was increased to 5 mm and a silicone tip (4 mm diameter) was used for the impact, fabricated from a Sylgard^{TM} 184 Silicone Elastomer Kit. Silicone elastomer solution was prepared with a 10:1 ratio of silicone to catalyst, syringed directly inside a custom-made Teflon mold before being placed inside an oven at 150 ºC for 1.5 Hours. The impact velocity was lowered to 0.4 m/s, with a depth of 2 mm and dwell time of 80 ms. For the DTBI model, the impactor tip was comprised of a stainless-steel disc (10 mm diameter x 3 mm thickness). There was no craniectomy as the mouse's skull was protected by a steel helmet of the same size as the impactor and secured to the midline of the exposed skull using an adhesive glue. Additionally, the mouse was placed onto a 1-in foam pad, with head placed onto a smaller foam pad (~15 mm), to dissipate the acceleration from impact.

3.2.4 Tissue Lysate Preparation

Mice from each group (N=3) were perfused with PBS with a pressure of 80 mmHg at 1, 3, and 7 days post injury. Brains were then harvested and separated into four

regions: left cortex (LC), right cortex (RC), left hippocampus (IH) and contralateral hippocampus (CH) using methods described previously [123]. Samples were homogenized using bead disruption with the TissueLyser II (Qiagen) in 300 µL of RIPA buffer (50 mM Tris HCl pH 8.0, 150 mM NaCl, 1% Triton X-100, 0.5% Na Deoxycholate, 0.1% SDS, 1 mM EOTA, 0.5 mM EGTA, 1 mM PMSF, 1 mM Na3VO4, 1 mM NaF). Samples were then sonicated using a horn sonicator for 20s at 20% pulse frequency and centrifuged in 4 ºC for 5 minutes at 17,740 rcf. Supernatants were collected and total protein content was measured using a bicinchoninic acid (BCA) Assay. Aliquoted tissue lysates were then loaded with B-Mercaptoethanol and 4x Laemlli Buffer (1:9 ratio), boiled at 95 °C for 5 minutes and stored at -20 °C.

3.2.5 Western Blot Analysis

For assessing SBDP's, polyacrylamide gels were casted at a thickness of 1 mm using two different percentages including: 1 mL of 12% on bottom, immediately followed by approximately 4 mL at 5%. Tissue lysates were loaded with a total volume of 5 µL in each well at a protein concentration of 1 µg/µl. For assessing all other markers, polyacrylamide gels were casted with a gel percentage at 13% and tissue lysates were loaded at 30 µg of total protein content. Proteins were separated through gel electrophoresis at 120 V for approximately 80 minutes. For all casted gels, proteins were transferred onto PVDF membranes, using a wet transfer tank overnight, at 25 V. Membranes were washed twice with TBS for 5 minutes and incubated for 1 hour at room temperature in blocking buffer (5% Blot-Quick Blocker Reagent in TBST). Membranes were then incubated overnight in primary antibody solution and washed three times with TBST for 5 min. Following washing, membranes were incubated with secondary

antibody for 1 hour and washed three times with TBST for 10 minutes. ECL was then added dropwise and left to set for approximately 5 minutes prior to imaging. Imaged bands were quantified using the adjusted volume quantity from drawn regions of interest.

3.2.6 Cryosection Preparation

Mice from each group (N=3) were perfused with 4% PFA at 3 days post injury, and brains were harvested and stored in 4% PFA for 24 hours. Fixed brains were rinsed and then washed with PBS twice for 5 minutes. After washing, brains were submerged in 30% sucrose and left to sink for 72 hours. Brains were then sliced through the coronal plane at approximately 2 mm below bregma, or the location of lesion from impact. Brains were then placed inside plastic molds, submerged in OCT and frozen over a methanol-dry ice slurry. Following the embedding procedure, brains were sliced coronally into 15 um thick sections and placed onto microscope slides. Slides were frozen at -80 °C prior to immunostaining.

3.2.7 Immunostaining

Slides were rinsed thrice with PBS and incubated with blocking buffer (PBS, 3% Donkey Serum, 0.3% Triton X-100, 0.1% Sodium Azide) for 1 hour at room temperature. Primary antibody dilutions were prepared, added dropwise, and slides are incubated for 24 hours at 4 °C. Slides were washed thrice for 5 minutes in blocking buffer, prior to the dropwise addition of secondary antibody. Slides were then covered to be protected from light and left to sit at room temperature for 1.5 hours. Following secondary antibody incubation, slides were washed thrice with blocking buffer and rinsed once with PBS. DAPI solution was applied and left to sit for 5 minutes, before washing twice with PBS and once with DDI water. Prolong Gold was applied dropwise over the center of each

coronal section and cover slips were applied. Slides were stored at -80 °C until imaged through confocal microscopy. Parameters used during confocal microscopy for 40x co-localization images for each respective antibody are provided here: LC3B (1.8%, 800 V) and LAMP1 (1.0% 680V)

3.2.8 Statistical Analysis

All data are represented as mean ± standard deviation (SD) with N=3 for all groups. Statistical analysis was performed using GraphPad Prism (version 9.3.1) and all graphs were generated using this software. Prior to running comparative analysis, all data was first analyzed for normality using the Shapiro-Wilk Test, and all data collected passed this test. For examining comparisons of injury timeline to control, data was analyzed using Two-way ANOVA with Dunnett's multiple comparisons test for post hoc analysis (#: CTRL vs Injury). For examining comparisons between injuries, data was analyzed using Two-Way ANOVA with Tukey's Honest Significantly Difference test for post hoc analysis (&: CTRL vs Mild and #: MTBI vs DTBI).

3.3 Results

3.3.1 Gross Neuropathology

Gross pathological changes following TBI are a direct consequence of both the mechanism and severity of primary impact. As such, examining differences in brain pathology is imperative for establishing spectrums of injury amongst various types of animal models. Additionally, these observations are useful for making comparisons to the neuroanatomical changes observed in a clinical setting through imaging techniques, including magnetic resonance imaging (MRI) and computed tomography imaging (CT). Following perfusions, brains were imaged at 1, 3, and 7 days post injury to observe

changes in gross pathology. These images were also used to evaluate the reproducibility between impacts and compare brain lesions, or lack thereof, against previously developed protocols. Impacts from the CCI model produced cortical lesions in the ipsilateral region observed at each time point following impact (Figure 3.1.). Visible hemorrhaging surrounding lesions was observed at 1 and 3 days post injury. Brain images following MTBI presented with similar results, however, lesion size and depth was reduced when compared with CCI at each time point. In contrast, no lesions were present in either hemisphere following DTBI. However, slight hemorrhaging was observed throughout the midline at 1 and 3 days post injury, and at the tentorium cerebelli, the space dividing the cerebrum and cerebellum at 3 days time point. These results provide gross pathological evidence for producing a spectrum of TBI variability with different injury mechanisms and severities, through modifications from one impactor device.

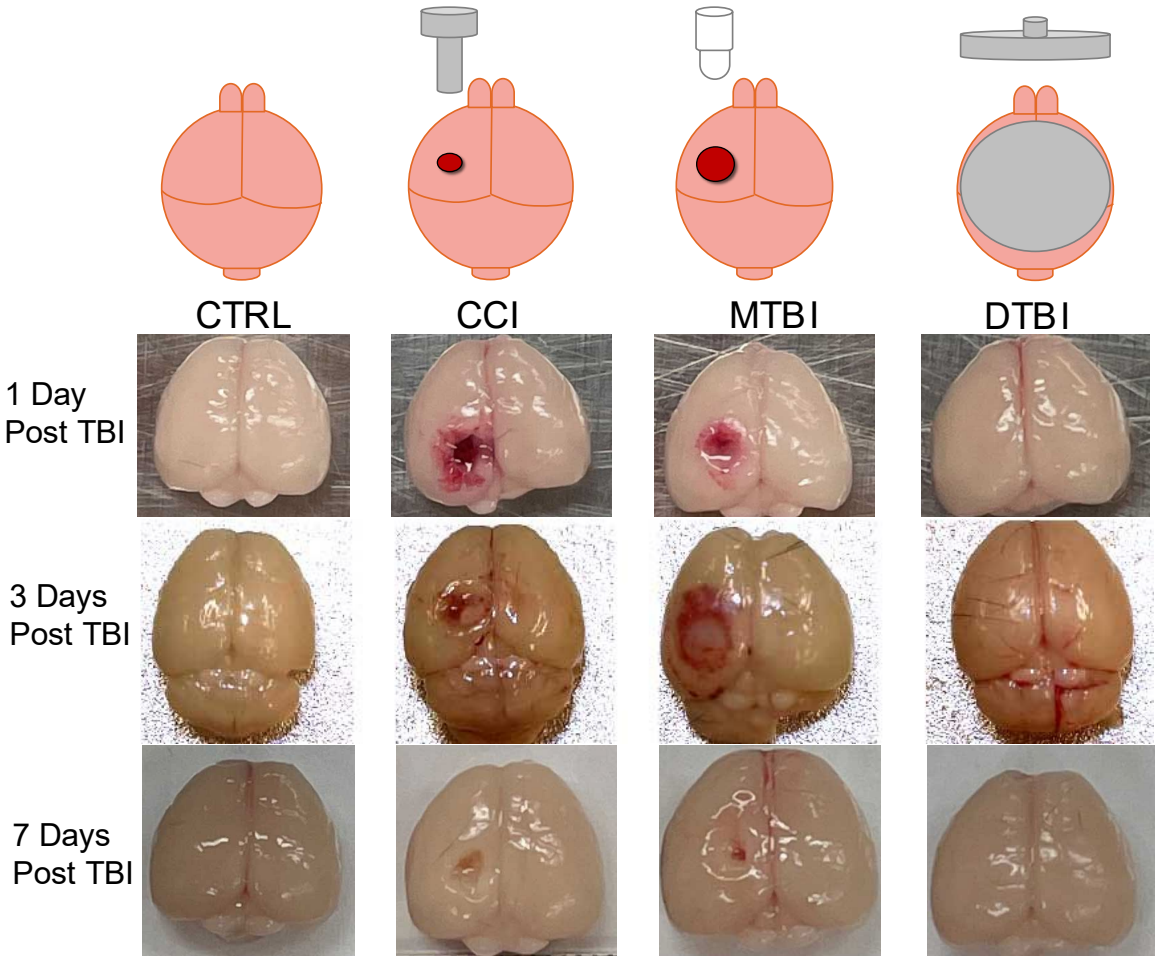

Figure 3.1. Schematic of experimental conditions and representative brain images collected from each of the impact models at 1, 3 and 7 days post injury. Cortical lesions were present at each time point following CCI impact. mTBI impacts produced similar focal lesions and hemorrhaging but was less pronounced at 7 days post injury. Impacts following dTBI impacts did not produce cortical lesions, and hemorrhaging was only observed in the midline at days 1 and 3 post injury. CTRL: Control; CCI: traditional controlled cortical impact; mTBI: mild impact with modified silicone tip; dTBI: diffuse impact with protective helmet.

3.3.2 Injury severity and the mechanisms of cell death

Gross pathological differences suggest distinct shifts in molecular pathophysiology, specifically regarding the spectrum of cell death. Thus, we investigated changes in the mechanisms of cell death, including apoptosis and necrotic oncosis (hereby referred to as oncosis), in the acute/subacute period following impact. Western

blot analysis was used to observe changes in protein expression from α-II-spectrin breakdown products (SBDPs). α-II-spectrin is a molecular scaffold protein involved in the linkage between the plasma membrane and the cell's cytoskeleton [77]. Following damage to the cell, the protein is cleaved through two independent pathways including calpain-mediated cleavage and caspase-mediated cleavage indicating changes in oncosis and apoptosis, respectively. SBDPs correlate to total cell death (150 kDa), oncosis (145 kDa), and apoptosis (120 kDa) and were normalized to control.

Following severe CCI, we observed a significant increase in oncotic cell death, which is consistent with previous pre-clinical CCI studies and clinical assessment of severe TBI [77, 128]. Oncosis peaked at 3 days post injury and was present in each of the four brain regions following impact (Figure 3.2.). In contrast, neither mild TBI model presented with changes in oncotic cell death. Indeed, even with observable changes in gross neuropathology, no significant changes in oncosis or apoptosis were observed following MTBI. (Figure 3.3.). These results indicate a dramatic reduction in injury severity, due to the softer tip and reduced depth, decreasing the molecular pathophysiological consequences following TBI. However, following DTBI, apoptosis was significantly increased in the cortex at each time point, and peaked at 3 days (Figure 3.4.). Additionally, total cell death peaked at 3 days in both the cortex and hippocampus, coinciding with changes in apoptosis. Overall, these results suggest a shift in pathophysiology due to the mechanism and severity of injury (Figure 3.5.).

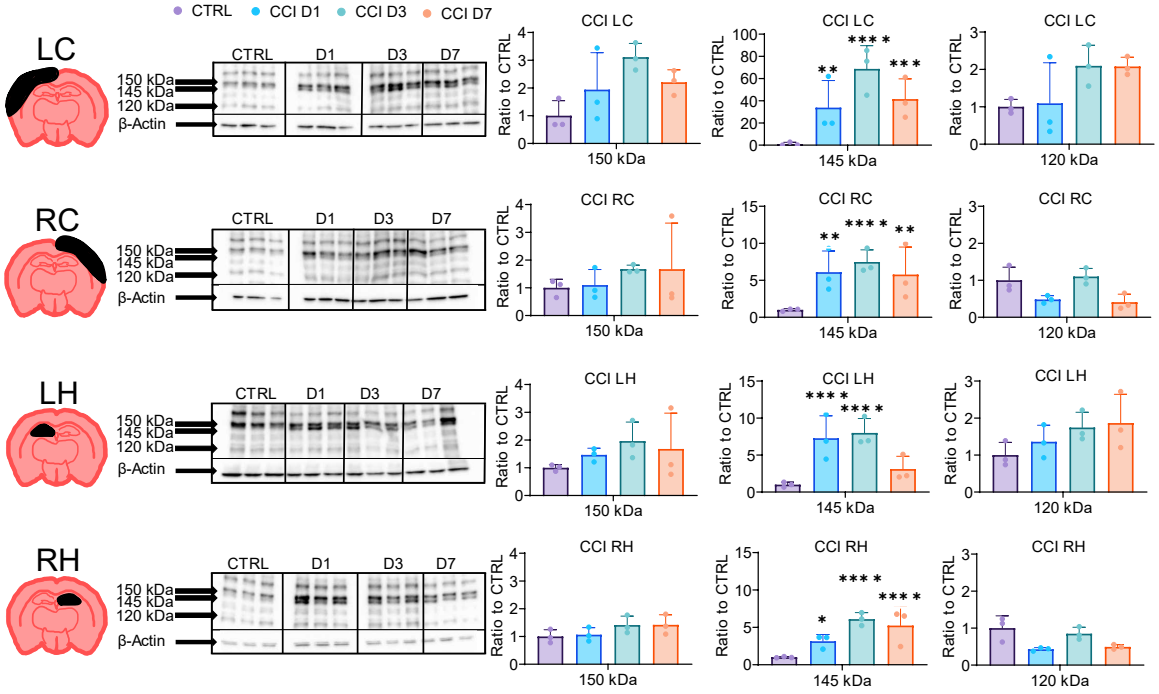

Figure 3.2. Western blot images and quantified data for SBDPs at 1, 3 and 7 days post CCI. Oncosis was present at each time point following impact and peaked at 3 days post injury in all four brain regions. No significant results were detected for total cell death or apoptosis.

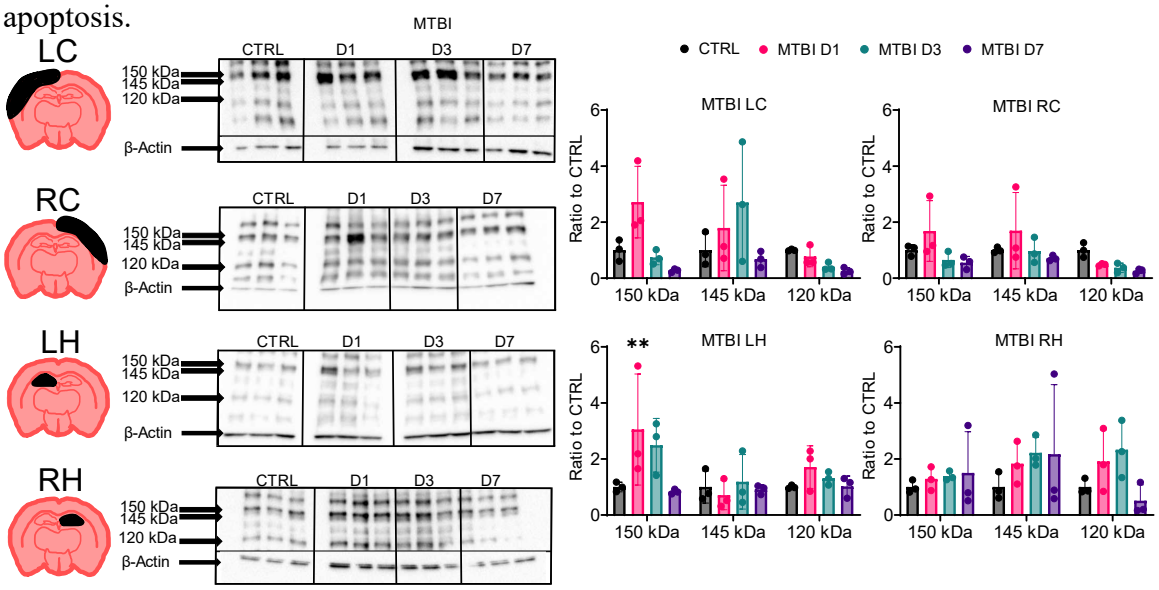

Figure 3.3. Western blot images and quantified data for SBDPs at 1, 3 and 7 days post MTBI. No significant changes were observed in oncosis or apoptosis, and total cell death peaked at 1 day in the left hemisphere (LH).

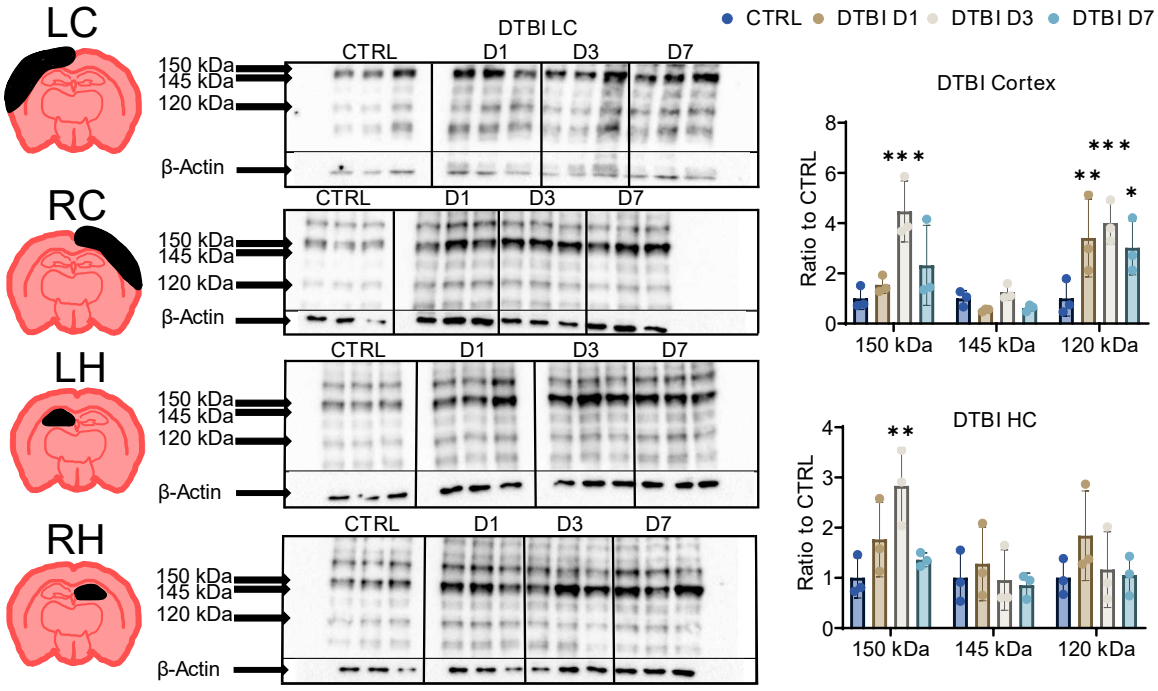

Figure 3.4. Western blot images and quantified data for SBDPs at 1, 3 and 7 days post DTBI. Apoptosis was present at each time point following impact in the cortex and peaked at 3 days post injury. Additionally, we observed corresponding peaks in total cell death in both the cortex and hippocampus. DTBI data was averaged between left and right hemispheres for the cortex and hippocampus (HC).

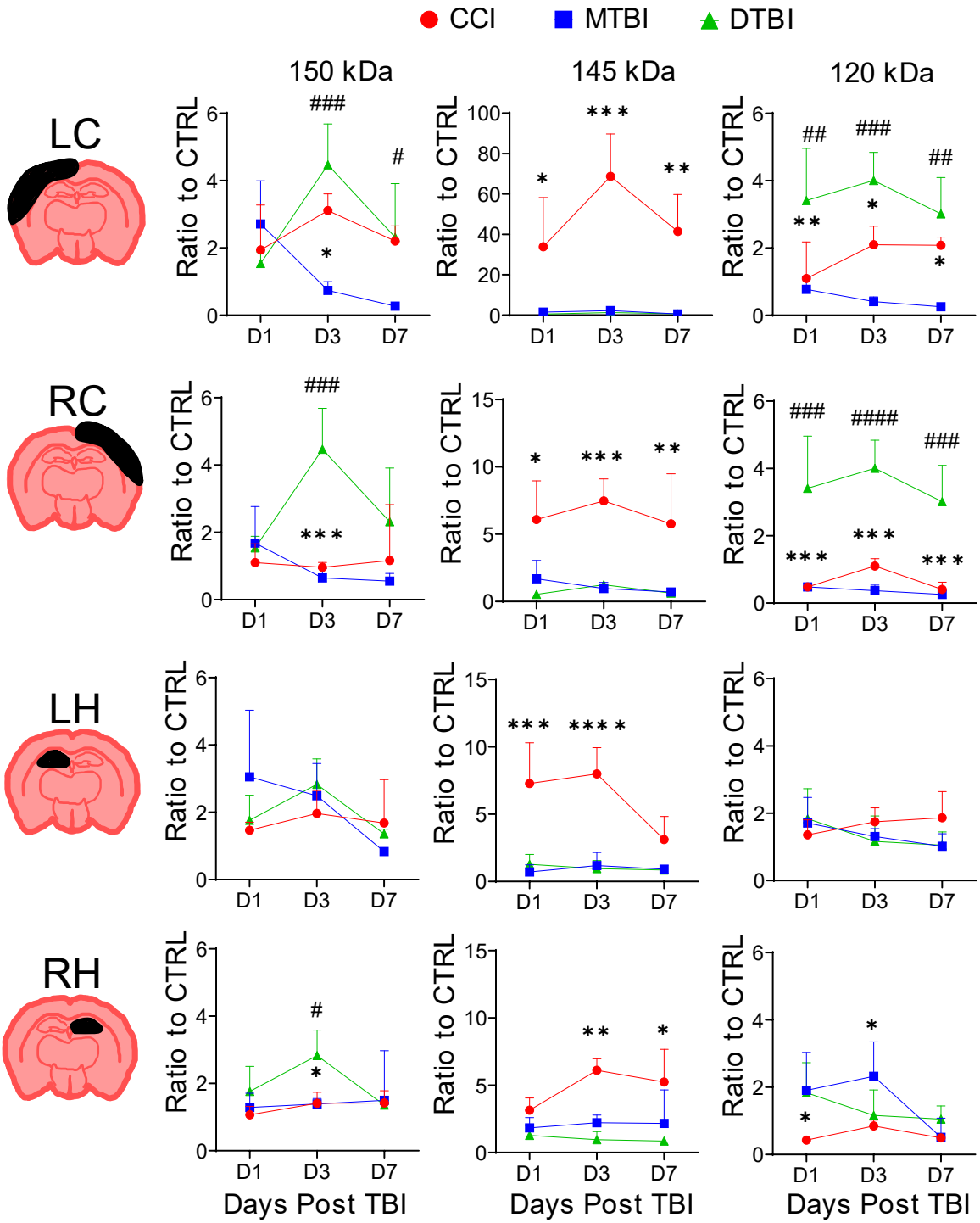

Figure 3.5. Injury timeline of quantified data for SBDPs at 1, 3 and 7 days post injury. Oncotic cell death and apoptotic cell death were only observed following impacts from CCI and DTBI models, respectively. *: CCI vs Mild; #: MTBI vs DTBI

3.3.3 Injury mechanism and apoptotic response

Due to the gross pathological changes following MTBI, we expected to see evidence of either oncotic or apoptotic cell death. Thus, we further investigated changes in apoptosis with the pro-apoptotic regulator, BAX. BAX plays a primary role in driving mitochondrial membrane permeabilization, leading to apoptosis [68]. Interestingly, both MTBI and DTBI resulted in increased BAX protein expression, confirming that apoptotic cell death is in fact present following mild impact. BAX peaked at 3 days post injury in the LC for both models, corresponding with increases in SBDP's for DTBI (Figure 3.6.). We also observed peak expression in the LH at 7 days following MTBI, indicating a progression of secondary damage post impact (Figure 3.7.). Additionally, differences between models were observed in the right hemisphere, providing additional evidence for injury mechanism influencing pathophysiology.

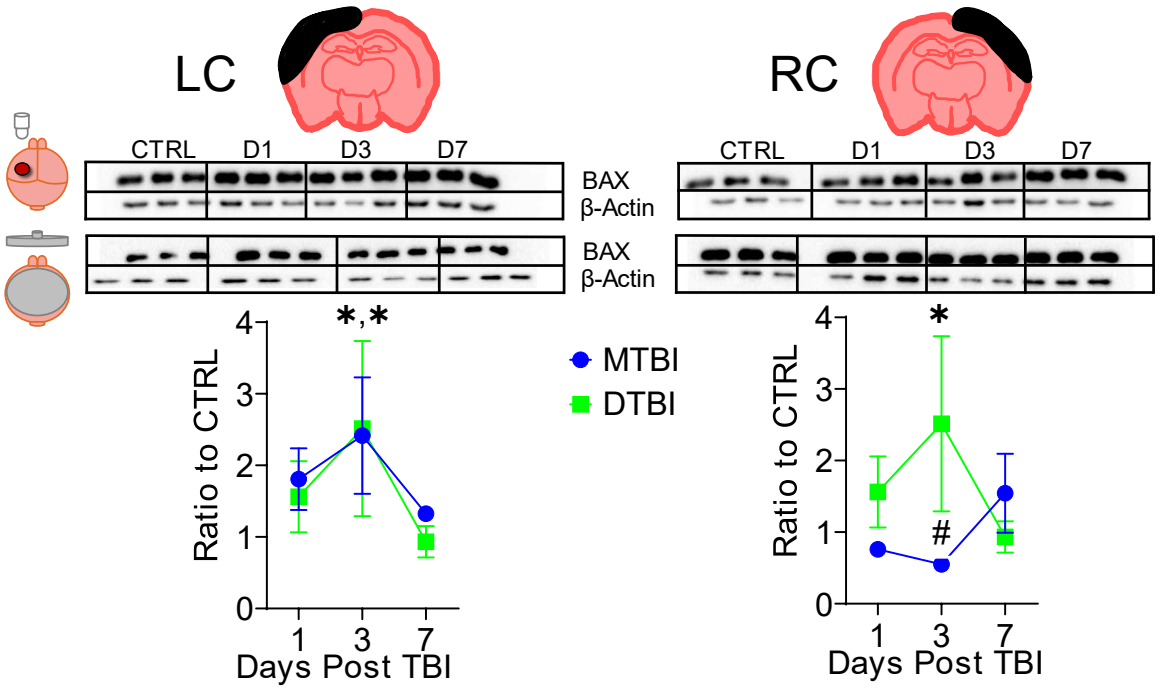

Figure 3.6. Western blot images and quantified data for BAX at 1, 3 and 7 days post mild TBI. BAX peaked in the LC at 3 days for both MTBI and DTBI, but no changes were observed following MTBI in the RC. DTBI data was averaged between left and right hemispheres for the cortex and hippocampus (HC). *: CTRL vs Injury; #: MTBI vs DTBI.

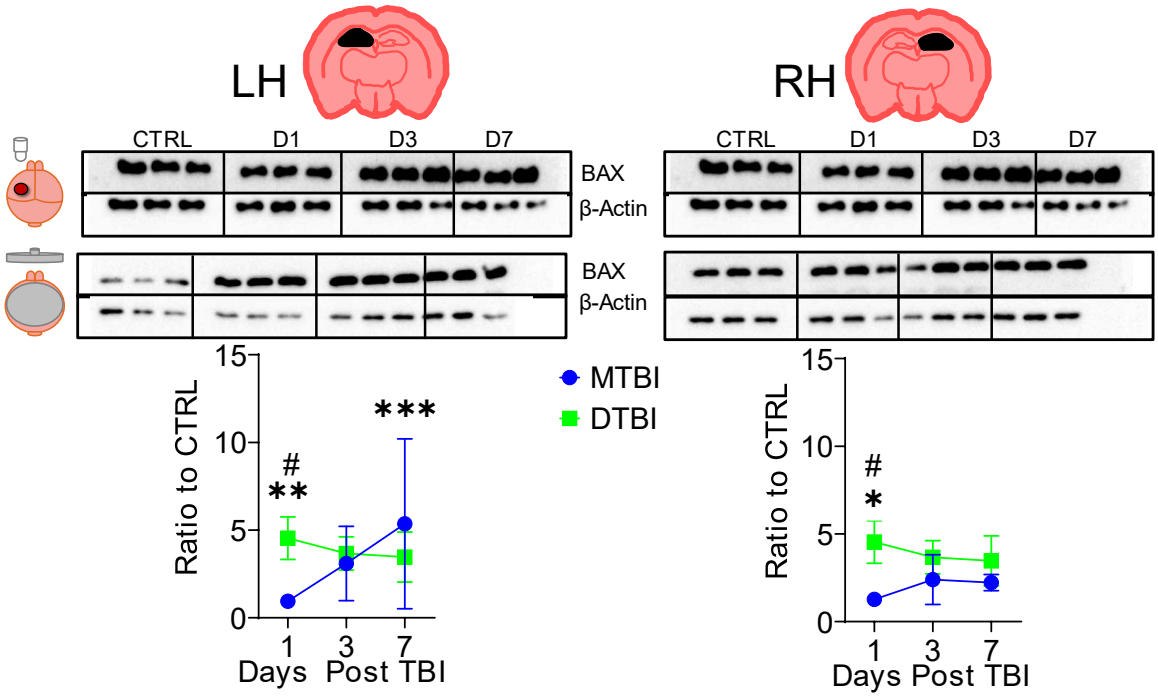

Figure 3.7. Western blot images and quantified data for BAX at 1, 3 and 7 days post mild TBI. BAX peaked at 7 days in the LH following MTBI, suggesting a progression of secondary injury. Additionally, we observed peak at 1 day in the HC following DTBI, suggesting differences in the induction of apoptosis due to injury mechanism. DTBI data was averaged between left and right hemispheres for the cortex and hippocampus (HC). *CTRL vs Injury; #MTBI vs DTBI.

3.3.4. Impaired autophagic flux independent of mechanism and severity

Previous literature has demonstrated that autophagy is impaired in the acute/subacute period following severe CCI [114, 115]. Autophagy is the major metabolic pathway involved in cellular turnover, involved in the accumulation and degradation of damaged or dysfunctional cellular components (Figure 3.8.) [89]. During periods of cellular stress, autophagy is induced through two primary upstream regulatory processes, including inhibition of the master regulatory protein complex, mechanistic target of rapamycin (mTOR), as well as activation of AMP-activated protein kinase (AMPK) [92, 93]. Inhibiting mTOR complex 1 (mTORC1) allows for the translocation of transcription factor EB (TFEB) into the nucleus, which acts as the key regulator in lysosomal

biogenesis and autophagy [93, 94]. AMPK activates unc-51 like autophagy activating kinase 1 (ULK1) complex, leading to the phosphorylation of Beclin1, a core subunit of the PI3K complex, which initiates the production of autophagosomes [92, 95, 96]. Autophagy related genes 3 & 7 (ATG3 and ATG7) are involved in the covalent linkage of phosphatidylethanolamine, converting LC3BI into LC3BII [97-99]. LC3BII, or Microtubule-associated protein 1A/1B light chain 3B, is involved in the formation of the autophagosome, specifically the elongation of the phagophore [97, 98]. During this process, ubiquitin-binding protein P62 (also referred to as SQSTM1), selectively binds to autophagic substrates tagging them for autophagic accumulation [100]. The autophagosome continues to grow, and expands around the tagged targets, until advancing into a mature autophagosome. The final steps in autophagy involve lysosomal fusion with the autophagosome leading to lysosomal degradation, where nutrients can be recycled for the specific needs of the cell [89].

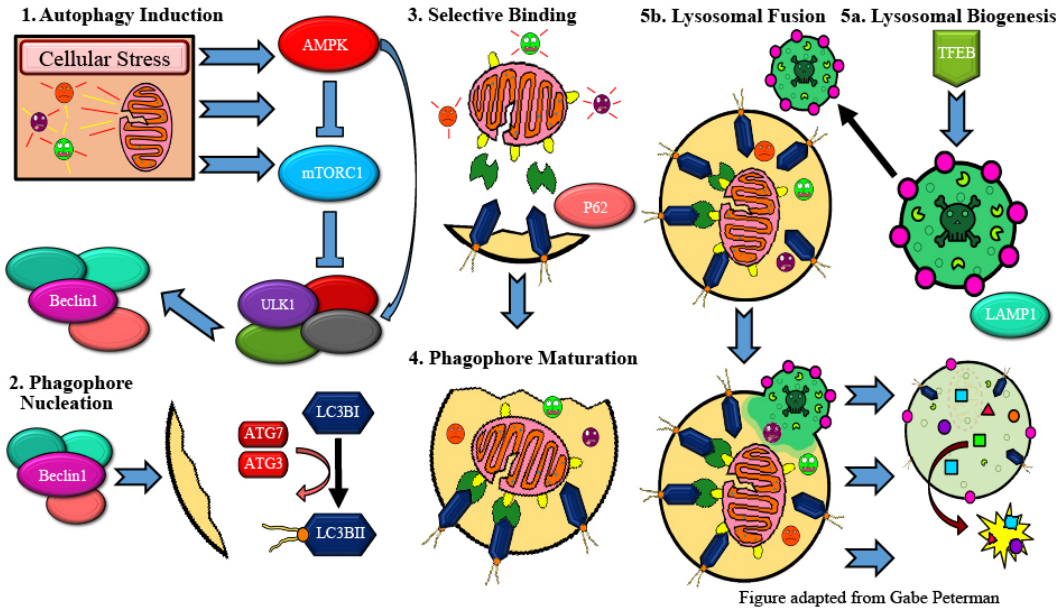

Figure 3.8. Brief overview of the mechanisms of autophagy. Autophagy is a primary mechanism of cellular turnover, involved in accumulating and degrading cellular components. Autophagic substrates are recycled and reused for further synthesis by the cell.

Autophagic flux refers to the activity of autophagic degradation. Both autophagosomes and their substrates are degraded by lysosomes following a complete cycle of cellular turnover. Thus, corresponding increases in LC3BII and SQSTM1, suggest autophagic flux is disrupted leading to an accumulation of cellular components in the lysosome. Impaired autophagic flux has been reported previously following severe injuries to the central nervous system and plays an active role in a variety of neurodegenerative processes[114, 115, 124, 125]. Thus, understanding how injury mechanism and severity influences autophagic flux could provide novel insight into designing effective therapeutics for treating injury heterogeneity associated with TBI.

Following CCI, we observed a peak in LC3BII at 1 day post injury in the LC and both hippocampi (Figure 3.9.). These results correspond to the initial increases in oncotic cell death confirmed with SBDP's. Autophagic flux was impaired at 1 day post injury in the LH. However, we did not observe autophagic dysfunction in either the LC or RH. These results were unexpected, as previous literature has shown a peak in autophagic dysfunction in the ipsilateral cortex following less severe models of CCI. However, using confocal microscopy, we did observe an increase in the co-localization of LC3BII with LAMP1, just below the site of lesion, at 3 days post impact (Figure 3.10.). These results suggest an accumulation of autophagosomes in the lysosome, indicating impaired autophagic flux. We believe these observed differences are due to autophagosome accumulation being localized to a small region beneath the impact site, when compared with Western blot results for the entirety of the left cortex. Impacts from MTBI resulted in impaired autophagic flux in the LC and LH, with peak accumulation at 3 days post injury (Figure 3.11.). Results from the ipsilateral hemisphere coincided with peak

increases in BAX following MTBI, suggesting impaired autophagic flux may be associated with apoptotic cell death. However, due to the diffuse mild impact associated with the MTBI model, we also observed autophagic dysfunction in the RH suggesting impaired autophagic flux is associated with the spread of secondary injury following TBI. Following DTBI, we observed significant increases in SQSTM1 at 3 days post injury in the cortex following DTBI, corresponding with peak changes in apoptotic cell death confirmed with both SBDP's and BAX (Figure 3.12). However, we did not observe corresponding increases in LC3BII in the cortex. In contrast, impaired autophagic flux was observed at 1 day post injury in the hippocampus, coinciding with peak increases in BAX protein expression. These results, coupled with changes in molecular pathophysiology associated with cell death, suggest impaired autophagic flux plays a primary role in the secondary consequences associated with TBI. Additionally, autophagic biomarkers may be valuable targets for evaluating the efficacy of therapeutics across a spectrum of injury heterogeneity.

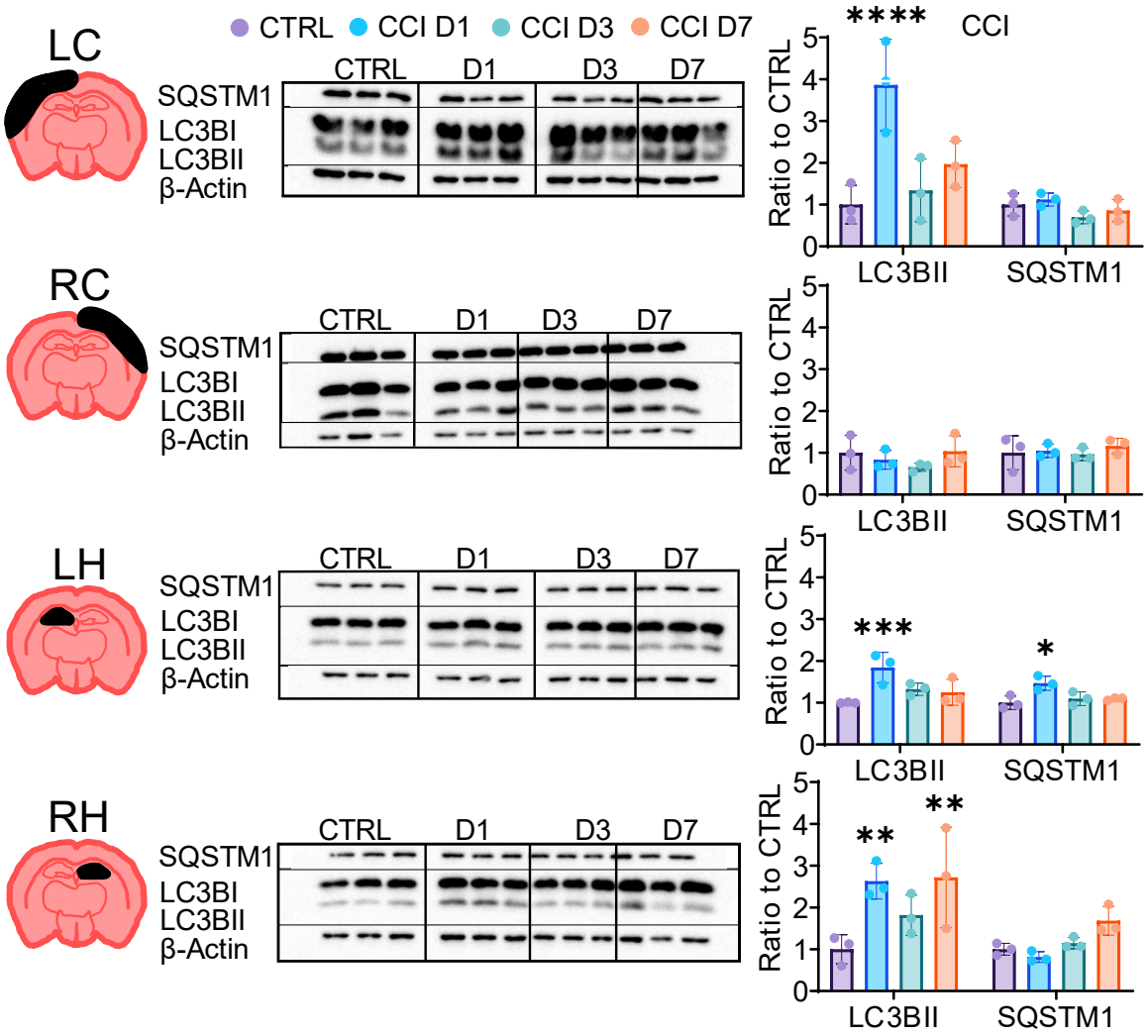

Figure 3.9. Western blot images and quantified data for autophagic markers, LC3BII and SQSTM1 at 1, 3 and 7 days post CCI. LC3BII peaked at 1 day in the LC, LH, and RH. Impaired autophagic flux was observed in the LH at 1 day post CCI.

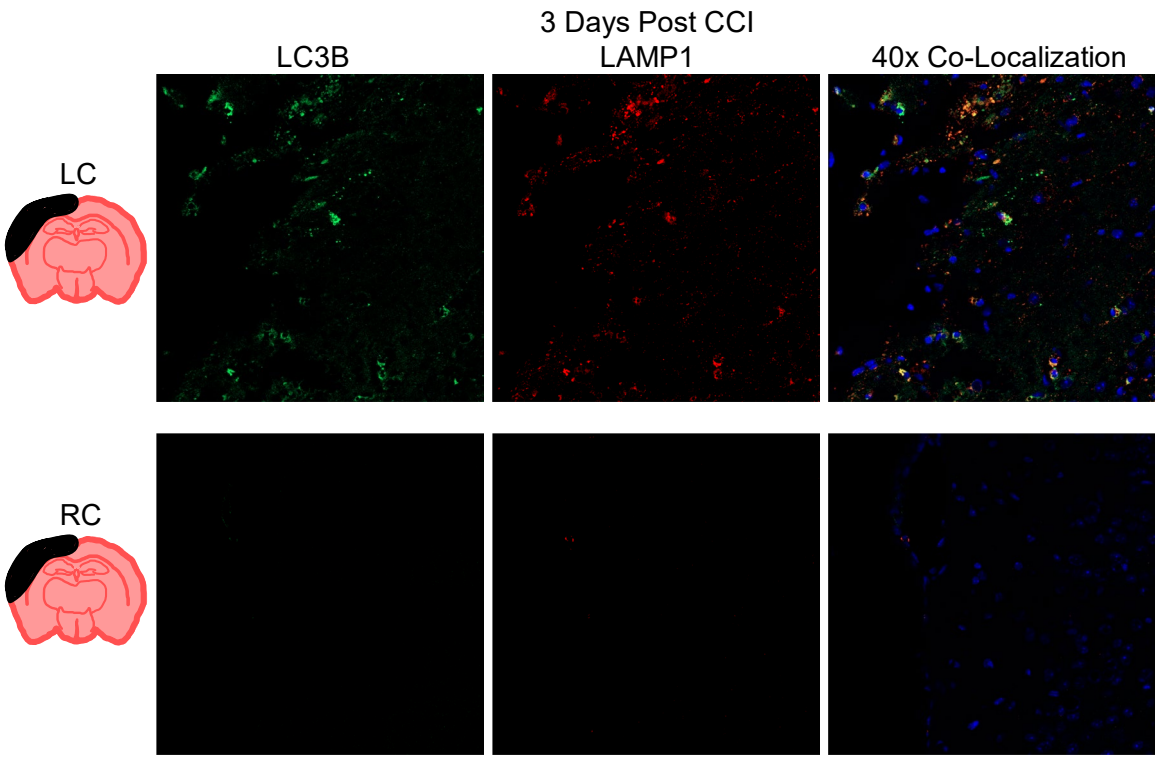

Figure 3.10. Images collected from confocal microscopy at 3 days post CCI in the ipsilateral (left) and contralateral (right) cortex. We observed a dramatic increase in autophagosomes (LC3B: Green) in the ipsilateral region, directly under the impact site. Additionally, these autophagosomes were shown to be localized with lysosomes (LAMP1: Red). In contrast, we did not observe any noticeable increases in either marker in the contralateral region. These results suggest an accumulation of autophagic substrates in the lysosome following CCI, indicating impaired autophagic flux.

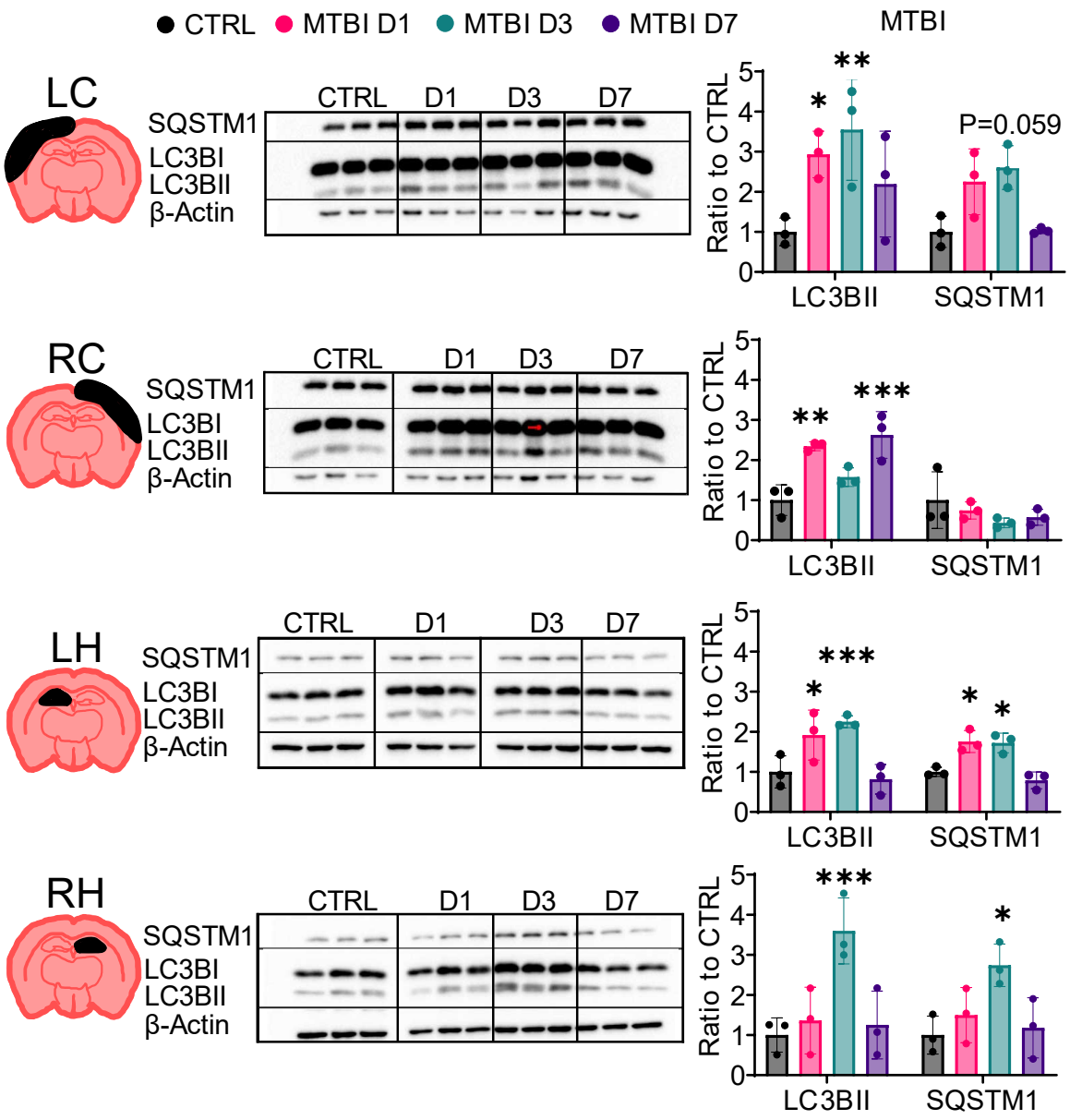

Figure 3.11. Western blot images and quantified data for autophagic markers, LC3BII and SQSTM1 at 1, 3 and 7 days post MTBI. Impaired autophagic flux was observed in both hippocampi and peaked at 3 days post MTBI. Additionally, LC3BII was increased in the RC, with no observed increases in SQSTM1.

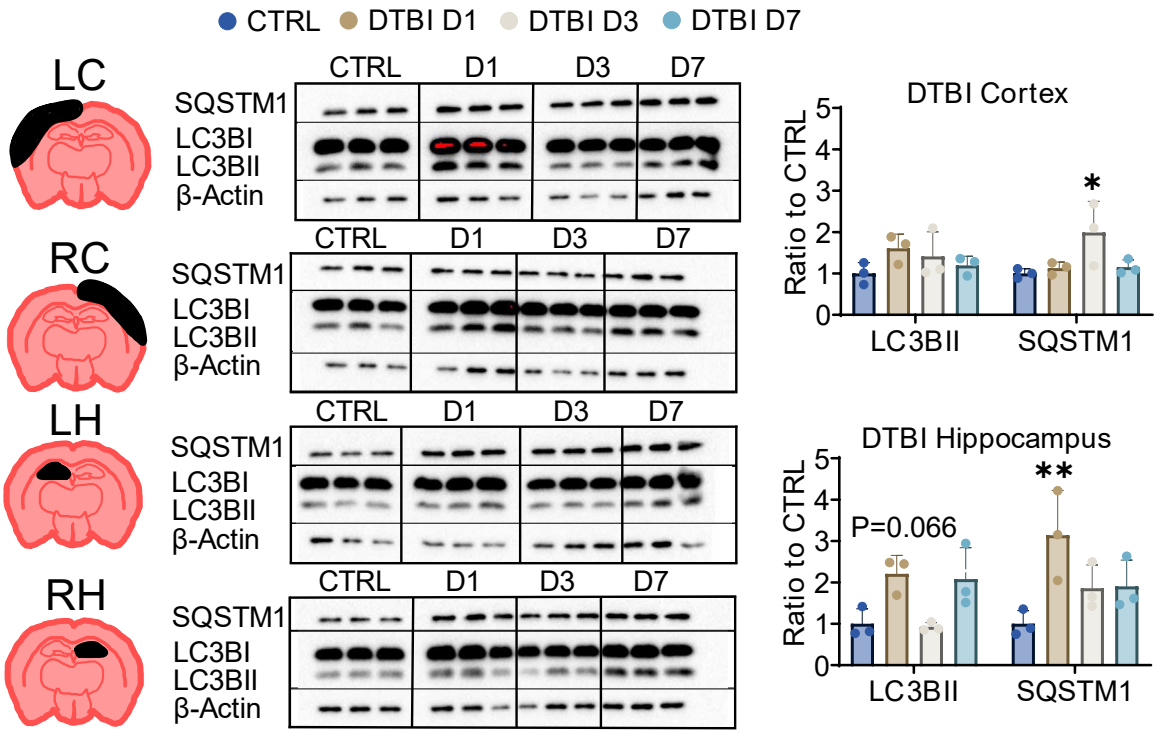

Figure 3.12. Western blot images and quantified data for autophagic markers, LC3BII and SQSTM1 at 1, 3 and 7 days post DTBI. SQSTM1 peaked at 3 days post DTBI in the cortex, and autophagic dysfunction may be present in the hippocampus at 1 day post injury.

3.4 Discussion and Limitations

Previous research has prioritized developing animal models, designed to simulate clinical TBI, to investigate pathophysiological changes associated with injury. However, evaluating individual models limits our scope of understanding how both injury mechanism and severity generate the continuum of cognitive and behavioral deficits observed clinically. Additionally, current challenges facing clinical trials and pre-clinical translation are highly impacted by injury heterogeneity at the population level. Thus, theranostic tools must be evaluated amongst of a spectrum of injuries to ensure adequate targeting and efficacious drug delivery. Our results provide evidence for establishing injury heterogeneity, with respect to both mechanism and severity, through modifications

of the controlled cortical impact model. Following impacts, gross neuropathological differences were observed between each injury, establishing three independent models for investigating pathophysiology. Cortical lesions were present at each time point following CCI, and a complete lack of lesion was observed following DTBI. However, injuries following MTBI did result in cortical lesions at each time point and noticeable hemorrhaging at days 1 and 3 post impact. These results are not reflective of the pathology observed following mild TBI and did not coincide with observations from previous methodology [43]. We believe these cortical lesions observed following MTBI are due to damage to the underlying dura when using the larger trephine drill tip. Indeed, through modifications to our current protocol, we produced an MTBI impact with no cortical lesions or gross cortical hemorrhaging (Figure .12.). These results are promising, suggesting these adjustments produced an injury more representative of mild injuries seen clinically. Future work will assess how biochemical changes from this updated mild injury, compares with our previous MTBI results. However, impacts from our MTBI model did result in reduced pathological insults when compared to CCI and were sufficient for producing significant differences in biochemical markers. Therefore, these brains were used for the remainder of the study.

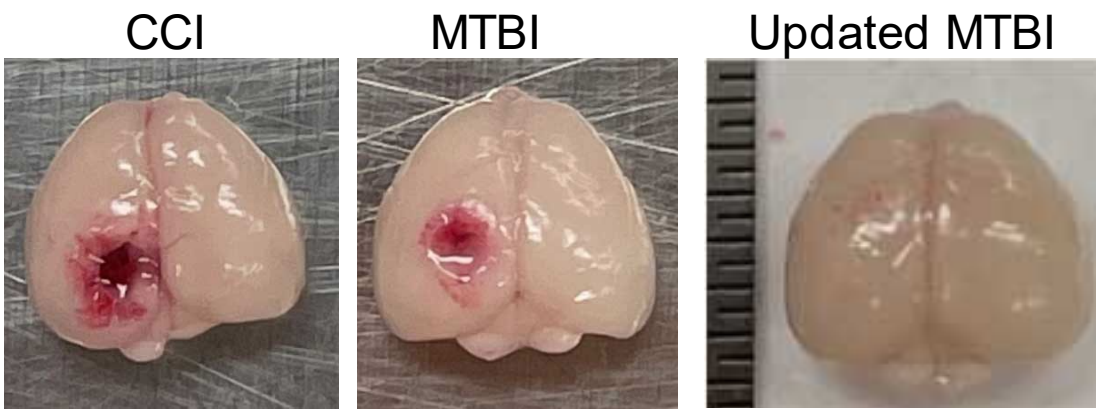

Figure 3.13. Comparison of brain images collected at 1 day post impact for CCI, MTBI, and updated MTBI protocol. Due to the updated surgery protocol for MTBI, we were able to produce impacts absent of gross neuropathological changes, suggesting injuries more representative of mild TBI.

Previous pre-clinical and clinical TBI studies have discovered several differences regarding mechanisms of cell death in response to injury severity [77, 83, 104, 115]. Results from these studies indicate an acute increase in oncotic cell death following severe TBI and these changes may influence the functionality of other cellular mechanisms. Due to the gross neuropathological changes observed following impact, we investigated how injury heterogeneity influenced the mechanisms of cell death. Severe CCI resulted in a dramatic increase in oncotic cell death, validated by SBDP's, which has been reported previously in pre-clinical studies and clinical assessment of severe TBI [77, 128]. While impacts from CCI are focal and are localized to the ipsilateral cortex, we observed changes in oncosis at 1 day post injury, peaking at 3 days, in each of the four brain regions. These results suggest the cascade of secondary damage associated with severe TBI is rapidly progressing, limiting the window for therapeutic intervention. In contrast, both MTBI and DTBI were absent of any significant changes in oncosis, suggesting these injuries are more representative of the greater patient population. However, SBDP's for apoptosis reported significant increases in apoptotic cell death in

the cortex following DTBI. Interestingly, apoptosis peaked at 3 days in the cortex, and markers for total cell death also peaked at 3 days in both the cortex and hippocampus. These corresponding peaks in oncotic and apoptotic cell death for CCI and DTBI respectively, suggest that while injury mechanism and severity differ, the timeline for the progression of cell damage remains unchanged. Additionally, we did not observe significant changes in SBDP's following MTBI, concluding that injury mechanism alone influences the evolution of pathophysiology. However, due to the gross neuropathological changes observed following MTBI, we expected to see corresponding changes in either oncotic or apoptotic cell death in the acute period following injury. Thus, we further investigated the mechanisms of apoptosis in both models of mild TBI through examining changes in protein expression for the apoptotic regulator, BAX. Interestingly, we did observe significant changes in the ipsilateral hemisphere following MTBI, suggesting that mild injuries due in fact elicit an apoptotic response. We observed a peak in BAX protein expression at 3 days in the LC, and at 7 days in the LH following MTBI, providing evidence for the continuum of secondary damage following diffuse, mild injury. Additionally, we observed a corresponding peak in BAX at 3 days post DTBI in the cortex. This peak in apoptosis corresponds with previous results from SBDP's, and has been reported previously following closed head TBI [85]. Interestingly, we observed a peak in BAX at 1 day in the hippocampus. We believe this early damage in the hippocampus could be due to the diffuse impact acceleration of closed skull impacts and could provide evidence for the acute cognitive deficits observed following mild injury.

Due to these corresponding changes between gross neuropathology and cellular pathophysiology, we investigated how injury mechanism and severity influenced the mechanisms of cell turnover, specifically autophagy. Previous literature has shown that autophagic flux is impaired following severe CCI [114, 115]. Acutely following impact, both LC3BII and SQSTM1 were upregulated in both the cortex and hippocampi, and these results provide justification for the discrepancies associated with autophagic intervention following TBI. Additionally, these studies concluded that autophagic impairment may be directly correlated with dramatic increases in oncotic cell death following severe injury. Therefore, we chose to examine autophagic flux acutely, following impacts from each model to determine how differences in cell death coincided with mechanistic changes in autophagy. Our results suggest that autophagic impairment is present in all models of TBI, regardless of injury mechanism and severity. Following CCI, we observed autophagic dysfunction in the LH. Both LC3BII and SQSTM1 peaked at 1 day post impact, coinciding with the initial increase in oncotic cell death following injury. Interestingly, we did not observe impaired autophagic flux in the LC, which had been reported previously. However, these studies used CCI models which were less severe, and we believe this lack of autophagic dysfunction could be due to the overwhelming abundance of oncotic cell death localized in the cortex following impact. Impaired autophagic flux was also present following MTBI, with peak changes at 3 days post injury, corresponding with peak changes in BAX. Interestingly, we also observed autophagic dysfunction in the RH, which correlates with the timeline of secondary progression seen following CCI and DTBI. Additionally, impacts from our DTBI model resulted in autophagy dysfunction in the hippocampus at 1 day post injury, which also

coincided with peak changes in BAX protein expression. Therefore, both oncotic and apoptotic cell death appear influenced by autophagic dysfunction.

Due to the plethora of secondary consequences experienced following TBI, establishing mechanistic links in molecular pathophysiology may provide researchers with unique upstream targets for therapeutic intervention. Previous literature has identified that impaired autophagic dysfunction is due to lysosomal membrane permeabilization (LMP) [114, 115]. LMP produces pores along the membrane of the lysosome, allowing cathepsins and other degradative enzymes to escape, which have shown to induce both apoptotic and oncotic cell death [116, 117]. Therefore, the upstream link between each of these pathophysiological processes may be LMP. LMP is induced through a variety of mechanisms, including increased production of reactive oxygen species (ROS) [118]. Thus, developing therapeutic strategies for mitigating the production of ROS, may mitigate LMP and lead to the physiological activation and continuation of autophagy.

CHAPTER 4: CONCLUSION AND FUTURE WORK

4.1 Conclusion

Due to the prevalence of mild TBI observed clinically, there is a critical need to evaluate the pathophysiological changes associated with injury severity, in addition to the outcomes influenced by impact mechanisms. Indeed, this research aimed to evaluate a closed head injury model using an electromagnetic impact device to determine the clinical translatability and the practicality of usage in producing repeated mild injuries. Interestingly, we observed that the input parameters from our electromagnetic CCI device were not correlated with outcome, specifically with respect to actual impact speed. Indeed, the actual impact speeds were far lower than anticipated, which has a dramatic effect on the direct comparison between pre-clinical models. We determined that the actual impact speed was highly dependent on both input velocity and depth, where regardless of input velocity, 9 mm and 15 mm impacts recorded the highest and lowest impact speeds, respectively. Thus, these results raise concern for researchers using an electromagnetic CCI device for producing diffuse, mild impacts and we suggest models should be characterized to ensure results are interpreted based on the actual impact conditions. Additionally, we investigated how impact speeds influenced pathophysiology, through examining biomarkers associated with cell turnover, specifically autophagy. Our results concluded that autophagic flux was impaired in the hippocampus, regardless of impact speed, providing rationale for evaluating autophagic flux in a range of impact severities and mechanisms.

Therefore, we investigated pathophysiological changes in multiple TBI animal models, including one severe, focal impact and two diffuse, mild impacts. Ultimately,

these impact models produced a spectrum of injuries, through modifications of a CCI device. Following impacts, we observed distinct differences in gross neuropathology, which corresponded with changes in the progression of cell death. Indeed, severe CCI resulted in dramatic increases in oncotic cell death, which has been shown in both pre-clinical and clinical severe TBI. In contrast, mild models resulted in differences regarding apoptotic response, suggesting injury mechanism alone shifts the progression of pathophysiology. Interestingly, each of the three impact models resulted in impaired autophagic flux, which coincided with changes in both oncotic and apoptotic cell death. Thus, these results suggest that examining biomarkers associated with autophagy may provide unique insight for evaluating the efficacy of potential therapeutics in a spectrum of injury models. Additionally, these results provide evidence that the pathophysiological mechanisms affiliated with TBI heterogeneity may be linked through common upstream events, namely impaired autophagic flux and lysosomal dysfunction. Therefore, therapeutic strategies designed to intervene in the amelioration of these consequences may alleviate molecular dysfunction, thus alleviating cognitive and behavioral deficits.

4.2 Future Work

The primary goal of this work was to establish injury heterogeneity through modifications in the CCI device and examine the differences and similarities in biochemical response. While we were able to achieve significant differences between severe and mild models, gross neuropathological changes following MTBI were more severe than previously expected. Thus, our future work will consist of reproducing MTBI injuries with our updated surgical protocol and examine secondary changes in molecular pathophysiology as discussed previously. We believe that these new results will provide

data that is more translatable to the mild injuries observed clinically and offer insight into how damage to the dura following craniectomy influences biochemical response. Additionally, this work only examined the pathophysiological differences associated with injury mechanism and severity. However, impact frequency also plays a primary role in the evolution of behavioral deficits observed clinically. Indeed, several studies have shown that repeated mild injuries are linked to the progression of neurodegenerative diseases. Thus, we are interested in determining how repeated closed head injuries influence the progression of cell death and contributes to the progression of impaired autophagic flux.

Additionally, due to the multitude of sequalae associated with TBI, establishing mechanistic links in molecular pathophysiology may provide researchers with unique upstream targets for therapeutic intervention. Previous literature has shown that impaired autophagic dysfunction is due to lysosomal membrane permeabilization (LMP) [114, 115]. LMP is induced through increased ROS production and contributes to both apoptotic and oncotic cell death [116-118]. Therefore, the upstream link between each of these pathophysiological processes may be LMP. Thus, developing therapeutic strategies for mitigating the production of ROS, may mitigate LMP and lead to the physiological activation and continuation of autophagy. Our previous work has focused on synthesizing, characterizing, and assessing the therapeutic efficacy of antioxidant nanoparticles following TBI. These nanoparticles have shown to effectively scavenge ROS, alleviate secondary pathophysiological damage, and ameliorate cognitive deficits associated with moderate to severe TBI [129-132]. Thus, our future work will assess how to improve the accumulation of these nanoparticles in less severe forms of injury,

examine how they influence the activation of autophagy and determine whether they provide an effect for ameliorating impaired autophagic flux.

APPENDIX

A. SAS Code used for generating the fitted regression model for impact speed.

SAS Code:

```
data a;  input x d v y;   datalines; *Data excluded* proc print; run;
proc mixed method=type3; class d v; model y = d v d*v;
contrast 'D Lin' d -1 0 1;
contrast 'D Quad' d 1 -2 1;
contrast 'V Lin' v -1 0 1;
contrast 'V Quad' v 1 -2 1;
contrast 'D Lin * V Lin' d*v 1 0 -1 0 0 0 -1 0 1;
contrast 'D Lin * V Quad' d*v -1 2 -1 0 0 0 1 -2 1;
contrast 'D Quad * V Lin' d*v -1 0 1 2 0 -2 -1 0 1;
contrast 'D Quad * V Quad' d*v 1 -2 1 -2 4 -2 1 -2 1;
lsmeans d v d*v; run; proc sort; by d v;
proc means; by d v; var y; output out=b mean=ym;
proc plot; plot ym*v=d / hpos=40 vpos=15; run;
proc glm; model ym= d v d*d v*v d*v; run;
data b; do d=3 to 15 by 1; do v=2 to 4 by 0.1;
y= -1.1559 + 0.2595*d + 1.42028*v - 0.0111*d*d - 0.1694*v*v - 0.0286*d*v;
output; end; end; run; proc g3d; plot v*d=y; run; run;
```

B. Multivariate implicit differentiation for obtaining the maximum impact speed.

$$\boldsymbol{Y = -1.156 + 0.26d + 1.42v - 0.011d^2 - 0.169v^2 - 0.029dv}$$

Step 1. Set equation equal to zero.

$$-1.156 + 0.26d + 1.42v - 0.011d^2 - 0.169v^2 - 0.029dv - y = 0$$

Step 2. Find partial derivatives.

$$\frac{\partial y}{\partial d} = 0.26 - 0.022d - 0.029v$$

$$\frac{\partial y}{dv} = 1.42 - 0.338v - 0.029d$$

Step 3. Solve for v, when $\frac{\partial y}{\partial v} = 0$.

$$\frac{\partial y}{\partial v} = 0 = 1.42 - 0.338v - 0.029d$$

$$v = \frac{(1.42 - 0.029d)}{0.338}$$

Step 4. Plug in v, when $\frac{\partial y}{\partial d} = 0$, and solve for d.

$$\frac{\partial y}{\partial d} = 0 = 0.26 - 0.022d - \frac{0.029(1.42 - 0.029d)}{0.338}$$

$$d = 7.08$$

Step 5. Plug in d, when $\frac{\partial y}{\partial v} = 0$, and solve for v.

$$\frac{\partial y}{dv} = 0 = 1.42 - 0.338v - 0.029(7.08)$$

$$v = 3.59$$

REFERENCES

[1] B.Z. McDonald, C.C. Gee, F.M. Kievit, The Nanotheranostic Researcher’s Guide for Use of Animal Models of Traumatic Brain Injury, Journal of Nanotheranostics 2(4) (2021) 224-268.

[2] A.I.R. Maas, D.K. Menon, P.D. Adelson, N. Andelic, M.J. Bell, A. Belli, P. Bragge, A. Brazinova, A. Buki, R.M. Chesnut, G. Citerio, M. Coburn, D.J. Cooper, A.T. Crowder, E. Czeiter, M. Czosnyka, R. Diaz-Arrastia, J.P. Dreier, A.C. Duhaime, A. Ercole, T.A. van Essen, V.L. Feigin, G. Gao, J. Giacino, L.E. Gonzalez-Lara, R.L. Gruen, D. Gupta, J.A. Hartings, S. Hill, J.Y. Jiang, N. Ketharanathan, E.J.O. Kompanje, L. Lanyon, S. Laureys, F. Lecky, H. Levin, H.F. Lingsma, M. Maegele, M. Majdan, G. Manley, J. Marsteller, L. Mascia, C. McFadyen, S. Mondello, V. Newcombe, A. Palotie, P.M. Parizel, W. Peul, J. Piercy, S. Polinder, L. Puybasset, T.E. Rasmussen, R. Rossaint, P. Smielewski, J. Soderberg, S.J. Stanworth, M.B. Stein, N. von Steinbuchel, W. Stewart, E.W. Steyerberg, N. Stocchetti, A. Synnot, B. Te Ao, O. Tenovuo, A. Theadom, D. Tibboel, W. Videtta, K.K.W. Wang, W.H. Williams, L. Wilson, K. Yaffe, T.P. In, Investigators, Traumatic brain injury: integrated approaches to improve prevention, clinical care, and research, Lancet Neurol 16(12) (2017) 987-1048.

[3] D. Najem, K. Rennie, M. Ribecco-Lutkiewicz, D. Ly, J. Haukenfrers, Q. Liu, M. Nzau, D.D. Fraser, M. Bani-Yaghoub, Traumatic brain injury: classification, models, and markers, Biochem Cell Biol 96(4) (2018) 391-406.

[4] J.B. Long, T.L. Bentley, K.A. Wessner, C. Cerone, S. Sweeney, R.A. Bauman, Blast overpressure in rats: recreating a battlefield injury in the laboratory, J Neurotrauma 26(6) (2009) 827-40.

[5] D.R. Namjoshi, W.H. Cheng, K.A. McInnes, K.M. Martens, M. Carr, A. Wilkinson, J. Fan, J. Robert, A. Hayat, P.A. Cripton, C.L. Wellington, Merging pathology with biomechanics using CHIMERA (Closed-Head Impact Model of Engineered Rotational Acceleration): a novel, surgery-free model of traumatic brain injury, Mol Neurodegener 9 (2014) 55.

[6] A.C. McKee, D.H. Daneshvar, The neuropathology of traumatic brain injury, Handb Clin Neurol 127 (2015) 45-66.

[7] J.A. Langlois, W. Rutland-Brown, M.M. Wald, The epidemiology and impact of traumatic brain injury: a brief overview, J Head Trauma Rehabil 21(5) (2006) 375-8.

[8] G. Neurobehavioral Guidelines Working, D.L. Warden, B. Gordon, T.W. McAllister, J.M. Silver, J.T. Barth, J. Bruns, A. Drake, T. Gentry, A. Jagoda, D.I. Katz, J. Kraus, L.A. Labbate, L.M. Ryan, M.B. Sparling, B. Walters, J. Whyte, A. Zapata, G. Zitnay, Guidelines for the pharmacologic treatment of neurobehavioral sequelae of traumatic brain injury, J Neurotrauma 23(10) (2006) 1468-501.

[9] K.W. McConeghy, J. Hatton, L. Hughes, A.M. Cook, A review of neuroprotection pharmacology and therapies in patients with acute traumatic brain injury, CNS Drugs 26(7) (2012) 613-36.

[10] M.R. Bullock, R. Chesnut, J. Ghajar, D. Gordon, R. Hartl, D.W. Newell, F. Servadei, B.C. Walters, J.E. Wilberger, G. Surgical Management of Traumatic Brain Injury Author, Surgical management of acute subdural hematomas, Neurosurgery 58(3 Suppl) (2006) S16-24; discussion Si-iv.

[11] R.K. Narayan, M.E. Michel, B. Ansell, A. Baethmann, A. Biegon, M.B. Bracken, M.R. Bullock, S.C. Choi, G.L. Clifton, C.F. Contant, W.M. Coplin, W.D. Dietrich, J.

Ghajar, S.M. Grady, R.G. Grossman, E.D. Hall, W. Heetderks, D.A. Hovda, J. Jallo, R.L. Katz, N. Knoller, P.M. Kochanek, A.I. Maas, J. Majde, D.W. Marion, A. Marmarou, L.F. Marshall, T.K. McIntosh, E. Miller, N. Mohberg, J.P. Muizelaar, L.H. Pitts, P. Quinn, G. Riesenfeld, C.S. Robertson, K.I. Strauss, G. Teasdale, N. Temkin, R. Tuma, C. Wade, M.D. Walker, M. Weinrich, J. Whyte, J. Wilberger, A.B. Young, L. Yurkewicz, Clinical trials in head injury, J Neurotrauma 19(5) (2002) 503-57.
[12] D.G. Stein, Embracing failure: What the Phase III progesterone studies can teach about TBI clinical trials, Brain Inj 29(11) (2015) 1259-72.
[13] S.M. Poloyac, R.J. Bertz, L.A. McDermott, P. Marathe, Pharmacological Optimization for Successful Traumatic Brain Injury Drug Development, J Neurotrauma 37(22) (2020) 2435-2444.
[14] R.B. Howard, I. Sayeed, D.G. Stein, Suboptimal Dosing Parameters as Possible Factors in the Negative Phase III Clinical Trials of Progesterone for Traumatic Brain Injury, J Neurotrauma 34(11) (2017) 1915-1918.
[15] E.M. Doppenberg, S.C. Choi, R. Bullock, Clinical trials in traumatic brain injury: lessons for the future, J Neurosurg Anesthesiol 16(1) (2004) 87-94.
[16] P.M. Kochanek, C.E. Dixon, S. Mondello, K.K.K. Wang, A. Lafrenaye, H.M. Bramlett, W.D. Dietrich, R.L. Hayes, D.A. Shear, J.S. Gilsdorf, M. Catania, S.M. Poloyac, P.E. Empey, T.C. Jackson, J.T. Povlishock, Multi-Center Pre-clinical Consortia to Enhance Translation of Therapies and Biomarkers for Traumatic Brain Injury: Operation Brain Trauma Therapy and Beyond, Front Neurol 9 (2018) 640.
[17] J.F. Malec, A.W. Brown, C.L. Leibson, J.T. Flaada, J.N. Mandrekar, N.N. Diehl, P.K. Perkins, The mayo classification system for traumatic brain injury severity, J Neurotrauma 24(9) (2007) 1417-24.
[18] B.Y. Gravesteijn, C.A. Sewalt, A. Ercole, C. Akerlund, D. Nelson, A.I.R. Maas, D. Menon, H.F. Lingsma, E.W. Steyerberg, C. Collaborative European NeuroTrauma Effectiveness Research for Traumatic Brain Injury, Toward a New Multi-Dimensional Classification of Traumatic Brain Injury: A Collaborative European NeuroTrauma Effectiveness Research for Traumatic Brain Injury Study, J Neurotrauma 37(7) (2020) 1002-1010.
[19] Y. Xiong, A. Mahmood, M. Chopp, Animal models of traumatic brain injury, Nat Rev Neurosci 14(2) (2013) 128-42.
[20] C.N. Bodnar, K.N. Roberts, E.K. Higgins, A.D. Bachstetter, A Systematic Review of Closed Head Injury Models of Mild Traumatic Brain Injury in Mice and Rats, J Neurotrauma 36(11) (2019) 1683-1706.
[21] N. Khatri, M. Thakur, V. Pareek, S. Kumar, S. Sharma, A.K. Datusalia, Oxidative Stress: Major Threat in Traumatic Brain Injury, CNS Neurol Disord Drug Targets 17(9) (2018) 689-695.
[22] G. Teasdale, B. Jennett, Assessment of Coma and Impaired Consciousness, The Lancet 304(7872) (1974) 81-84.
[23] G. Teasdale, A. Maas, F. Lecky, G. Manley, N. Stocchetti, G. Murray, The Glasgow Coma Scale at 40 years: standing the test of time, The Lancet Neurology 13(8) (2014) 844-854.
[24] G.L. Sternbach, The Glasgow Coma Scale, The Journal of Emergency Medicine 19(1) (2000) 67-71.

[25] V. Di Pietro, K.M. Yakoub, G. Caruso, G. Lazzarino, S. Signoretti, A.K. Barbey, B. Tavazzi, G. Lazzarino, A. Belli, A.M. Amorini, Antioxidant Therapies in Traumatic Brain Injury, Antioxidants (Basel) 9(3) (2020).
[26] C.T. Forde, S.K. Karri, A.M. Young, C.S. Ogilvy, Predictive markers in traumatic brain injury: opportunities for a serum biosignature, Br J Neurosurg 28(1) (2014) 8-15.
[27] C.f.D. Control, Prevention, Report to Congress on mild traumatic brain injury in the United States: steps to prevent a serious public health problem, Atlanta, GA: Centers for Disease Control and Prevention 45 (2003).
[28] C.A. Tagge, A.M. Fisher, O.V. Minaeva, A. Gaudreau-Balderrama, J.A. Moncaster, X.L. Zhang, M.W. Wojnarowicz, N. Casey, H. Lu, O.N. Kokiko-Cochran, S. Saman, M. Ericsson, K.D. Onos, R. Veksler, V.V. Senatorov, Jr., A. Kondo, X.Z. Zhou, O. Miry, L.R. Vose, K.R. Gopaul, C. Upreti, C.J. Nowinski, R.C. Cantu, V.E. Alvarez, A.M. Hildebrandt, E.S. Franz, J. Konrad, J.A. Hamilton, N. Hua, Y. Tripodis, A.T. Anderson, G.R. Howell, D. Kaufer, G.F. Hall, K.P. Lu, R.M. Ransohoff, R.O. Cleveland, N.W. Kowall, T.D. Stein, B.T. Lamb, B.R. Huber, W.C. Moss, A. Friedman, P.K. Stanton, A.C. McKee, L.E. Goldstein, Concussion, microvascular injury, and early tauopathy in young athletes after impact head injury and an impact concussion mouse model, Brain 141(2) (2018) 422-458.
[29] M. Prins, T. Greco, D. Alexander, C.C. Giza, The pathophysiology of traumatic brain injury at a glance, Dis Model Mech 6(6) (2013) 1307-15.
[30] J.J. Nissen, P.A. Jones, D.F. Signorini, L.S. Murray, G.M. Teasdale, J.D. Miller, Glasgow head injury outcome prediction program: an independent assessment, J Neurol Neurosurg Psychiatry 67(6) (1999) 796-9.
[31] P.V. Dong, O.L. Cremer, Limitations of the use of the Glasgow Coma Scale in intensive care patients with non-neurological primary disease: a search for alternatives, Critical Care 15(S1) (2011).
[32] T.M. Andriessen, B. Jacobs, P.E. Vos, Clinical characteristics and pathophysiological mechanisms of focal and diffuse traumatic brain injury, J Cell Mol Med 14(10) (2010) 2381-92.
[33] A.Y. Abramov, M.R. Duchen, Mechanisms underlying the loss of mitochondrial membrane potential in glutamate excitotoxicity, Biochim Biophys Acta 1777(7-8) (2008) 953-64.
[34] J.V. Rosenfeld, A.C. McFarlane, P. Bragge, R.A. Armonda, J.B. Grimes, G.S. Ling, Blast-related traumatic brain injury, The Lancet Neurology 12(9) (2013) 882-893.
[35] J. Cheng, J. Gu, Y. Ma, T. Yang, Y. Kuang, B. Li, J. Kang, Development of a rat model for studying blast-induced traumatic brain injury, J Neurol Sci 294(1-2) (2010) 23-8.
[36] Y. Chen, W. Huang, Non-impact, blast-induced mild TBI and PTSD: concepts and caveats, Brain Inj 25(7-8) (2011) 641-50.
[37] B.D. Stemper, A.S. Shah, F.A. Pintar, M. McCrea, S.N. Kurpad, A. Glavaski-Joksimovic, C. Olsen, M.D. Budde, Head rotational acceleration characteristics influence behavioral and diffusion tensor imaging outcomes following concussion, Ann Biomed Eng 43(5) (2015) 1071-1088.
[38] I. Cernak, Animal models of head trauma, NeuroRx 2(3) (2005) 410-422.
[39] N. Osier, C.E. Dixon, The Controlled Cortical Impact Model of Experimental Brain Trauma: Overview, Research Applications, and Protocol, Methods Mol Biol 1462 (2016) 177-92.

[40] H. Alluri, C.A. Shaji, M.L. Davis, B. Tharakan, A Mouse Controlled Cortical Impact Model of Traumatic Brain Injury for Studying Blood-Brain Barrier Dysfunctions, Methods Mol Biol 1717 (2018) 37-52.
[41] C. Edward Dixon, G.L. Clifton, J.W. Lighthall, A.A. Yaghmai, R.L. Hayes, A controlled cortical impact model of traumatic brain injury in the rat, Journal of Neuroscience Methods 39(3) (1991) 253-262.
[42] J. Romine, X. Gao, J. Chen, Controlled cortical impact model for traumatic brain injury, J Vis Exp (90) (2014) e51781.
[43] Y. Chen, H. Mao, K.H. Yang, T. Abel, D.F. Meaney, A modified controlled cortical impact technique to model mild traumatic brain injury mechanics in mice, Front Neurol 5 (2014) 100.
[44] A. Marmarou, M.A. Foda, W. van den Brink, J. Campbell, H. Kita, K. Demetriadou, A new model of diffuse brain injury in rats. Part I: Pathophysiology and biomechanics, J Neurosurg 80(2) (1994) 291-300.
[45] C.R. Marmarou, R. Prieto, K. Taya, H.F. Young, A. Marmarou, Marmarou Weight Drop Injury Model, Animal Models of Acute Neurological Injuries2009, pp. 393-407.
[46] L. Xu, J.V. Nguyen, M. Lehar, A. Menon, E. Rha, J. Arena, J. Ryu, N. Marsh-Armstrong, C.R. Marmarou, V.E. Koliatsos, Repetitive mild traumatic brain injury with impact acceleration in the mouse: Multifocal axonopathy, neuroinflammation, and neurodegeneration in the visual system, Exp Neurol 275 Pt 3 (2016) 436-449.
[47] I. Cernak, R. Vink, D.N. Zapple, M.I. Cruz, F. Ahmed, T. Chang, S.T. Fricke, A.I. Faden, The pathobiology of moderate diffuse traumatic brain injury as identified using a new experimental model of injury in rats, Neurobiol Dis 17(1) (2004) 29-43.
[48] R. Daneman, A. Prat, The Blood–Brain Barrier, Cold Spring Harbor Perspectives in Biology 7(1) (2015).
[49] A. Chodobski, B.J. Zink, J. Szmydynger-Chodobska, Blood-brain barrier pathophysiology in traumatic brain injury, Transl Stroke Res 2(4) (2011) 492-516.
[50] H. Alluri, K. Wiggins-Dohlvik, M.L. Davis, J.H. Huang, B. Tharakan, Blood-brain barrier dysfunction following traumatic brain injury, Metab Brain Dis 30(5) (2015) 1093-104.
[51] G.R. de Lores Arnaiz, M.G.L. Ordieres, Brain Na(+), K(+)-ATPase Activity In Aging and Disease, Int J Biomed Sci 10(2) (2014) 85-102.
[52] M.L. Hernandez, T. Chatlos, K.M. Gorse, A.D. Lafrenaye, Neuronal Membrane Disruption Occurs Late Following Diffuse Brain Trauma in Rats and Involves a Subpopulation of NeuN Negative Cortical Neurons, Frontiers in neurology 10 (2019) 1238-1238.
[53] F.D. Lima, M.A. Souza, A.F. Furian, L.M. Rambo, L.R. Ribeiro, F.V. Martignoni, M.S. Hoffmann, M.R. Fighera, L.F.F. Royes, M.S. Oliveira, C.F. de Mello, Na+,K+-ATPase activity impairment after experimental traumatic brain injury: Relationship to spatial learning deficits and oxidative stress, Behavioural Brain Research 193(2) (2008) 306-310.
[54] Y. Zhou, N.C. Danbolt, Glutamate as a neurotransmitter in the healthy brain, J Neural Transm (Vienna) 121(8) (2014) 799-817.
[55] C. Ménard, R. Quirion, Group 1 Metabotropic Glutamate Receptor Function and Its Regulation of Learning and Memory in the Aging Brain, Frontiers in Pharmacology 3 (2012).

[56] D. Belov Kirdajova, J. Kriska, J. Tureckova, M. Anderova, Ischemia-Triggered Glutamate Excitotoxicity From the Perspective of Glial Cells, Front Cell Neurosci 14 (2020) 51-51.
[57] R.M. Guerriero, C.C. Giza, A. Rotenberg, Glutamate and GABA imbalance following traumatic brain injury, Curr Neurol Neurosci Rep 15(5) (2015) 27-27.
[58] M. Schieber, N.S. Chandel, ROS function in redox signaling and oxidative stress, Curr Biol 24(10) (2014) R453-R462.
[59] S.J. Schimmel, S. Acosta, D. Lozano, Neuroinflammation in traumatic brain injury: A chronic response to an acute injury, Brain Circ 3(3) (2017) 135-142.
[60] Y. Xiong, A. Mahmood, M. Chopp, Current understanding of neuroinflammation after traumatic brain injury and cell-based therapeutic opportunities, Chin J Traumatol 21(3) (2018) 137-151.
[61] Y.J. Jung, D. Tweedie, M.T. Scerba, N.H. Greig, Neuroinflammation as a Factor of Neurodegenerative Disease: Thalidomide Analogs as Treatments, Frontiers in Cell and Developmental Biology 7 (2019).
[62] L. Galluzzi, I. Vitale, S.A. Aaronson, J.M. Abrams, D. Adam, P. Agostinis, E.S. Alnemri, L. Altucci, I. Amelio, D.W. Andrews, M. Annicchiarico-Petruzzelli, A.V. Antonov, E. Arama, E.H. Baehrecke, N.A. Barlev, N.G. Bazan, F. Bernassola, M.J.M. Bertrand, K. Bianchi, M.V. Blagosklonny, K. Blomgren, C. Borner, P. Boya, C. Brenner, M. Campanella, E. Candi, D. Carmona-Gutierrez, F. Cecconi, F.K. Chan, N.S. Chandel, E.H. Cheng, J.E. Chipuk, J.A. Cidlowski, A. Ciechanover, G.M. Cohen, M. Conrad, J.R. Cubillos-Ruiz, P.E. Czabotar, V. D'Angiolella, T.M. Dawson, V.L. Dawson, V. De Laurenzi, R. De Maria, K.M. Debatin, R.J. DeBerardinis, M. Deshmukh, N. Di Daniele, F. Di Virgilio, V.M. Dixit, S.J. Dixon, C.S. Duckett, B.D. Dynlacht, W.S. El-Deiry, J.W. Elrod, G.M. Fimia, S. Fulda, A.J. Garcia-Saez, A.D. Garg, C. Garrido, E. Gavathiotis, P. Golstein, E. Gottlieb, D.R. Green, L.A. Greene, H. Gronemeyer, A. Gross, G. Hajnoczky, J.M. Hardwick, I.S. Harris, M.O. Hengartner, C. Hetz, H. Ichijo, M. Jaattela, B. Joseph, P.J. Jost, P.P. Juin, W.J. Kaiser, M. Karin, T. Kaufmann, O. Kepp, A. Kimchi, R.N. Kitsis, D.J. Klionsky, R.A. Knight, S. Kumar, S.W. Lee, J.J. Lemasters, B. Levine, A. Linkermann, S.A. Lipton, R.A. Lockshin, C. Lopez-Otin, S.W. Lowe, T. Luedde, E. Lugli, M. MacFarlane, F. Madeo, M. Malewicz, W. Malorni, G. Manic, J.C. Marine, S.J. Martin, J.C. Martinou, J.P. Medema, P. Mehlen, P. Meier, S. Melino, E.A. Miao, J.D. Molkentin, U.M. Moll, C. Munoz-Pinedo, S. Nagata, G. Nunez, A. Oberst, M. Oren, M. Overholtzer, M. Pagano, T. Panaretakis, M. Pasparakis, J.M. Penninger, D.M. Pereira, S. Pervaiz, M.E. Peter, M. Piacentini, P. Pinton, J.H.M. Prehn, H. Puthalakath, G.A. Rabinovich, M. Rehm, R. Rizzuto, C.M.P. Rodrigues, D.C. Rubinsztein, T. Rudel, K.M. Ryan, E. Sayan, L. Scorrano, F. Shao, Y. Shi, J. Silke, H.U. Simon, A. Sistigu, B.R. Stockwell, A. Strasser, G. Szabadkai, S.W.G. Tait, D. Tang, N. Tavernarakis, A. Thorburn, Y. Tsujimoto, B. Turk, T. Vanden Berghe, P. Vandenabeele, M.G. Vander Heiden, A. Villunger, H.W. Virgin, K.H. Vousden, D. Vucic, E.F. Wagner, H. Walczak, D. Wallach, Y. Wang, J.A. Wells, W. Wood, J. Yuan, Z. Zakeri, B. Zhivotovsky, L. Zitvogel, G. Melino, G. Kroemer, Molecular mechanisms of cell death: recommendations of the Nomenclature Committee on Cell Death 2018, Cell Death Differ 25(3) (2018) 486-541.
[63] J.C. Reed, Mechanisms of Apoptosis, The American Journal of Pathology 157(5) (2000) 1415-1430.

[64] B.F. Trump, I.K. Berezesky, S.H. Chang, P.C. Phelps, The pathways of cell death: oncosis, apoptosis, and necrosis, Toxicol Pathol 25(1) (1997) 82-8.
[65] Z. Yu, N. Jiang, W. Su, Y. Zhuo, Necroptosis: A Novel Pathway in Neuroinflammation, Front Pharmacol 12 (2021) 701564.
[66] S. Elmore, Apoptosis: a review of programmed cell death, Toxicol Pathol 35(4) (2007) 495-516.
[67] P.B. Bhosale, S.E. Ha, P. Vetrivel, H.H. Kim, J.-A. Kim, K.-I. Park, S.M. Kim, G.S. Kim, Flavonoid-induced apoptotic cell death in human cancer cells and its

mechanisms, Journal of Biomedical Translational Research 21(2) (2020) 50-58.
[68] S.W. Tait, D.R. Green, Mitochondria and cell death: outer membrane permeabilization and beyond, Nat Rev Mol Cell Biol 11(9) (2010) 621-32.
[69] R. Shakeri, A. Kheirollahi, J. Davoodi, Apaf-1: Regulation and function in cell death, Biochimie 135 (2017) 111-125.
[70] S. Fulda, K.M. Debatin, Extrinsic versus intrinsic apoptosis pathways in anticancer chemotherapy, Oncogene 25(34) (2006) 4798-811.
[71] P. Mehlen, D.E. Bredesen, Dependence receptors: from basic research to drug development, Sci Signal 4(157) (2011) mr2.
[72] A. Strasser, P.J. Jost, S. Nagata, The many roles of FAS receptor signaling in the immune system, Immunity 30(2) (2009) 180-92.
[73] L.S. Dickens, I.R. Powley, M.A. Hughes, M. MacFarlane, The 'complexities' of life and death: death receptor signalling platforms, Exp Cell Res 318(11) (2012) 1269-77.
[74] N. Yatim, S. Cullen, M.L. Albert, Dying cells actively regulate adaptive immune responses, Nat Rev Immunol 17(4) (2017) 262-275.
[75] T. Vanden Berghe, N. Vanlangenakker, E. Parthoens, W. Deckers, M. Devos, N. Festjens, C.J. Guerin, U.T. Brunk, W. Declercq, P. Vandenabeele, Necroptosis, necrosis and secondary necrosis converge on similar cellular disintegration features, Cell Death Differ 17(6) (2010) 922-30.
[76] P. Golstein, G. Kroemer, Cell death by necrosis: towards a molecular definition, Trends Biochem Sci 32(1) (2007) 37-43.
[77] S. Chen, Q. Shi, S. Zheng, L. Luo, S. Yuan, X. Wang, Z. Cheng, W. Zhang, Role of alpha-II-spectrin breakdown products in the prediction of the severity and clinical outcome of acute traumatic brain injury, Exp Ther Med 11(5) (2016) 2049-2053.
[78] R. Raghupathi, D.I. Graham, T.K. McIntosh, Apoptosis after traumatic brain injury, J Neurotrauma 17(10) (2000) 927-38.
[79] P. Weerasinghe, L.M. Buja, Oncosis: an important non-apoptotic mode of cell death, Exp Mol Pathol 93(3) (2012) 302-8.
[80] C. Del Nagro, Y. Xiao, L. Rangell, M. Reichelt, T. O'Brien, Depletion of the central metabolite NAD leads to oncosis-mediated cell death, J Biol Chem 289(51) (2014) 35182-92.
[81] A. Murao, M. Aziz, H. Wang, M. Brenner, P. Wang, Release mechanisms of major DAMPs, Apoptosis 26(3-4) (2021) 152-162.
[82] N.D. Osier, S.W. Carlson, A. DeSana, C.E. Dixon, Chronic Histopathological and Behavioral Outcomes of Experimental Traumatic Brain Injury in Adult Male Animals, Journal of neurotrauma 32(23) (2015) 1861-1882.
[83] J.R. Kulbe, I.N. Singh, J.A. Wang, J.E. Cebak, E.D. Hall, Continuous Infusion of Phenelzine, Cyclosporine A, or Their Combination: Evaluation of Mitochondrial

Bioenergetics, Oxidative Damage, and Cytoskeletal Degradation following Severe Controlled Cortical Impact Traumatic Brain Injury in Rats, J Neurotrauma 35(11) (2018) 1280-1293.
[84] J.E. Slemmer, C. Zhu, S. Landshamer, R. Trabold, J. Grohm, A. Ardeshiri, E. Wagner, M.I. Sweeney, K. Blomgren, C. Culmsee, J.T. Weber, N. Plesnila, Causal Role of Apoptosis-Inducing Factor for Neuronal Cell Death Following Traumatic Brain Injury, The American Journal of Pathology 173(6) (2008) 1795-1805.
[85] V. Tashlykov, Y. Katz, V. Gazit, O. Zohar, S. Schreiber, C.G. Pick, Apoptotic changes in the cortex and hippocampus following minimal brain trauma in mice, Brain Research 1130 (2007) 197-205.
[86] W. Jiang, P. Jin, W. Wei, W. Jiang, Apoptosis in cerebrospinal fluid as outcome predictors in severe traumatic brain injury: An observational study, Medicine 99(26) (2020).
[87] X. Liu, T. Van Vleet, R.G. Schnellmann, The Role of Calpain in Oncotic Cell Death, Annual Review of Pharmacology and Toxicology 44(1) (2004) 349-370.
[88] Z. Yang, D.J. Klionsky, Eaten alive: a history of macroautophagy, Nat Cell Biol 12(9) (2010) 814-22.
[89] N. Mizushima, Autophagy: process and function, Genes Dev 21(22) (2007) 2861-73.
[90] K. Vijayakumar, G.-W. Cho, Autophagy: An evolutionarily conserved process in the maintenance of stem cells and aging, Cell Biochemistry and Function 37(6) (2019) 452-458.
[91] J.F. Halling, H. Pilegaard, Autophagy-Dependent Beneficial Effects of Exercise, Cold Spring Harb Perspect Med 7(8) (2017).
[92] R.A. Saxton, D.M. Sabatini, mTOR Signaling in Growth, Metabolism, and Disease, Cell 168(6) (2017) 960-976.
[93] G.Y. Liu, D.M. Sabatini, mTOR at the nexus of nutrition, growth, ageing and disease, Nat Rev Mol Cell Biol 21(4) (2020) 183-203.
[94] C. Settembre, C. Di Malta, V.A. Polito, M. Garcia Arencibia, F. Vetrini, S. Erdin, S.U. Erdin, T. Huynh, D. Medina, P. Colella, M. Sardiello, D.C. Rubinsztein, A. Ballabio, TFEB links autophagy to lysosomal biogenesis, Science 332(6036) (2011) 1429-33.
[95] C. Wang, H. Wang, D. Zhang, W. Luo, R. Liu, D. Xu, L. Diao, L. Liao, Z. Liu, Phosphorylation of ULK1 affects autophagosome fusion and links chaperone-mediated autophagy to macroautophagy, Nature Communications 9(1) (2018) 3492.
[96] E. Wirawan, S. Lippens, T. Vanden Berghe, A. Romagnoli, G.M. Fimia, M. Piacentini, P. Vandenabeele, Beclin1: a role in membrane dynamics and beyond, Autophagy 8(1) (2012) 6-17.
[97] I. Tanida, T. Ueno, E. Kominami, LC3 and Autophagy, in: V. Deretic (Ed.), Autophagosome and Phagosome, Humana Press, Totowa, NJ, 2008, pp. 77-88.
[98] S.R. Yoshii, N. Mizushima, Monitoring and Measuring Autophagy, Int J Mol Sci 18(9) (2017) 1865.
[99] N. Mizushima, T. Yoshimori, How to interpret LC3 immunoblotting, Autophagy 3(6) (2007) 542-5.
[100] G. Bjørkøy, T. Lamark, S. Pankiv, A. Øvervatn, A. Brech, T. Johansen, Monitoring autophagic degradation of p62/SQSTM1, Methods Enzymol 452 (2009) 181-97.
[101] L. Zhang, H. Wang, Autophagy in Traumatic Brain Injury: A New Target for Therapeutic Intervention, Frontiers in Molecular Neuroscience 11 (2018).

[102] J. Wu, M.M. Lipinski, Autophagy in Neurotrauma: Good, Bad, or Dysregulated, Cells 8(7) (2019) 693.
[103] T. Diskin, P. Tal-Or, S. Erlich, L. Mizrachy, A. Alexandrovich, E. Shohami, R. Pinkas-Kramarski, Closed Head Injury Induces Upregulation of Beclin 1 at the Cortical Site of Injury, Journal of Neurotrauma 22(7) (2005) 750-762.
[104] A.K. Au, R.K. Aneja, H. Bayır, M.J. Bell, K. Janesko-Feldman, P.M. Kochanek, R.S.B. Clark, Autophagy Biomarkers Beclin 1 and p62 are Increased in Cerebrospinal Fluid after Traumatic Brain Injury, Neurocrit Care 26(3) (2017) 348-355.
[105] M. Su, Y. Mei, S. Sinha, Role of the Crosstalk between Autophagy and Apoptosis in Cancer, J Oncol 2013 (2013) 102735.
[106] A. Thorburn, Apoptosis and autophagy: regulatory connections between two supposedly different processes, Apoptosis 13(1) (2008) 1-9.
[107] R.T. Marquez, L. Xu, Bcl-2:Beclin 1 complex: multiple, mechanisms regulating autophagy/apoptosis toggle switch, Am J Cancer Res 2(2) (2012) 214-221.
[108] G. Robert, C. Gastaldi, A. Puissant, A. Hamouda, A. Jacquel, M. Dufies, N. Belhacene, P. Colosetti, J.C. Reed, P. Auberger, F. Luciano, The anti-apoptotic Bcl-B protein inhibits BECN1-dependent autophagic cell death, Autophagy 8(4) (2012) 637-649.
[109] L. Luo, A.M. Lu, Y. Wang, A. Hong, Y. Chen, J. Hu, X. Li, Z.H. Qin, Chronic resistance training activates autophagy and reduces apoptosis of muscle cells by modulating IGF-1 and its receptors, Akt/mTOR and Akt/FOXO3a signaling in aged rats, Exp Gerontol 48(4) (2013) 427-36.
[110] S. Erlich, A. Alexandrovich, E. Shohami, R. Pinkas-Kramarski, Rapamycin is a neuroprotective treatment for traumatic brain injury, Neurobiol Dis 26(1) (2007) 86-93.
[111] X. Lin, L. Han, J. Weng, K. Wang, T. Chen, Rapamycin inhibits proliferation and induces autophagy in human neuroblastoma cells, Biosci Rep 38(6) (2018) BSR20181822.
[112] Y. Lai, R.W. Hickey, Y. Chen, H. Bayir, M.L. Sullivan, C.T. Chu, P.M. Kochanek, C.E. Dixon, L.W. Jenkins, S.H. Graham, S.C. Watkins, R.S. Clark, Autophagy is increased after traumatic brain injury in mice and is partially inhibited by the antioxidant gamma-glutamylcysteinyl ethyl ester, J Cereb Blood Flow Metab 28(3) (2008) 540-50.
[113] C.L. Luo, B.X. Li, Q.Q. Li, X.P. Chen, Y.X. Sun, H.J. Bao, D.K. Dai, Y.W. Shen, H.F. Xu, H. Ni, L. Wan, Z.H. Qin, L.Y. Tao, Z.Q. Zhao, Autophagy is involved in traumatic brain injury-induced cell death and contributes to functional outcome deficits in mice, Neuroscience 184 (2011) 54-63.
[114] C. Sarkar, J.W. Jones, N. Hegdekar, J.A. Thayer, A. Kumar, A.I. Faden, M.A. Kane, M.M. Lipinski, PLA2G4A/cPLA2-mediated lysosomal membrane damage leads to inhibition of autophagy and neurodegeneration after brain trauma, Autophagy 16(3) (2020) 466-485.
[115] C. Sarkar, Z. Zhao, S. Aungst, B. Sabirzhanov, A.I. Faden, M.M. Lipinski, Impaired autophagy flux is associated with neuronal cell death after traumatic brain injury, Autophagy 10(12) (2014) 2208-22.
[116] P. Boya, G. Kroemer, Lysosomal membrane permeabilization in cell death, Oncogene 27(50) (2008) 6434-6451.
[117] U. Repnik, M. Hafner Česen, B. Turk, Lysosomal membrane permeabilization in cell death: Concepts and challenges, Mitochondrion 19 (2014) 49-57.

[118] X. Cai, Y. Liu, Y. Hu, X. Liu, H. Jiang, S. Yang, Z. Shao, Y. Xia, L. Xiong, ROS-mediated lysosomal membrane permeabilization is involved in bupivacaine-induced death of rabbit intervertebral disc cells, Redox Biol 18 (2018) 65-76.
[119] D.H. Smith, D.F. Meaney, W.H. Shull, Diffuse Axonal Injury in Head Trauma, The Journal of Head Trauma Rehabilitation 18(4) (2003).
[120] M.I. Hiskens, M. Angoa-Pérez, A.G. Schneiders, R.K. Vella, A.S. Fenning, Modeling sports-related mild traumatic brain injury in animals-A systematic review, J Neurosci Res 97(10) (2019) 1194-1222.
[121] B. Fehily, M. Fitzgerald, Repeated Mild Traumatic Brain Injury: Potential Mechanisms of Damage, Cell Transplant 26(7) (2017) 1131-1155.
[122] M.L. Prins, D. Alexander, C.C. Giza, D.A. Hovda, Repeated mild traumatic brain injury: mechanisms of cerebral vulnerability, Journal of neurotrauma 30(1) (2013) 30-38.
[123] S. Spijker, Dissection of Rodent Brain Regions, in: K.W. Li (Ed.), Neuroproteomics, Humana Press, Totowa, NJ, 2011, pp. 13-26.
[124] S. Liu, Y. Li, H.M.C. Choi, C. Sarkar, E.Y. Koh, J. Wu, M.M. Lipinski, Lysosomal damage after spinal cord injury causes accumulation of RIPK1 and RIPK3 proteins and potentiation of necroptosis, Cell Death & Disease 9(5) (2018) 476.
[125] F.M. Menzies, A. Fleming, A. Caricasole, C.F. Bento, S.P. Andrews, A. Ashkenazi, J. Füllgrabe, A. Jackson, M. Jimenez Sanchez, C. Karabiyik, F. Licitra, A. Lopez Ramirez, M. Pavel, C. Puri, M. Renna, T. Ricketts, L. Schlotawa, M. Vicinanza, H. Won, Y. Zhu, J. Skidmore, D.C. Rubinsztein, Autophagy and Neurodegeneration: Pathogenic Mechanisms and Therapeutic Opportunities, Neuron 93(5) (2017) 1015-1034.
[126] G. Wei, X.C. Lu, X. Yang, F.C. Tortella, Intracranial pressure following penetrating ballistic-like brain injury in rats, J Neurotrauma 27(9) (2010) 1635-41.
[127] W.S. Carbonell, M.S. Grady, Regional and temporal characterization of neuronal, glial, and axonal response after traumatic brain injury in the mouse, Acta Neuropathologica 98(4) (1999) 396-406.
[128] M.E. Schober, D.F. Requena, L.J. Davis, R.R. Metzger, K.S. Bennett, D. Morita, C. Niedzwecki, Z. Yang, K.K.W. Wang, Alpha II Spectrin breakdown products in immature Sprague Dawley rat hippocampus and cortex after traumatic brain injury, Brain research 1574 (2014) 105-112.
[129] D. Yoo, A.W. Magsam, A.M. Kelly, P.S. Stayton, F.M. Kievit, A.J. Convertine, Core-cross-linked nanoparticles reduce neuroinflammation and improve outcome in a mouse model of traumatic brain injury, ACS nano 11(9) (2017) 8600-8611.
[130] J. Xu, M. Ypma, P.A. Chiarelli, J. Park, R.G. Ellenbogen, P.S. Stayton, P.D. Mourad, D. Lee, A.J. Convertine, F.M. Kievit, Theranostic oxygen reactive polymers for treatment of traumatic brain injury, Advanced Functional Materials 26(23) (2016) 4124-4133.
[131] A.W. Tarudji, C.C. Gee, S.M. Romereim, A.J. Convertine, F.M. Kievit, Antioxidant thioether core-crosslinked nanoparticles prevent the bilateral spread of secondary injury to protect spatial learning and memory in a controlled cortical impact mouse model of traumatic brain injury, Biomaterials 272 (2021) 120766.
[132] A. Priester, R. Waters, A. Abbott, K. Hilmas, K. Woelk, H.A. Miller, A.W. Tarudji, C.C. Gee, B. McDonald, F.M. Kievit, Theranostic Copolymers Neutralize Reactive Oxygen Species and Lipid Peroxidation Products for the Combined Treatment of Traumatic Brain Injury, Biomacromolecules 23(4) (2022) 1703-1712.